Aalto University
School of Engineering

Eetu Peltoluhta

Design of a Testbed for Hybrid Electric Vehicle Hardware-in-the-Loop Simulations

Thesis submitted for examination for the degree of Master of Science in Technology.

Espoo, 27.5.2019
Supervisor: Prof. Kari Tammi
Advisor: D.Sc. (Tech.) Alexander Smirnov

Aalto University
School of Engineering

Aalto University, P.O. BOX 11000, 00076 AALTO
www.aalto.fi
Abstract of master's thesis

Author Eetu Peltoluhta

Title of thesis Design of a Testbed for Hybrid Electric Vehicle Hardware-in-the-Loop Simulations

Master programme Master's Programme in Mechanical Engineering **Code** ENG25

Thesis supervisor Prof. Kari Tammi

Thesis advisor D.Sc. (Tech.) Alexander Smirnov

Date 27.5.2019 **Number of pages** 97+2 **Language** English

Abstract

Recent changes to vehicle type-approval regulations have increased demand for testing methods, which better represent real-world driving conditions. *Hardware-in-the-Loop* (HIL) simulation is seen as an attractive alternative for pure simulations and real-world operation measurements.

The goal of this work was to provide a functional testbed for engine testing, as well as for HIL simulations of *Hybrid Electric Vehicles* (HEVs). In addition, a state-of-the-art review of HIL was considered an important goal of the work.

The theory behind HIL, and real-time systems in general, is depicted using a wide variety of examples from automotive applications relating to hybrid power sources. The knowledge gained from the literature was used to design and build a testbed in a form of an engine dynamometer. The testbed can be used to emulate rotational forces, such as load torques on a driveshaft. The testbed's fast hardware connections enable real-time testing. The scope of the design was in mechanical design and in specification of the hardware components.

Initial *Internal Combustion Engine* (ICE) steady-state and transient tests were done to partially validate the testbed. However, the performance was assessed to not be at an acceptable level. For example, only speed tracking passed the non-road transient cycle tracking assessment. Torque tracking and the derived power curves failed the assessment narrowly. However, the test results indicate that with proper tuning of the control software, the system performance should get better. The system response was slow at this point, but the transient behavior itself was fast. Also, in steady-state, torque and speed ripple were low.

Only the preparations for HIL simulation were carried out, since the testbed was not validated to be functional enough for the much more demanding HIL tests. The preparations involved building a simulation model of a series-parallel hybrid *Refuse-Collecting Vehicle* (RCV), which is to be used for the verification of the designed system's HIL capabilities. The model was independently verified to be suitable to be used for the physical tests.

Keywords HIL, dynamometer, testbed, design, simulation, HEV

Aalto University
School of Engineering

Aalto-yliopisto, PL 11000, 00076 AALTO
www.aalto.fi
Diplomityön tiivistelmä

Tekijä Eetu Peltoluhta

Työn nimi Testialustan Suunnittelu Hybridiajoneuvojen Hardware-In-The-Loop Simulaatioihin

Maisteriohjelma Konetekniikan Maisteriohjelma **Koodi** ENG25

Työn valvoja Prof. Kari Tammi

Työn ohjaaja TkT Alexander Smirnov

Päivämäärä 27.5.2019 **Sivumäärä** 97+2 **Kieli** Englanti

Tiivistelmä

Viimeaikaiset muutokset ajoneuvojen tyyppihyväksyntään ovat lisänneet tarvetta testausmetodeille, jotka paremmin vastaavat oikean elämän ajo-olosuhteita. HIL-simulaatio nähdään houkuttelevana vaihtoehtona pelkälle simulaatiolle sekä ajoneuvon ajonaikaisille mittauksille.

Tämän työn tavoitteena on tarjota toimiva testilaite moottoridynamometritestaukseen sekä hybridiajoneuvojen HIL-simulaatioihin. Lisäksi, HIL:in nykytilanteen kuvausta pidettiin tärkeänä työn tavoitteena.

HIL:in, ja yleisemmin reaaliaikaisen testauksen, tausta ja teoria selvitettiin laaja-alaisesti käyttäen esimerkkejä hybridivoimanlähteisiin liittyvistä ajoneuvoalan käyttökohteista. Kirjallisuutta hyödyntäen, testipenkki suunniteltiin ja rakennettiin. Testipenkkiä voidaan käyttää emuloimaan pyöriviä voimia, kuten vetoakseliin kohdistuvia vääntöjä. Testipenkin nopeat yhteydet mahdollistavat reaaliaikaisen testauksen. Suunnittelu oli rajattu pääasiassa mekaaniseen suunnitteluun ja komponenttien määrittelyyn. Sähkö- ja ohjelmistosuunnittelu määriteltiin yleisellä tasolla.

Alustavat polttomoottorilla tehdyt vakaiden ajopisteiden ja transienttiajojen testit toteutettiin testipenkin osittaiseksi validoinniksi. Kuitenkin, laitteen suorituskyky ei yltänyt halutulle tasolle. Esimerkiksi, ainoastaan nopeusseuranta läpäisi transienttiajo-testin, mutta vääntö- ja voimaseurannat epäonnistuivat täpärästi. Tulokset kuitenkin osoittavat luottamusta siitä että testipenkki saadaan aikanaan halutulle tasolle ohjelmistopuolen kontrollereja säätämällä. Tällä hetkellä systeemin vasteaika on liian pitkä, vaikka muuten dynamiikka on nopeaa. Lisäksi, vakaissa ajopisteissä vääntö- ja nopeushuojunta ovat alhaisia.

Ainoastaan valmistelut HIL-simulaatiota varten saatiin toteutettua, sillä testipenkkiä ei saatu reaaliaikasta testausta vaativalle tasolle. Valmistelut sisälsivät hybridijäteauton simulaatiomallin rakentamisen, jota tullaan aikanaan käyttämään testipenkin HIL-toimivuuden validointiin. Simulaatiomalli varmistettiin itsenäisenä toimivaksi, ja siten soveltuvaksi tuleviin fyysisiin testiajoihin.

Avainsanat HIL, dynamometri, testilaite, suunnittelu, simulaatio, hybridiajoneuvo

Preface

I ended up doing my thesis for VTT after several weeks of searching. I knew that I would only work on a project, which I would find thoroughly interesting. Eventually, I contacted professor Kari Tammi about thesis possibilities, and was pointed to the direction of Mr. Jukka Lehtomäki from VTT. I found out about their planned eDyno project and soon I was on board. For giving me this possibility, I would like to thank both of them. Of course, Kari then became my thesis supervisor, and I have thoroughly enjoyed having him as a supervisor, but also as a teacher in a few of my favorite courses.

From VTT's side, Dr. Alexander Smirnov was assigned as my official advisor. He helped me immeasurably with the HIL-side of the thesis, and a huge credit goes to him for proofreading this paper and giving me great advice all-around.

From the beginning, the project was known to be too much for one measly student. Thus, a huge thank you goes to all the people who were involved in the project by assembling the system, running the cables, installing the components etc. From that lot, one man requires a special mention. The man most involved with the project, and my unofficial thesis advisor, Mr. Timo Murtonen. In addition, I would like to thank Mr. Valtteri Kuusinen for taking care of the software development for the eDyno.

I would also like to thank all my friends, old and new, for making these past years so great and memorable.

Finally, I would like to thank my family for always supporting me.

Espoo, 27.5.2019

Eetu Peltoluhta

Contents

Symbols

A_f	[m^2]	vehicle frontal area
C_d	[-]	aerodynamic drag coefficient
C_T	[Nm/rad]	torsional stiffness
F_brake	[N]	braking force
F_drag	[N]	aerodynamic force
F_friction	[N]	frictional force
F_prop	[N]	accelerating (propelling) force
F_total	[N]	total force acting on the vehicle
F_α	[N]	gravitational force resulting from the road grade
$J_\mathrm{driveshaft}$	[kgm^2]	driveshaft moment of inertia
J_total	[kgm^2]	total vehicle moment of inertia
J_trans	[kgm^2]	transmission moment of inertia
P_aux	[W]	auxiliary power consumption
P_dyn	[W]	vehicle power need from the dynamic elements
$P_\mathrm{pumpmotor}$	[W]	pump motor power
P_total	[W]	total vehicle power need
Q	[m^3/s]	flow rate
T_eng	[Nm]	carrier gear torque
T_gen	[Nm]	sun gear torque
T_m	[Nm]	traction motor torque
T_r	[Nm]	ring gear torque
V	[m^3]	volume
a	[$\mathrm{m/s}^2$]	acceleration
f_r	[-]	rolling resistance coefficient
f_0	[Hz]	natural frequency
g	[$\mathrm{m/s}^2$]	gravitational acceleration
i_g	[-]	final drive gear ratio
k	[-]	planetary gear ratio
m	[kg]	mass
n	[rpm]	rotational frequency
p	[Pa]	pressure
r_e	[m]	tire dynamic radius
v	[m/s]	longitudinal velocity
α	[%]	road inclination
η_m	[-]	mechanical efficiency
η_t	[-]	transmission efficiency
η_V	[-]	volumetric efficiency
ω_eng	[rad/s]	carrier gear rotational velocity
ω_gen	[rad/s]	sun gear rotational velocity
ω_r	[rad/s]	ring gear rotational velocity
ρ	[$\mathrm{kg/m}^3$]	air density

Abbreviations

AC	Alternating Current
BIL	Battery-in-the-Loop
BMS	Battery Management System
CAN	Controller Area Network
CIL	Controller-in-the-Loop
CPU	Central Processing Unit
DC	Direct Current
DUT	Device Under Test
ECU	Electronic Control Unit
EIL	Engine-in-the-Loop
EM	Electric Machine
ER-EV	Extended-Range Electric Vehicle
EV	Electric Vehicle
FC	Fuel Cell
FCEV	Fuel Cell Electric Vehicle
FPGA	Field Programmable Gate Array
GVW	Gross Vehicle Weight
HEV	Hybrid Electric Vehicle
HIL	Hardware-in-the-Loop
I/O	Input/Output
ICE	Internal Combustion Engine
MIL	Model-in-the-Loop
NEDC	New European Driving Cycle
NRTC	Non-road Transient Cycle
PC	Personal Computer
PEV	Pure Electric Vehicle
PHEV	Plug-in Hybrid Electric Vehicle
PI	Proportional-Integral
PL	Performance Level
PMSM	Permanent Magnet Synchronous Machine
RCV	Refuse-Collecting Vehicle
RT	Real-Time
SoC	State of Charge
UC	Ultracapacitor
WLTC	Worldwide Harmonized Light Vehicle Drive Cycle

1 Introduction

European commission has focused on the reduction of vehicle emissions during the last two decades, and new testing regulations are being proposed and introduced gradually as an on-going process throughout the upcoming years. In Europe, the *New European Driving Cycle* (NEDC) has been used for passenger vehicle type-approval in the form of laboratory dynamometer testing. The reasons for these new regulation changes are in the noticeable discrepancy between type-approval testing and real-world emissions [1]. Real driving emissions testing is being implemented alongside dynamometer type-approval testing by means of portable emissions measurement systems, which eventually will be used as the main type-approval platform. However, dynamometer-based testing will remain prevalent for CO_2-emission measurement for the sake of repeatability and compatibility between different vehicle models. Improvements have also been made in dynamometer tests: in 2017, NEDC was replaced by *Worldwide Harmonized Light Vehicle Drive Cycle* (WLTC) as the new standard for type-approval dynamometer tests. WLTC was designed to represent practical driving cycle better than NEDC. [2]

The automotive industry is under pressure to develop cleaner solutions and to reduce vehicle emissions due to changes in emission regulations and rising fuel prices. Other contributing factors come from a shifting consumer bias with the help from supportive regional policies and cost reductions to favor *Electric Vehicles* (EVs) and HEVs. The industry has responded well, and the production of electric and hybrid vehicles has been increasing rapidly in the last few years, as seen in figure 1. At the Eighth Clean Energy Ministerial in 2017, EV30@30 campaign was launched, which aims for 30% market penetration of EVs in the total of all vehicles by 2030. This will be achieved by supporting the deployment of chargers, helping policy makers and establishing co-operative global EV pilot city program. By the year 2030, the overall number of EVs is estimated to be between 130 and 230 million units, depending on the used projection scenario. [3]

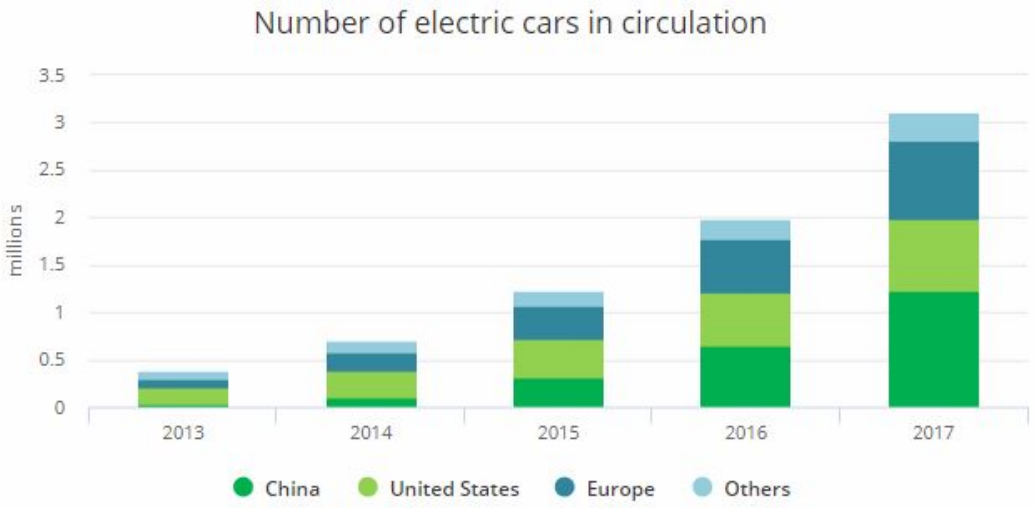

Figure 1. Number of electric vehicles by region [3]

Even though dynamometer testing will have a lesser role as part of regulatory testing in the future, it will have significant use in research and development of innovative technologies,

especially in the areas of EVs and HEVs. In heavy-duty machinery, where the focus is on higher productivity, operator comfort and lower operating costs, research in powertrain hybridization might give a significant edge in the market [4], thus increasing demand for faster development processes.

Field-testing and measurement of vehicles, for example for emissions and efficiency, is time consuming, expensive and hard to create in a reproducible way. Therefore, vehicle manufacturers need faster prototyping methods to meet the consumer and regulatory demands. Another extremity is to run simulations of the systems as part of design and verification. However, even though simulations make testing consistent, less expensive and save time, the results never completely represent real-life. A technology combining the best of both worlds is called HIL simulation. HIL combines these two methods by connecting a physical machine to a simulation. This way, it is possible to make real-life measurements of isolated components in a simulated real-world representation, while keeping testing reproducible and fast, improving convenience and cost effectiveness [5]. It also allows for simplified simulation complexity.

HIL testing has an especially important application in vehicle development as it can be used to reproduce various operational and environmental conditions a vehicle meets in its real-world operation. HIL testing can be used to run performance tests of individual components, such as ICE transient operation. Other applications include the design and development of vehicle drivetrain configuration or control strategies. HIL testing is widely used to validate designed controllers by implementing them as physical components, which control a virtual object, thus preventing possible dangerous and costly hardware failures. Vice versa, control logics can be developed virtually while testing their functionality in a physical setup without manufacturing the physical control boards. Using HIL testing, many integration issues and design flaws can be found in early design phases with negligible risk involved. [6]

In this work, HIL is implemented to provide a platform for vehicle control unit rapid development of a hybrid electric refuse truck including a generalized work hydraulic cycle. For this, a simulation model of a refuse truck is built virtually, while a physical testbed is built as an electric motor/generator dynamometer, which emulates loads to a physical diesel engine according to the torque loading behavior generated in the simulation model.

The distinction between simulation and emulation should be explained, for they are often used as synonyms, but are important in the topic of HIL. Both processes represent a system, but emulation only mimics the behavior of the system, which can be observed from the outside. It does not matter how the resulting behavior is achieved. On the other hand, simulation tries to mimic the system's inner states as realistically as possible. A well modeled simulation should emulate the system. In the case study, the simulation model includes component models, which use lookup tables to emulate the component's behavior, but the overall model is built around correct component causalities, thus simulating the vehicle. The testbed itself emulates the engine loads from the model to the physical engine, i.e. the testbed emulates the simulation model.

Dynamometers are used for multiple purposes related to rotating machinery measurements. Most commonly, people associate dynamometers with measurement of vehicle torque and power. These kinds of dynamometers are called chassis dynamometers, where the prime

mover is not directly in contact with an absorption unit. When a prime mover is directly coupled to an absorption unit, it is usually regarded as an engine dynamometer. Electric motor/generator dynamometers have an *Electric Machine* (EM) as an absorption unit, thus making the dynamometer universal, meaning that it can be used to apply a load to the prime mover as a generator, but also to run it as a motor. This creates a possibility for brake dust measurement, which the designed dynamometer will be used in the future as well. The need for brake dust measurement comes from the regulatory bodies pushing for non-exhaust emission regulations to be added alongside exhaust regulations [7].

The other important advantage of having a motor/generator dynamometer is its use in engine transient testing. Most other types of dynamometers can only be utilized to provide static loads or slow transients for the prime mover, or are not universal, whereas the fast and precise controllability of an EM allows for good tracking of quickly varying load cycles. This is important, as results from static tests do not match well with real-world emissions, especially for NO_x and soot emissions, which show large spikes of particulate concentrations during engine transients [8].

The above stated reasons and applications define the need for a transient multipurpose engine dynamometer. Thus, VTT Technical Research Centre of Finland Ltd (later referred as VTT) wants to invest in having one. VTT is a research facility based in Finland, which serves both the private and the public sector; focusing on innovating new solutions and helping their customers create profit from new technologies. For a while, VTT has had a need for a transient multipurpose dynamometer testbed, which could be applied to different HIL applications, testing conventional engine and for brake dust measurements.

1.1 Research problem

This work documents the process of designing a system, which will be referred to as eDyno, and can be applied to all of the previously mentioned uses, mainly focusing on HIL simulation. The research problem is multidisciplinary and consists of mechanical design, instrumentation and measuring technology, electronic control and simulation. Additionally, hydraulic design, electric design and software implementation are briefly discussed. The HIL application is the focus of this work and provides a valid answer to the question of *whether a Hardware-in-the-Loop simulation for Hybrid Electric Vehicles is achieved with the designed engine dynamometer testbed*.

1.2 Objectives

The objective is to provide a functional setup as an outcome of this thesis work, which can be applied for conventional engine dynamometer testing. In addition, the system is expected to be used for HEV HIL simulations, where a physical engine is used. The system design and implementation process should be documented in system level without going into too detailed specifications. The work also aims to contribute by explaining the overall theory behind HIL simulations and providing reference for different HIL applications of HEVs.

1.3 Scope

The scope of this work is the design, documentation and implementation of the eDyno testbed. The scope of HIL is limited to general description and to relevant applications with one case

study. For the case study, a simulation model will be constructed, a test sequence prepared and validated on the eDyno. Part of the hardware design had already been specified by means of selection of the motor and the inverter before the start of this thesis work, and thus most of the design work is limited to the design of the testbed frame, connections and driveline. Overall documentation of the testbed consists of 2D and 3D -models, system specifications, operation manual and of other necessary documentation. Most of the system specifications are presented in this work, but e.g. dimensions are usually left out unless they provide information that can be considered important. Any manuals provided as part of this work also remain as part of VTT's own archives. Hardware and software specifications are within the scope of this work, but assembly and software programming are not. The scope of the eDyno verification is in running non-standardized tests as a conventional engine dynamometer and as a HIL testbed. Brake dust measurement application is not in the scope of this work.

1.4 Methods

The design of the eDyno testbed will be done using PTC Creo Parametrics 3 computer-aided design software. The system is implemented and verified with steady-state and transient tests with a physical diesel engine. A literature survey of HIL is done, which presents its general description along with its applications related to research topics in electric and hybrid powertrains and hybrid power sources.

As a case study, a HIL simulation model of a hybrid electric RCV is done using The MathWorks, Inc. Simulink® Software (later referred as Simulink). A series-parallel powertrain topology is implemented for the truck, which involves a diesel engine, a starter-generator, a traction motor, a DC-DC converter, a battery and the vehicle dynamic model. Additionally, a reduced model of the hydraulics is modeled in combination of an electric motor, which is used to power the hydraulic actuators during waste collection. The model should be compared to a physical HIL simulation where the modeled diesel engine is replaced with the physical test setup by *Input/Output* (I/O) connections between the virtual and physical environments. The Simulink model will be integrated to National Instruments LabVIEW® software, which provides a bidirectional communication to National Instruments data acquisition hardware. Software development for this communication is outsourced to a third-party company.

2 Hardware-in-the-Loop

This section discusses the background and theory behind HIL testing. First, the general idea and characteristics behind it are explained by starting broadly from explaining real-time systems, describing HIL specific advantages and requirements, and finally going for a more detailed look about system architecture and modeling. Second, previous literature about HIL applications are presented concerning electric and hybrid electric powertrains, hybrid power sources and other applications outside automotive industry. Finally, a brief introduction is given of typical HIL test equipment.

2.1 HIL in general

Testing is an important part of any design or research project. Testing validates the hypothesis and expectations put on a system. In this work, testing is considered from a vehicle design approach, where manufacturers use testing methods to validate the component-, subsystem- and system-level performances of structures and control methods. Tight regulations restrict the design of a vehicle, and these regulations often have strictly determined the acceptable testing methods and conditions as well as the passing test results. Testing can also be unregulated and part of internal development of new designs. The manufacturer creates its own test plan with methods and objectives. The objective can be arbitrarily selected to reflect the goal of the new design, e.g. different drivetrain topologies are tested to find the one with the best efficiency.

Laboratory testing is used for mechanical systems usually to assess their behavior under indented operational domain or dynamic characteristics. Typical testing consists of measurements under emulated in-service loading conditions in terms of motion, force or strain, where actuators are used to excite the system. [5] Actuator output is often determined by numerical calculations using simplified estimations. Regulatory testing procedures use standardized test cycles and methods, which the system has to fulfill. However, these tests rarely represent real-world conditions well [2], and thus more sophisticated tests should be used in addition, at least in early design phases for the more critical parts of the system.

HIL simulation is mostly used in these early design phases to test, validate and calibrate partial systems or single components. Other common HIL uses are to test different control strategies, system configuration, power management or system optimization [9]. For this work, no information was found on HIL testing being used as a regulated test method.

The idea of HIL testing is to "fool" a system into thinking that it is operating in real-world conditions, when in reality it is operated in highly controlled laboratory environment [9]. In [10], HIL is defined as *"a setup that emulates a system by immersing faithful physical replicas of some of its subsystems within a closed-loop virtual simulation of the remaining subsystems"*. Two key aspects arise from this definition: HIL simulator is a *closed-loop system* and has *bidirectional interactions*. Closed-loop system means that the input of the system is determined by the previous output of the system. Nowadays, detailed mathematical models exist of the most commonly used mechanical and electrical systems, which enable the use of simulated models in place of physical components. In HIL simulation, the test specimen is partly real and partly virtual, in which the virtual component is a computer simulation. The real and virtual components interact with each other in real-time in a closed loop. [11] Because both the physical and virtual components affect each other, their interaction is bidirectional.

Unidirectional physical-virtual partitioned simulations can be made, but they are not HIL simulations by definition [10]. Such example would be a physical vehicle chassis interacting with a virtual road model. Here, the chassis responds to the virtual road profile, but the road is not affected by the chassis, as shown in figure 2.

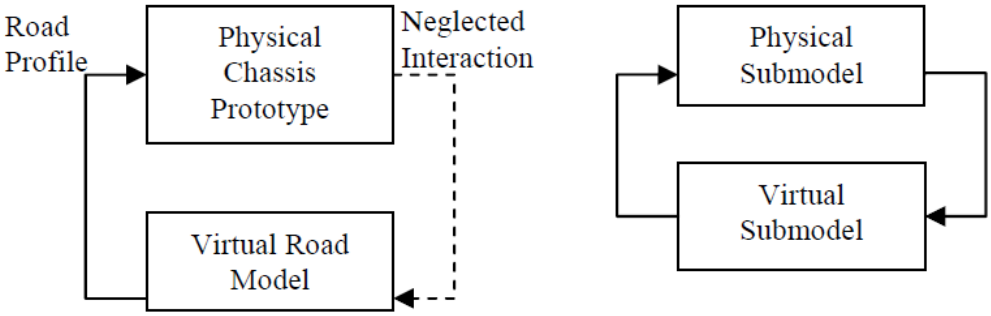

Figure 2. Physical-virtual partitioned simulation. Left: unidirectional interaction. Right: bidirectional interaction (HIL). [10]

Sometimes, other similar terms and definitions are used to define HIL, such as *Controller-in-the-Loop* (CIL), *Engine-in-the-Loop* (EIL) or *Battery-in-the-Loop* (BIL). These terms can be considered special cases of HIL and are used to put an emphasis on the tested object. Similarly, new terms can be derived. CIL is a traditional HIL application, which is used to refer controller prototyping where a physical controller is validated with a virtual subsystem. CIL has become common use in aerospace, defense, marine and automotive industries [10]. EIL is traditionally used for engine mapping, but increasingly more as a system prototyping tool. The designed HIL system in this thesis work is also considered as an EIL. BIL is usually referred in vehicle battery testing.

Model-in-the-Loop (MIL) is a term often used in the automotive industry, and in general means the same thing as HIL as both terms are used in a general context as opposed to defining the tested component [5]. However, in HIL, a plant is being controlled by a real-time simulation, but in MIL it is extended so that the dynamics of the testing equipment such as actuators and sensors, interface with the simulation, as shown in figure 3.

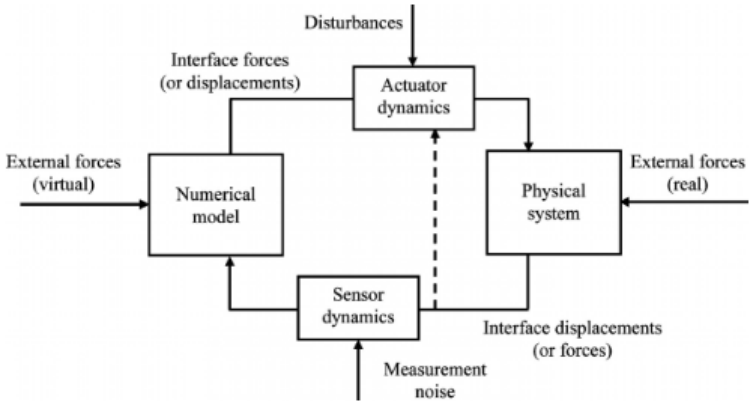

Figure 3. Actuator and sensor interaction in MIL [5]

HIL simulation may require a physical emulator, which can be considered as a link between the physical and virtual parts. For example, this can be an electrical power source controlling the battery voltage or a dynamometer, which applies a countering torque to a prime mover according to the loads determined by a virtual simulation model. Figure 4 depicts an example HIL philosophy where the measured output torque of a real component is used as an input to a virtual component, which then calculates and outputs a speed reference for a dynamometer. A common application where emulators are not needed is *Electronic Control Unit* (ECU) testing, in which only the ECU is physical and all of the other elements are virtual. This is also known as CIL. Typically, no outside variables affect the ECU, and thus no physical emulation is needed.

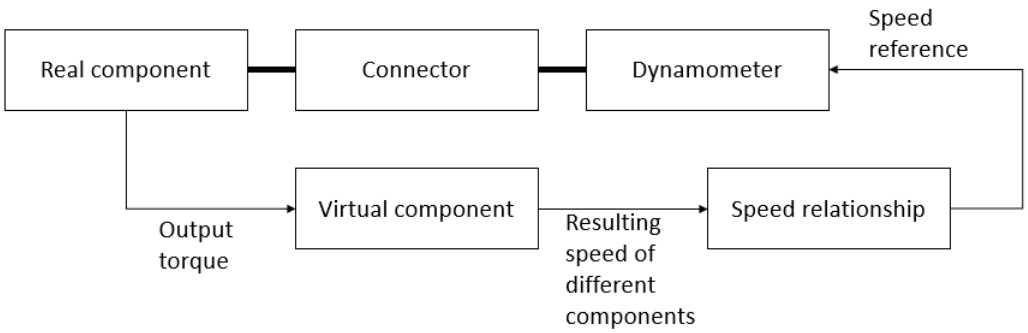

Figure 4. Typical speed reference based HIL philosophy

2.1.1 Real-time systems

Before going further into HIL, it is important to explain *Real-Time* (RT) systems, which HIL is in essence. It is not in the scope of this work to go into details about the subject, but fundamental knowledge is important. RT systems are thoroughly explained in the literature [12, 13].

RT systems have varying definitions, but essentially, they are systems, which are limited by the dynamics of a physical process. The system behavior depends on logical results of the computations and on the physical computation time. Real-time does not always equal fast computing, and the term is often misused for marketing purposes. Rather, real-time means that at the least the computation speed has to match the behavior of the physical system.

An RT system is often used in an embedded system or in a physical-virtual system, such as in HIL simulation. RT is needed when the system has tight interaction with the physical environment via sensors and actuators. Many control systems utilize RT processing. A control system can simply have one sensor and an actuator, a controlled plant, a controller and signal processing. Such control system schematic is presented in figure 5.

RT systems have many challenges compared to purely simulated control. Because the pace of the system is inherited from the environment, RT system is forced to have reactive behavior i.e. the system can only make predictions at look-ahead time, but actual results are always bound to real-time. In addition, the system behavior is hard to maintain deterministic and reproducible due to concurrency of the operation executions. The behavior should be predictable even at the worst-case scenario, and the system response times are usually required to stay under deadlines. A deadline is defined as the time at which a specific result is produced. System environment always dictates the deadlines in RT applications. Implementation of RT systems proves

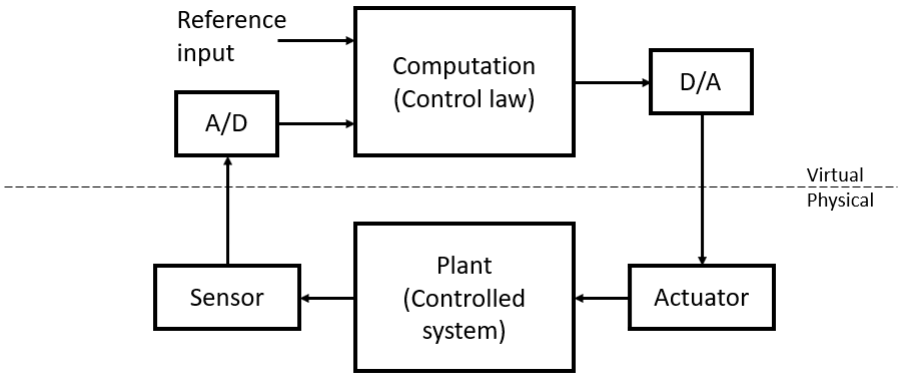

Figure 5. A simple control system

a challenge, since often they are expected to work right the first time to prevent hardware failures. Therefore, reliability and safety requirements should be designed carefully before implementation to the target platform. Physical system properties and environmental effects should be considered in RT systems, such as processing power, temperature or electromagnetic interference.

RT systems are usually classified to three categories: soft, firm and hard. The difference comes from whether the result of a computation still has utility after a deadline. In a soft case, the result still has utility, in a firm case, it has zero utility and in a hard case, missing a deadline may be catastrophic. When a deadline is missed, and the system has potential to become unstable, a safe operation should be enforced. A system can be either a fail-safe or a fail-operational system. In a system failure, a fail-safe system can reach a safe state — an operation point, which is known to be safe. An example could be a complete power cut-off in an engine dynamometer, i.e. termination of the control system and making the physical system completely non-operational. A fail-operational system cannot reach a safe state in a system failure. Rather, a minimum level of operation should be available in a failure. Airplane flight control is an example where fail-operational systems are used. Active redundancy is often used to provide minimum operational proficiency.

In soft RT systems, meeting the iteration deadline is not guaranteed, and the correctness of the results usually cannot be made analytically. Error detection is on user's responsibility, but safety is also non-critical. In hard RT systems, timeliness must be guaranteed by sufficient (computational) resources and analytically evaluated correctness. Error detection at a system level must be present. Under failure or at rare events, the system operation must be predictable, and redundancy should be used.

2.1.2 HIL advantages

An important advantage of HIL simulation is the simplicity of the test setup. Rather than having a complete system, e.g. a vehicle, only a small part of the overall system has to be physical, as other components can be modeled virtually. Of course, the key component(s) with unknown dynamics always has to be part of the physical setup. Some advantages of HIL simulation have already been mentioned, but to give a complete overview of the main advantages, a short list is provided below based on [10]:

- Cost effectiveness: Less hardware results in HIL simulation being cost effective compared to physical prototyping.
- Rapid prototyping: HIL setups are usually faster to build than physical prototypes.
- Fidelity: Purely virtual simulations are always simplifications of real systems, and thus cannot reach the levels of fidelity HIL simulations do.
- Simulation speed: Swapping virtual components to physical hardware reduce the computational effort.
- Repeatability: By incorporating virtual models to testing, variables can be removed, which would otherwise affect test results in physical testing.
- Non-destructiveness: Enables possibility to simulate destructive events.
- Operating conditions: Possibility to emulate in-service conditions, which would otherwise be hard to replicate in laboratory, for example, aerodynamics. Testing conditions can also be changed in fast and easy manner by changing the simulation parameters.
- Safety: HIL simulators can be used for operator training e.g. pilots in flight simulators. Also, virtualization of high-power components improves safety in testing and prototyping.
- Concurrent engineering: Different subsystems can be developed simultaneously with HIL simulation while keeping track of the integration issues.

2.1.3 HIL Requirements

A successful HIL simulation system has some key requirements, which are mostly related to real-time simulation, as more elaborated in [8], [9] and [10]:

- Sensors and actuators: The associated sensors and actuators must have sufficient fidelity and bandwidths. HIL simulator is basically a control system, where a physical subsystem tries to follow a reference set by the virtual subsystem. Accurate measurements and control are needed for this tracking. However, the actual fidelity and bandwidth of the sensors and actuators can vary greatly, depending on the type of the HIL system, and still obtain good results. For example, there can be an order of magnitude difference in fidelity in EIL and BIL. Fast instrumentation and data acquisition hardware are needed to accurately correlate test data to the test cycle. This is more important in HIL simulations with fast transients such as in [9], where engine emissions were measured with state-of-the-art NO_x analyzer and a differential mobility particulate spectrometer.
- Hardware/software integration: Hardware/software partitioning, i.e. the selection of the physical components and the virtual models, must be made according to the research and design goals. The bare minimum is to have the key test specimen to be physical, but it also might be beneficial to use other physical components in addition, if their modeling would prove difficult or otherwise impractical or lead to significant measurement errors of the key component. Proper hardware/software partitioning is essential in rapid prototyping of system configurations such as vehicle drivelines, where HIL can be

used to quickly swap components, for example, to compare components from different manufacturers.

- Signals: Digital signal processing and conditioning by the use of lead-lag filtering is critical for system integration in terms of reduction in disturbances, noise and time delays. Typical signal processing includes digital signal decoding, anti-alias filtering and noise attenuation. The use of a separate digital signal processor is recommended for these tasks.

- Proper modeling: Proper modeling is required to get reliable test data. However, modeling accuracy increases the need for calculation power, and thus may compromise real-time simulation. Therefore, model reduction techniques are often used, such as energy-based automated model reduction [14].

- Real-time simulation: Bidirectional interaction requires that the physical and virtual component frames match exactly. Real-time simulation requires fast processors and software capable of handling real-time simulation. The simulation environment should run in fixed step-size to continuously synchronize with real time. Different types and architectures of real-time systems are explained in [12].

2.1.4 System architecture

A HIL system is relatively simple and consists of only three main components: a real-time processor, an operator interface and I/O for connections. The real-time processor is the most crucial part of the test system and is responsible for the test execution. Everything is connected to it in one way or another: I/O communication, sensor data logging, actuator/emulator excitation etc. The simulation is needed to run in real-time for accurate representation of the virtual components. The model itself can be built in a remote *Personal Computer* (PC), but it is usually sent out to a target PC for execution. Additionally, an important part of system development is to guarantee a safe operation in non-ideal conditions. Fault insertion modules can be inserted between I/O and *Device Under Test* (DUT) to emulate faulty behavior, such as bad signal quality, short-to-ground circuits or open circuits. Figure 6 shows a block diagram of the main connections of the system.

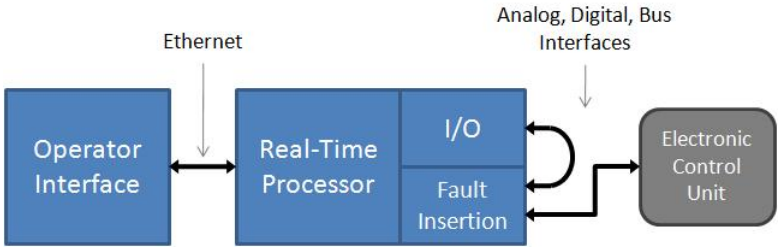

Figure 6. HIL system architecture has three main components: an operator interface, a real-time processor and I/O. Signal fault behavior can be tested with fault insertion. [15]

A target PC can generally be of any type a PC running on any operating system, as long as it has enough processing power for real-time execution and has the hardware and software capabilities to implement all of the I/Os. The MathWorks, Inc. offers a software called xPC

Target, which adds a real-time processing environment to implement Simulink and Stateflow® models. Modeling for HIL applications is discussed in section 2.1.5. The benefits of xPC target are its low cost and good calculation efficiency and use of existing PC hardware [16]. There are also several commercially available target machines specifically designed for real-time simulation and HIL testing. For example, Mathworks has a partnership with Speedgoat — a company, which creates real-time simulation and testing applications. They offer a wide range of target machines depending on the customer requirements. The benefit of using Speedgoat hardware is the out-of-the-box implementation of Simulink models to the target hardware. The Simulink model parameters can be changed on-the-fly in the Simulink environment without having to re-compile the model. National Instruments offers a modular approach for building a tailored HIL test system. CompactRIO by National Instruments is used in this work as a target machine. Usually, the benefits of these special real-time target machines is their programmability, extensibility and option for *Field Programmable Gate Array* (FPGA)-implementation.

Operator interface is usually implemented by the use of a host computer, which is a separate computer connected to the target machine via transmission control protocol / internet protocol, i.e. a network connection [17]. The host computer is used by the operator to provide test commands and the user interface typically involves visualization tools for test monitoring. Other host computer tasks involve test automation, test report generation, analysis and configuration management. For example, in some platforms, it is possible to write an optimization script in The MathWorks, Inc. MATLAB® software (later referred as Matlab), which runs a set of HIL simulations with parameter iteration to reach an optimization goal. It is also possible to run a simulation and modify its parameters on the fly. This can be used e.g. to tune control system parameters while monitoring the impact to the physical system in real-time.

I/O interfaces are used to connect the physical and virtual components together. The signals interacting with the DUT can be analog, digital or bus signals. Especially when developing and testing controllers, it is useful to have the same I/O as would be used in the fully physical system. *Controller Area Network* (CAN) bus signals are often used in the automotive industry, where ECU communicates with a wide range of devices inside a vehicle. Thus, CAN bus communication in HIL simulations is quite common.

As HIL setups get more complicated by the addition of more physical components and controllers, processing power needs to be increased, while the system wiring should not become too complex. Usually no additional system components are needed, and one target machine with sufficient I/O may be enough. However, for example, automobile, aircraft and wind farm applications often have multiple DUTs networked together in a HIL simulation, which increase the processing power and I/O need. In very power-hungry applications, one real-time processor cannot provide enough processing power, even with today's multi-core processors. In that case, multiple target machines can be linked to provide extra processing power and to extend I/O capabilities if the channel count is too high for one target machine. This is called distributed processing. Sometimes, a single processor may even have to be dedicated solely for simulation model processing, if the model is too complex and of a high fidelity. Distributed processing may require shared trigger, timing and data signals between the target machines, depending on the task distribution. Figure 7 shows a simple distributed architecture layout.

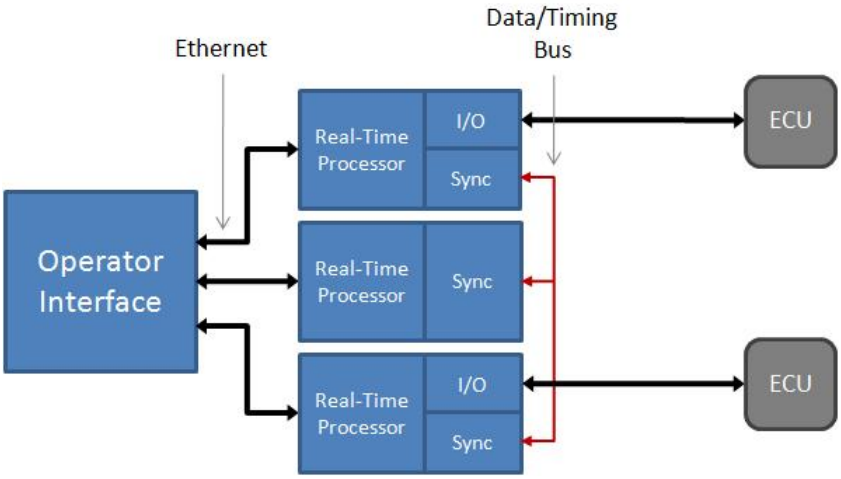

Figure 7. Distributed processing uses multiple target machines to provide extra processing power and to extend I/O capabilities. Synchronization may be necessary. [15]

Wiring schemes can be simplified with deterministic distributed wiring. I/O interfaces are separated from the real-time processor and located as close as possible to their respective DUTs. This keeps the wiring between I/O and DUT as short as possible, and the modularity of distributed I/O allows for easy scaling of the HIL setup. Modular I/O interfaces are connected to their real-time processors via bus channels.

2.1.5 Modeling

In a mechatronic field a system often has characteristic speeds in a large disparity, i.e. both fast and slow dynamics are present in a system, usually related to electrical and mechanical dynamics, respectively. A good example of fast dynamics is the pulse width modulation used in inverters, whereas mechanical dynamics such as motor rotation can be considered to be significantly slower. This speed disparity in a model is defined as virtual model stiffness [10].

As discussed in section 2.1.3, proper modeling is needed for successful HIL simulation. Even with lower simulation fidelity compared to full vehicle simulation, HIL simulation model design proves a challenge. Integration of accurate vehicle system dynamic models into the simulation increases real-world similarity, with the expense of execution speed, which may compromise real-time simulation [6]. Additionally, emulator control and overall platform control with precise physical-virtual system matching presents their own challenges.

Proper modeling techniques are often used for stiff models to eliminate fast dynamics, since they usually have low impact on the overall system response, but require the most processing power. A proper model is easily achieved by modeling the components with fast dynamics as simplified versions. For example, if the response of a component is known, it may be enough to use lookup tables in place of models that are based on the underlying physical equations. Lookup tables are especially useful for replacing engine, motor and inverter characteristics when the simplification has little impact on the inspected phenomenon. Another commonly used model simplification method in vehicle modeling is when measuring results, such as fuel and energy consumption over a long period of a drive cycle; it is not worth to model lateral, vertical or tire dynamics, when vehicle longitudinal dynamics are often enough. If model simplification needs to be avoided, a reduction algorithm can be applied on the model

to reduce model stiffness. In such algorithms, model fidelity is measured and balanced against simulation execution speed to optimize the simulation accuracy and computational effort. In [9] a high-fidelity vehicle and driveline models are first used and then reduced by eliminating the least active elements, i.e. the model elements that contribute the least to the overall system, using an algorithm called model order reduction algorithm. [18]

In case it is not possible to alleviate model stiffness, different model dynamics can be simulated at different integration sample rates. This is called multirate integration, and it requires the use of multiple processors, one for each integration process. Multithreaded processors can also be used, but generally as good of results are not obtained as with separate processors. Multirate integration can cause synchronization issues, which are further discussed in literature [10].

Virtual I/O is usually implemented into the simulation model and configured accordingly to send and receive data from the I/O hardware. For example, in Simulink it is possible to place CAN bus blocks to communicate with the CAN bus module on the target machine. In other words, the physical DUT can be completely replaced by virtual I/O blocks in the simulation model, depending on the causality of the model. Some simulation and integration platforms allow the use of simpler input and output blocks, which are configured external from the model.

The simulation preferences should be set for fixed time-step integration to achieve matching with real-world connectivity. Once the model is configured properly and communication links have been established, the model is automatically built into an executable algorithm and downloaded to the target machines processor(s). [17]

Gao et al. [19] modeled a fuel cell stack in electrical, fluid and thermal physical domains. The model complexity and nonlinearities required a well thought approach in modeling for the simulation to run in real-time. To keep the system portable and compatible, the stack model was coded in C-language-based S-function in Simulink. S-functions are blocks in Simulink, which execute scripts written in various other programming languages. They can be used to replace the graphical block modeling typically used in Simulink. The model dynamics are represented in nonlinear state-space matrices A, B, C and D using the physical equations of the system. These matrices are written in C-code as 1-D and 2-D table structures. This state-space representation allows the use of generic ordinary differential equation system solver, which is able to resolve complex differential equations efficiently, allowing real-time simulation of the model.

The simulation models are processed in the target machine as automatically generated C-code. These C-code generated simulation algorithms are usually implemented in *Central Processing Unit* (CPU)-based target machines, which are widely available and easiest to implement, but their time step is limited to ≤ 10 μs due to large bus latencies in the processor [20].

Many applications in power system simulation use detailed models of power electronics, such as converters. These components often use high-frequency switches controlled by pulse-width modulation signals, which can be up to 100 kHz [21]. When such signals are used in real-time simulations such as in HIL, the simulation time step needs to be faster than what the switching frequency of the DUT is. Graphics processing unit -based processing provides an alternative to CPU-processing, as they have good parallel processing capabilities. However,

they still have similar drawbacks as CPUs when it comes to real-time simulation [22]. Often, the only solution is to use FPGA processing, which combines excellent parallel processing and low bus latencies, which can be as low as 1.5 μs. These attributes make FPGA ideal for high-frequency HIL applications. The disadvantage of FPGA is the additional effort in simulation implementation [21] as the programming has to be done at lower-level. [20]

Measured signals always include some noise and also some time delays. Before using these signals in the model, some processing is usually required. At least with slow dynamic systems, fast signal dynamics are not needed, and thus implementing a low-pass filter is recommended to clean the signal from noise. Communication delays from the sensor measurements can be compensated, for example, using a lead-lag compensator. Lead-lag compensator shifts the signals phase via a transfer function. In [9], a lead-lag filter was designed by taking engine speed and throttle position measurements at various steady states and creating empirical models of the engine dynamics and setup's noise. Using these models, a lead-lag filter was designed by loop shaping.

In HIL simulation one of the first steps in modeling is to decide the connection causality, i.e. which properties are to be used as inputs and which signals are received as outputs. This decision may have significant impact on real-time simulation performance. Poorly designed model may result in limited control and unstable performance.

In vehicle simulation, two fundamental modeling techniques are used: forward and backward-facing models, as further described in the literature [23, 24, 25]. Forward-facing models are considered to have the correct causality, representing real-world physical correlations. The model starts with a driver model, often implemented as a *Proportional-Integral* (PI)-controller, following a reference, which is usually a longitudinal drive cycle or a vehicle maneuver. Based on the driver model, torque demands are generated for the power source(s), which transmit the torque flow all the way to the wheels through the implementation of transmission and vehicle dynamics.

In backward-facing vehicle modeling, it is assumed that a drive cycle reference can always be tracked. Therefore, the method cannot be used in computing best-effort performance, where the vehicle does not have capabilities to follow the reference. From the reference, necessary tire-contact forces are calculated based on the vehicle dynamics and are then converted back to the main power source(s) through the transmission. Figure 8 presents a generalized block diagram of both fundamental modeling techniques as would be used for a simple conventional vehicle. HEV energy management is usually implemented at two levels: local and global. To successfully manage local energy flow, a causal vehicle model is more appropriate. A local controller is also needed. Since forward-facing model is able to represent physical power flow and dynamics, it is suitable for low-level energy control.

While backward-facing models have their advantages mostly in their ease of implementation and fast processing times due to a common use of quasi-static and steady-state component models, they are not suitable for proper simulation of vehicle dynamics or HIL simulation. Essentially, they do not support feedback control of the subsystem level components, and correct physical connections such as throttle command are not present. Therefore, HIL simulation models should be implemented as forward-facing models unless it is enough to study top-level energy strategies or vehicle behavior. For example, Hentunen et al. [4, 26]

successfully used backward-facing modeling in their series HEV HIL simulation. This was possible because the study goal was to design a global energy management strategy by a load sharing algorithm. Backward-facing modeling is also very efficient for initial component sizing tasks, where the sizing is based on fulfilling the power needs of a drive cycle. After the sizing is done, a forward-facing model can be built using the selected component parameters. This model can further be used in HIL simulations.

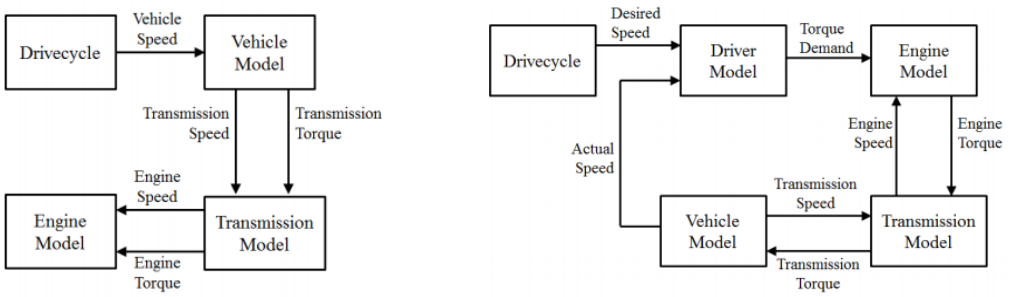

(a) *(b)*

Figure 8. Backward-facing (a) and forward-facing (b) vehicle models [24]

Filipi et al. [9] notes that even though good pure simulation results are gathered in vehicle simulation when controlling the engine torque and measuring engine speed, EIL simulators may show limited system controllability. Their designed EIL simulation continued to present control problems even after careful control gain tuning. The problem was cleared after switching the connection causality of the model from engine torque control and speed measurement to controlling engine speed and measuring the torque. The difference in performance was explained by pointing out that engine torque control essentially represents acceleration control of the engine's crank shaft. Acceleration is of a higher order in comparison to velocity, and higher order signals are noisier and require higher actuator bandwidths.

2.2 HIL applications

Three methods can be considered for in-vehicle engine investigation: real-world measurements on open roads, a chassis dynamometer with driving cycles or an engine dynamometer. First option gives the best results, but test repeatability is poor and a fully built vehicle is required. Second option makes testing repeatable, but still at least a fully operational powertrain, chassis and wheels are required. Third option only couples the engine to a dynamometer, which can be run in a test cell in controlled laboratory settings. An engine dynamometer can be used to determine engine specific dynamics, responses and emissions, but more promising is its use for HIL testing, where the rest of the vehicle is virtually built around the engine. This way, vehicle-specific dynamics, responses and emissions can be determined, and different configurations can be tested easily by changing model parameters. [27]

Model-based software development and rapid control prototyping are widely used in the automotive industry. Laboratory verification is considered important, because the systems in focus are typically high-powered, and thus could be dangerous to do in other ways, especially in early development where there is more risk involved. Therefore, HIL is frequently used due to its benefits in rapid prototyping.

Where measurements from static engine loads can be useful in some cases, real-world driving involves frequent changes in velocity with multiple starts and stops [9]. This resulting driving cycle is crucial for engine measurements since the speed and load of the engine wary greatly during the cycle. These transients play a large role in engine emissions, as the particulate (or soot) emissions resulting from transient spikes may make up to half of the total emissions over a city driving cycle [8]. Since simulating particulate emissions requires high-level computational fluid dynamics models and chemical kinetics, EIL simulation for system design and control is proposed in [27] to minimize fuel consumption and NO_x emissions. The optimization problem here is that minimizing fuel consumption (by engine cut-offs) increases NO_x emissions.

On the subject of fuel efficiency, [28] proposes a HIL simulation for measuring the performance of traffic mobility and connected vehicle applications, such as cooperative adaptive cruise control, by measuring actual fuel consumption and emissions from a physical vehicle powertrain that is connected to a microscopic traffic simulator. The simulator determines vehicle power demand based on vehicle dynamics, road condition and target vehicle information. While the engine is operated through a fuel consumption optimization protocol, a hydrostatic dynamometer then tracks the engine load.

Vehicle powertrain simulation using a dynamometer typically emulates loads and component inertias to a physical prime mover, e.g., an engine or an EM. Because a dynamometer and couplings usually have smaller combined inertias than that of the actual vehicle, the inertia should ideally be increased. Inertia can either be increased by attaching physical elements to the setup, or by taking the inertia difference into account when calculating reference loads to the dynamometer. [6]

Hardie et al. [29] built a dynamometer-based testbed for engine management unit automation. According to the paper, the process had been typically done by manually adjusting engine and dynamometer parameters to build an engine map that represents the tuned engine parameters, such as ignition timing and air-fuel ratio at a specific speed-throttle point. This process was automated by creating an algorithm, which controls both the engine and the dynamometer in a closed-loop, and tunes the engine management unit based on an optimization goal, which is usually either good fuel economy or maximum power output. Essentially, this closed-loop control of a physical engine dynamometer is HIL simulation, even though the term was not used in the referenced paper.

2.2.1 Electric and hybrid electric powertrain

HIL simulation has gained an important role in the automotive industry particularly for the development of electric and hybrid electric vehicles. The reason behind this is the nature of the powertrains in these vehicles, which have to be dimensioned with better precision than conventional powertrains, and their designs typically have more to gain from optimized control and power management strategies. [4]

The principle behind all electric vehicles is the utilization of an EM, with or without a conventional ICE. EV powertrains, i.e. vehicles without an ICE, are typically simpler than hybrid ones, with the basic idea of energy flow from an electric battery to an EM through an inverter. HEVs, on the other hand, can be classified in more than one way. The standard definition for HEV states it as a vehicle with two or more energy storage systems [30], most

often implemented as a combination of battery and fuel storage. A dated, but still often used division is made between series, parallel and power-split hybrid vehicles. Generally, the powertrain architectures can be simplified by defining series powertrain topology having the EM as the only prime mover while the ICE runs a generator, which powers the EM and charges the battery. Parallel topology would be defined combining both an EM and an ICE to drive the wheels, and power-split topology combining both by creating a possibility for (dis)engaging the ICE propulsion using a clutch.

In recent years, HEV topology variety and complexity has increased, muddling the classification. Terms like series-parallel and complex hybrids have been used to describe topologies, which are not clearly neither series or parallel [31]. Figure 9 shows the four basic HEV topologies, which work as a base for further classification. Guang et al. [32] extends the classification of electrified vehicles into more detailed architectures, and gives a comprehensive overview and comparison of them. The top level classifications of series, parallel and power-split powertrains are quite non-descriptive, and thus the paper classifies all electric vehicles into five categories based on their electrification levels: micro HEV, mild HEV, strong HEV, *Plug-in Hybrid Electric Vehicle* (PHEV) and *Extended-Range Electric Vehicle* (ER-EV). In addition, the classification includes *Pure Electric Vehicle* (PEV) and *Fuel Cell Electric Vehicle* (FCEV). However, some papers include FCEVs into HEV category [33]. Figure 10 presents a classification involving some of the electrification level based HEV classes, ICE vehicle and FCEV based on the propulsion device and energy source. PHEV and ER-EV could be placed at whatever part of the HEV classes in this presentation.

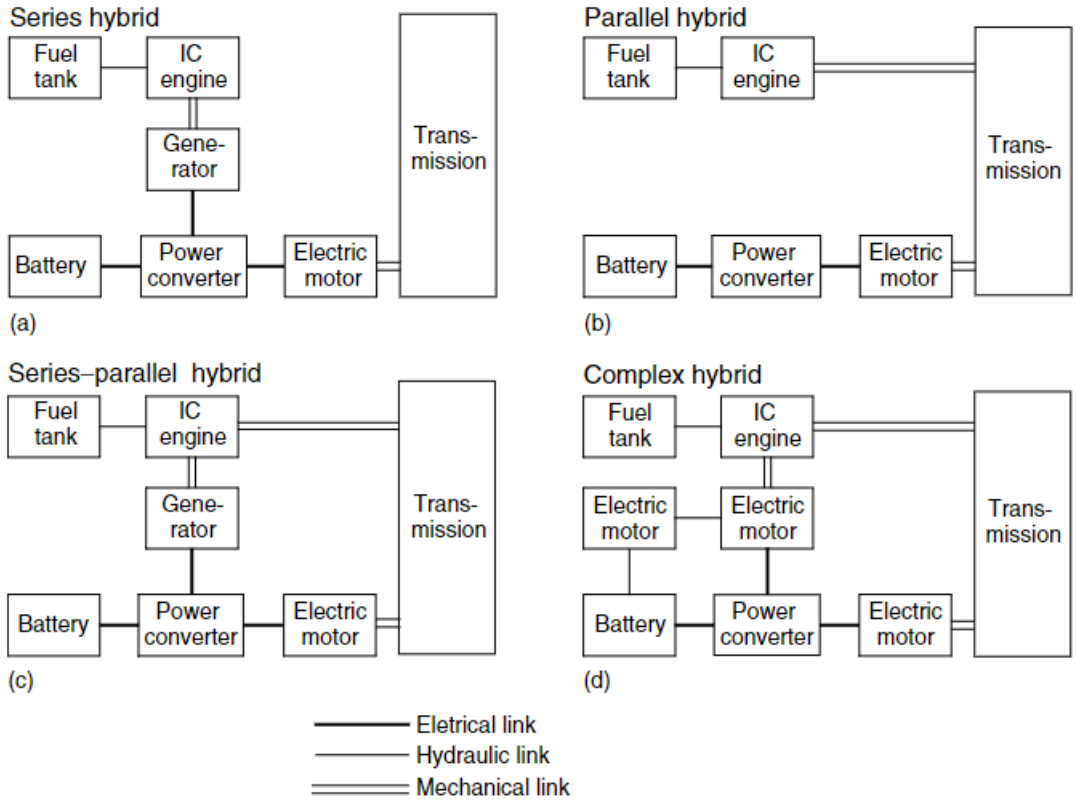

Figure 9. HEV classification based on powertrain topology [31]

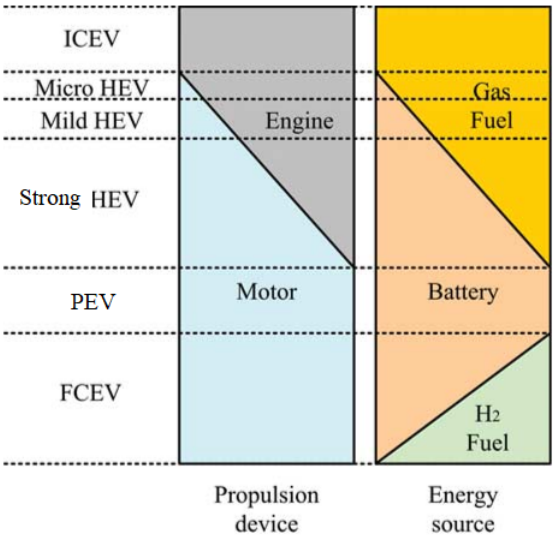

Figure 10. Vehicle classification based on propulsion device and energy source [33]

Of course, hybridization can refer to any type of power source combination, whether or not they appear in classifications such as was shown in figures 9 and 10. For example, *Fuel Cells* (FCs) can be combined with an ICE, a battery or even a supercapacitor. Virtually any combination is possible, but often may not make sense.

A great benefit of hybridization is that it allows ICE downsizing, since it no longer is the only source of traction. Downsized ICE inherently has lower fuel consumption and emissions. Additionally, electric motor's high traction from the very beginning of its speed range makes it ideal for use in driving cycles with frequent starts and stops at low average and maximum velocities, i.e. in urban driving scenarios and with many work machines such as loaders.

Hentunen et al. [4] designed an HIL environment for the specific purpose of HEV verification. It is a prime example on how well HIL can be extended to larger setups as well, rather than only having a single DUT. The physical setup emulates the power components of a series HEV and consists of an ICE generator set, an ultracapacitor, a battery with bidirectional *Direct Current* (DC)-DC boost converter, a traction motor and an inverter. This only leaves the vehicle body and dynamics to be virtually modeled. The load torque from the simulation is emulated with a dynamometer, which is connected to the traction motor via mechanical coupling. The dynamometer can either track a torque reference with speed limit or speed reference with a torque limit. The simulation model is backward-facing and provides information of large signal behaviors rather than including fast switching transients, because the load cycles are long and no detailed knowledge of the components was available. Thus, the simulation time-step could be kept rather long at 1 ms. In addition, a simulation model of the entire powertrain was modeled, and simulated and measured values were compared with mostly good matching. For example, two different ultracapacitor modeling techniques, constant capacitance and variable capacitance models, were used and compared. A simulation model that matches well with measured data can be considered well-modeled. Thus, HIL simulation can be used as a model development and validation tool. Also, a previously verified model can be used to validate a designed HIL system. While the presented HIL setup was designed for full-scale HEV powertrain verification, it has since been used for various other related

applications. For example, it has been used to measure efficiencies of electric machines, power electronic converters and hydraulic pumps. Also, plant models and control algorithms can be validated with the test setup, and device properties can be characterized by assuming a black box and identifying the system's response.

A lot of research is put into new technologies to improve the fuel economy of heavy-duty vehicles, such as trucks and off-road work machines [4, 27, 34, 35]. According to [27], implementation of lightweight structures for a truck is not a viable way to reduce its fuel economy, since it is likely to increase the payload carrying capacity, rather than reduce the *Gross Vehicle Weight* (GVW). Also, the aerodynamic properties are difficult to optimize for delivery trucks, since the carrying compartment mostly dictates them, and is already optimized for maximum capacity. Moreover, there is little left to gain from diesel engine development as they are already highly efficient. This leaves hybridization as the only viable option to significantly reduce fuel consumption and emissions for heavy-duty vehicles. Most of these gains are reached through regenerative braking, engine shut-downs and by utilizing a down-sized engine in its optimal operation point.

Energy management strategies are used in HEVs to control and optimize the fuel economy and emissions. This is an important research topic since HEVs have multiple power sources, which can co-operate in countless of ways. The strategies involve transitioning between multiple operation modes, typically to optimize energy consumption. However, sometimes a control strategy may be used to maximize the power output. Mode transitions often involve engagements in mechanical couplings, and sudden changes in torque transmission may be uncomfortable to passengers. [11]

Zhang et al. [11] utilized HIL simulation for controller verification for a robust mode transitioning in a series-parallel HEV. The controller's purpose was to reduce jerkiness resulting from clutch engagements present in transitions between different operation modes of the vehicle. The proposed controller was designed for a HEV, which comprised of an ICE with an integrated starter/generator, a transmission and an EM between the transmission and the final drive. The first operation mode is fully electric, when the battery is able to provide enough power to meet the speed/load requirements. As the required power gets too high or the battery *State of Charge* (SoC) drops below a specified threshold, the integrated starter/generator starts the engine and the clutch is engaged. At this point, the vehicle is operating in a hybrid or engine-only mode. The proposed mode transition control uses the EM to compensate for torques resulting from the clutch engagement and for other sudden spikes in the transmission. The proposed controller was verified in a HIL simulator consisting of three dynamometers, which were emulating the ICE output torque and the wheel torques. The physical output torque of the transmission was set as the input for the virtual model and was calculated based on the real transmission parameters. Rest of the vehicle was modeled virtually. The HIL simulation proved that the proposed controller was able to reduce transmission jerkiness. Also, the controller robustness against parameter uncertainties and torque disturbances was verified; the control was successful with only a small performance loss when using 5% errors in the parameter values.

Possibilities of HIL for regenerative braking is researched and discussed in [36]. The paper concludes that accurate results considering energy consumption can be made using a simple HIL setup where only a traction motor is physically under load. However, this required

introduction of brake distribution controller model that incorporates friction brake blending.

Marcel et al. [37] built a HIL testing facility with the specific focus on validation of FCEVs. Because FC stacks are still expensive and potentially dangerous, their thorough testing is important before actual implementation to a real vehicle power system. The designed test facility allowed for setting up all necessary FC powertrain components used in most common battery-FC configurations. The test platform involved a small-scale FC HEV powertrain consisting of an FC stack, a battery, a DC-DC converter and a *Permanent Magnet Synchronous Machine* (PMSM) with an inverter. The loads were emulated with a small DC motor and resistive loads for the DC-DC converter. A simulated model of the facility was also created and compared to the experimental results, showing that FC stack inclusion in HIL simulation is a viable option for development of FCEVs.

In the heart of most electric vehicles is the traction motor and other core components related to it. Accurate powertrain modeling is often a prerequisite for successful EV HIL simulation development. Real-time simulation has its set of boundaries in terms of modeling, which need to be addressed. In [20], Herrera et al. presented an FPGA-based real-time simulation of power converters and EMs, which can be used for EV HIL applications. An example HIL model was built with an algorithm for machine saturation characteristics and electrical and thermal behavior modeling of the power converter.

While traction motor modeling has reached a point where highly accurate behavior can be replicated, there is still benefit for testing EMs in a real-life condition emulation. HIL simulation can be especially useful when trying to make a decision between multiple similar motors from different manufacturers, because of the fast and concurrent testing in a HIL setup, where comparing different components is only a matter of swapping the DUT. Schupbach and Balda [38] built a relatively low cost HIL testbed for traction motor testing for the purpose of electric vehicle development and research in university facilities. The interactions of the HIL testbed are presented in figure 11.

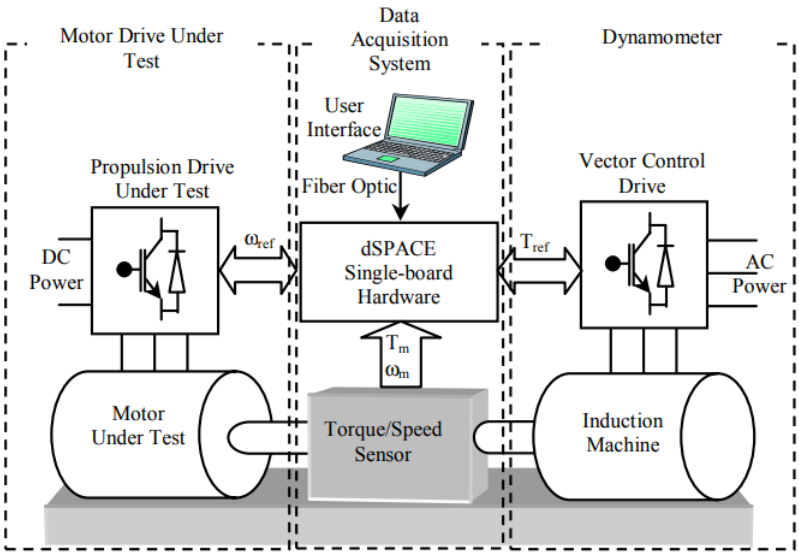

Figure 11. Schematic of HIL platform for EV and HEV development by utilizing an Alternating Current *(AC) dynamometer to emulate loads on a traction motor [38]*

2.2.2 Hybrid power sources

The reasoning behind vehicle hybridization has been stated previously and some configurations and combinations have been discussed. In this section, a closer look is taken at how HIL testing is utilized in the development of different power sources for HEVs; batteries, fuel cells, ultracapacitors and hydraulic power sources.

Usually, one source of energy does not provide good results as each solution has their own limitations. Batteries have lifetime constraints from degradation, while fuel cells have issues in power transfer [39]. Especially for heavier vehicles the amount of energy flow required can be extremely high, thus requiring fast energy discharges. This can be a problem for conventional energy storages i.e. batteries. Frequent rapid charging-discharging cycles cause battery overheating, which often reduces its charging rate capacity [27].

Therefore, hybridization offers a good solution. However, the combination of suitable power sources should be carefully decided based on available resources and energy demands, because the vehicle characteristics change drastically based on the power source. The downside of hybridization is the complexity of said systems. Sometimes very sophisticated control logics have to be implemented for optimal results, as the solution is not as simple as tuning an engine to run at its optimal region. Energy management strategies are constantly developed for multi-source vehicles, where most prevalent approaches are rule-based and optimization-based approaches [39].

Because the multi-source systems are complex, they take considerably more time and effort in development than conventional single-source vehicles. The power source characteristics are typically highly proportional to the environmental conditions and their dynamics can be hard to estimate or simulate. Thus, the main issue in the development process is in the model fidelity and therefore in the real-time implementation of the systems. The implementation of untested components can even be dangerous if limitations such as overcharge and temperature restrictions have not been considered properly. This is why the components should be tested thoroughly under various expected conditions before actual implementation. Power-HIL simulation has been used to configure power system components and control strategies in real-time before actual implementation in a real vehicle. [39]

Battery

For many EV applications battery power is still the most convenient solution. Lithium-ion batteries are widely used due to their long life, somewhat high power and high energy density and low self-discharge [40]. A battery pack consists of hundreds or even thousands of single battery cells, which are connected in both parallel and series to meet power and capacity requirements, determined in the initial component sizing process in the early development phase of the vehicle powertrain. For lithium-ion batteries, and for other types as well, a known limitation is the need for sophisticated strategies to protect the battery from electric and thermal abuse [41]. These control strategies are implemented with the use of a *Battery Management System* (BMS) in order to balance the cells. For each individual cell, BMS takes data such as SoC and temperature, while it also monitors and controls the battery pack current and voltage. SoC estimation is important part of BMS and can improve battery efficiency, lifetime and even the EV driving range [40, 41].

Even slight characteristic differences between the individual cells may result in uneven battery operation, where some cells may end up being overcharged. Thus, BMS development is clearly important for battery electric vehicles. These differences can be caused in manufacturing processes, further amplified by environmental variations, for example, in temperature. Therefore, BIL simulation is widely used in the automotive industry to test new sophisticated cell-balancing circuits and algorithms because of the difficult dynamic modeling of the cells [42].

HIL simulation can be employed on an actual battery or on hardware that emulates the battery dynamics using virtual battery models. In automotive applications, BIL is used to evaluate batteries, verify virtual battery models, validate BMSs as well as power and energy management strategies, or used as a part of a larger HIL simulation with other components. Barreras et al. [41] mentions multiple studies regarding each BIL application.

For development and verification of control strategies virtual battery models are sometimes used. In these, the controller is built physically and is verified by controlling a virtual model, much like with other controller verifications using HIL simulation. Other methods use simulators, which emulate the cell dynamics. The battery simulators usually are simplifications or downsized equivalents of the actual battery that the HIL system is addressing. For example, a simulated battery only has a small number of cells that are actually tested. This is because the charge/discharge loads are emulated with one bidirectional isolated power interface for each cell in series, which regulate the battery currents according to the test cycle and the virtual model of the cell dynamics. Pack-based battery modeling is more frequent than cell-based modeling in the literature. However, a complete validation of BMS strategy requires cell-based modeling, because proper charging/discharging control requires monitoring of pack voltage and current, but also voltages and temperatures at single cell level. Thus, cell-based HIL simulation is used in most cases only to validate BMS strategies or to test cell-balancing. Pack-based HIL simulation on the other hand is used to simulate more holistic strategies, such as power and energy management, HIL concept verification, electric powertrain evaluation and vehicle control unit testing. [41]

Lee et al. [42] devised a battery simulator for HIL testing of cell balancing circuits. The developed setup emulated voltages of four battery cells with current sourcing and sinking capabilities. The cell simulators require a parametrized model of a lithium-polymer cell by extracting parameters from real measurements. Once the cell models were implemented to the simulators, different load profiles could be simulated. The simulators were connected to a physical cell-balancing circuit, which was the DUT in the experiment. The proposed HIL platform overview is shown in figure 12. The HIL simulator and the battery model were verified with the same physical 4-cell lithium-polymer battery, from which the model parameters were extracted. The simulated and actual results using the developed cell-balancing circuit were close, verifying the HIL simulator to give representative estimates for cell-balancing circuit testing. The HIL simulator proved that significant time saving is possible when compared to testing with real battery modules. The preparation time itself for the real module was 14.6 hours, because the cells had to be preconditioned to have uneven balancing. Using the simulator, an operator was able to simply put the initial values into the system and run the simulation.

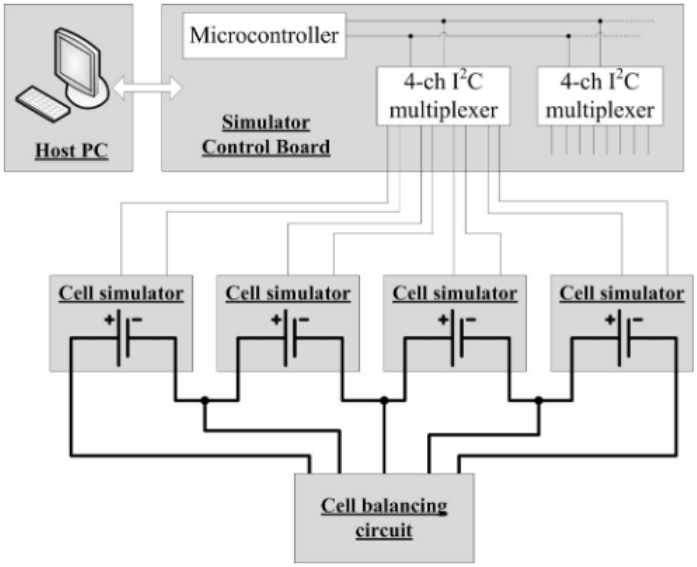

Figure 12. Schematic of the HIL platform for battery cell balancing circuit testing. The HIL system shares the same general elements as dynamometer-based HIL testing; a host computer, which initializes the test scenarios, a target machine, which runs the simulation (the microcontroller in the battery simulator), an emulator, which links the physical and virtual environments (dynamometer emulates torque loads while each battery simulator emulates voltages and currents of single battery cells) and a DUT(s). [42]

Along with cell balancing, other objectives of novel BMS strategies are validated using HIL, such as optimal current consumption of the BMS, as presented in [43]. According to the paper, typical BMSs draw currents in the region of several hundred milliamperes. A power consumption control strategy was developed to switch between different operating modes. The strategy was verified using a complete battery pack with the BMS control board involved as the physical DUT. Environmental conditioning was emulated using an environment chamber, which follows a temperature variation during a drive cycle. A power supply and an electronic load instrument were used to charge and discharge the battery according to the drive cycle power demand. The HIL simulation verified the power consumption control strategy, as positive results were gathered.

Fuel Cell

FCs are somewhat recently implemented technology in the automotive industry, but because of their potential they will probably eventually replace ICEs [4, 44, 45]. FCs are under extensive research because they provide an efficient, quiet and environmentally clean alternative for energy generation. However, their currently high cost is holding back implementation in masses. Other challenges, such as volume and safety concerns need to be fully addressed before implementation for transportation applications is viable.

FCs are based on a chemical reaction where oxygen and hydrogen react producing electricity and water as a byproduct [45]. The generated voltage of an individual fuel cell is only around 1 V (compared to lithium-ion cell voltage of approximately 3.7 V), and thus for an actual fuel cell power supply, the fuel cells need to be connected in series to be useful for practical applications [44].

Because of the high cost of a FC, a lot of research is made using modeled simulation. Zhao et al. [45] developed a 12 kW fuel cell model to test the proposed air supply compressor. Compressors are key elements in efficient operation of FC power supplies, since they are responsible for providing oxygen for the cells. A multi-physical FC model was built based on an actual fuel cell and added to a virtual vehicle model, which was used to validate the proposed compressor design in a HIL simulation. However, the model was built with reduced fidelity, because the research objective was deemed to be relevant without highly accurate modeling of the complex dynamics (for comparison, Gao et al. [19] studied HIL simulation with a high-fidelity FC model). The motor-compressor and a corresponding controller were built physically in combination with relevant sensors and actuators, which are used for oxygen supply control. The setup diagram is shown in figure 13. The HIL simulation validated the compressors performance, and the average power consumption was measured to be only 4.2 % of the FCs output power.

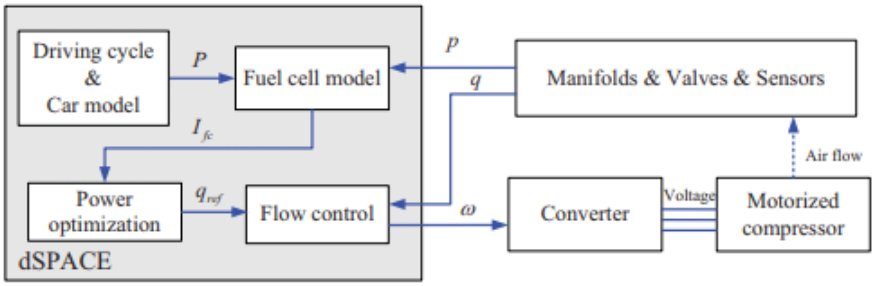

Figure 13. HIL setup diagram for FC air supply compressor validation [45]

Complete FC stacks are mostly used in HIL simulations of vehicle powertrains. Such HIL simulator was presented in [37], which was already discussed in this paper's section 2.2.1.

Lindahl et al. [44] proposes an alternative technique for FC development and testing. According to the paper, researchers typically test fuel cells using individual cells under emulated loads or use virtual FC stack models under realistic loads. The paper describes a technique of using a real FC as a reference cell, which is scaled up using the specific amplifier to emulate the performance of a full stack. Realistic loads can now be used with one-to-one correspondence to the amplified FC voltage and current. Some limitations are still persistent when using the technology, such as temperature differences of individual cells in a stack. However, it is noted that the amplifier-emulator concept can be expanded to take a small reference stack instead of reference cell. The proposed HIL testing technique makes it especially useful for studying system integration and control systems for load management, because it allows studying of real correlations between FC output and loads.

Ultracapacitor

An *Ultracapacitor* (UC), which is also known as a supercapacitor, is a type of an energy source, which is similar to a conventional capacitor, but offers much higher power and energy density and capacity. Its efficiency is better than that of a battery and it can provide large power peaks, which are ideal for vehicle applications where accelerations and decelerations at high power levels are frequent. According to [4], even 50 % ICE downsizing can be achieved when using UCs as another power source. However, environmental challenges, cost and charge leakage remain an issue for larger market penetration [27].

Even though UCs generally have higher energy capacities than conventional capacitors, on their own they are usually not enough for transportation applications. Thus, UCs are often combined with other power sources to create a hybrid powertrain. Perhaps most often battery-UC combinations are used. The battery provides high specific energy for the longer and more constant duty and drive cycles, while the UC provides high specific power at higher peak loads.

Battery-UC HEVs have been researched extensively and like for most other hybrid powertrains, HIL testing provides a fast and cost-effective way for research and development. Papers have implemented HIL xPC-target-based simulations with good results [16, 17] to validate the hybrid combination and power management control methods.

Hydraulics

For similar reasons as was mentioned with regards to ultracapacitors, hydraulic hybrid powertrains are emerging as a significant alternative to conventional powertrains, especially in heavy-vehicle industry [27]. Also, similarly, they offer high specific power density, which for hydraulic pump/motors can be an order of magnitude higher than that of an EM. For its power density and excellent round-trip efficiency, a hydraulic pressure accumulator providing power to the hydraulic actuators also seems like an attractive option over an electric battery. However, they have relatively low energy densities, making them impractical as the only power source because the accumulator size is often physically restricted in vehicles. On the positive side, hydraulic accumulators can take great advantage of regenerative braking. [46, 47] Table 1 shows a comparison between a typical hydraulic accumulator and a typical electric lithium-ion battery.

Table 1. Hydraulic accumulators versus electric batteries [47]

	Power density (kW/kg)	Energy density (kJ/kg)	Round-trip efficiency (%)
Hydraulic accumulator	5	4-11	94
Electric battery Li-ion	0.5	150	81

Filipi et al. [27] created a HIL simulation platform for power management control of an ICE-hydraulic hybrid propulsion of a heavy vehicle to maximize fuel economy and emission benefits. Figure 14 presents the developed HIL setup, which can be considered as an EIL simulation, because the ICE is the only physical component of the powertrain. The hydraulic system, including an accumulator and a hydraulic pump/motor were virtually modeled along with the rest of the vehicle dynamics, using physics-based Simulink models. The studied hydraulic hybrid topology was of a series hybrid type, where the ICE was only run at its optimal point to charge the hydraulic accumulator. The accumulator would then provide high pressure fluid flow to the hydraulic pump/motor, which then turns the wheels. Thus, in the EIL setup, an AC dynamometer would emulate loads that would result from the accumulator charging/discharging process.

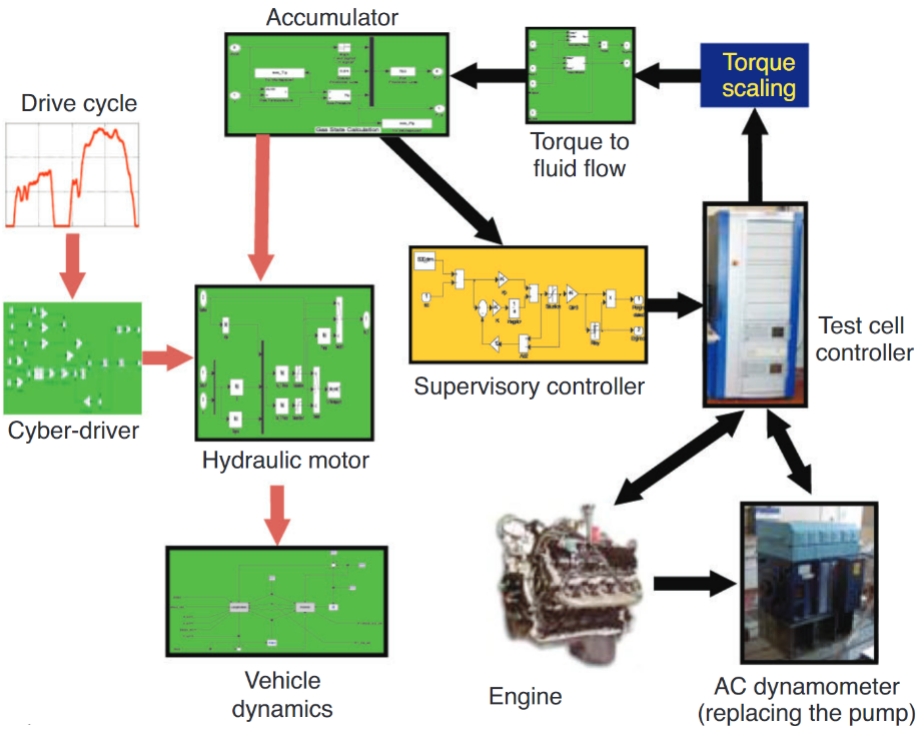

Figure 14. HIL setup diagram for hydraulic hybrid propulsion of a heavy vehicle [27]

2.2.3 HIL outside the automotive industry

This work focuses on the use of HIL simulation for HEV applications, but it is worth mentioning that HIL is used widely outside automotive industry as well. HIL market as a whole, including industries such as automotive, aerospace, marine, defense and power electronics, is increasing at a high rate due to shortened time to market and increasing design complexity of embedded systems. Back in 2014, HIL market was valued at USD 480.8 million and an overall growth rate of 9.37 % was estimated from 2015 to 2020, so that 2020 market value would be USD 826.7 million [48]. HIL simulation applications are e.g. development of safety systems, powertrain controllers, unmanned systems and defense systems. [10]

Non-commercially, HIL is also used in research and education sectors. According to [49], control engineering education requires laboratory exercises for the students to understand the theory and concepts of control at a deeper level. A low-cost HIL setup was built for students to design programmable logic controller data acquisition and control algorithms. Queiroz et al. [50] echoes the importance of proper education, focusing on students of industrial process control, saying that incomplete knowledge and practices learned in school translate to under-performing system design in the industry. Students require hands-on experience of their possible professions rather than solely relying on theoretical lectures. The need for low-cost and safe equipment is brought up, since the cost of using industrial level systems is often not feasible and may be too dangerous for education purposes. While HIL simulators in industry are already cost efficient, industry level data acquisition hardware and software can be quite expensive. For this reason, [50] presents a HIL platform based on free open source software. In [51], a HIL setup was designed for educational purposes in mechatronics and robotics. In it, a remote laboratory was built to educate robotic arm manipulation by using a physical

setup consisting of a controller and a 2-degree of freedom manipulator. The manipulator has a driving motor and a motor for emulating load torque on the joints.

In civil engineering field, HIL simulation is used for testing purposes on structures by combining a partial substructure and a simulated numerical model, since it is impractical or even impossible to test full scale structures. The idea is the same as in HIL, but terms like 'substructuring' or 'real-time hybrid testing' are more prevalent in this field [5]. Overview of real-time hybrid testing on a substructure is presented in [52]. The paper was also first to propose a compensation method for actuator delay, which is often involved with large scale substructure testing.

2.3 Test equipment

The hardware setup of HIL simulation can typically be divided into actuators, computer hardware and instrumentation. Computer hardware and instrumentation typically have some requirements and limitations, which have been discussed in earlier sections, but the actual testbed, and more importantly the emulator is basically only limited by the goals of the HIL simulation. There is no universal emulator, and it can consist of varying mechanical actuators or electrical devices, depending on what features need to be emulated on to the test specimen.

Commonly, force/motion relationship is researched for many applications. A variety of mechanical systems have been emulated with hydraulic actuators. For example, flight simulators typically use hydraulic actuation to introduce feel-force. Hydraulics can also be used to emulate loads on the test specimen, such as loads on a drive cylinder in an injection molding machine or loads experienced by rotating machinery. In motorsports high-speed hydraulic actuators are used in 4- or 7-post shaker rig configuration to emulate road and/or aerodynamic load effects on the vehicle, mainly for suspension tuning but also for lap simulation. [5]

As previously mentioned, HIL can be utilized for battery testing, and commonly the changes in battery voltage are emulated using an electronic load tester. The simulation determines the total electric load of the system on the battery, and according to that information the electronic load tester charges and discharges the battery. Usually the load tester also monitors the terminal voltage and the current drawn. [16]

For EIL simulation, by far the most common method is to use a dynamometer. However, real-time HIL simulation places requirements on the dynamometer properties so that the dynamometer can accurately emulate any loads it is meant to. Most importantly, the dynamometer needs to be able to follow speed and torque profiles with little error and delay. Also, in many applications the dynamometer should be able to change between positive and negative power, preferably as fast as possible. This property is necessary, for example, when simulating regenerative braking or downhill driving. In HEV applications, this enables specific studies of characteristics such as power flow in an electric DC bus. With that in mind, an EIL setup often should include the possibility to regenerate power into the supply line. Otherwise the generated power needs to be dumped to a resistive load where it is dissipated as heat energy. [38]

3 Testbed design

This chapter describes the process related to the design and implementation of the system to be used for HIL simulation. First, the main design requirements are set for both the hardware and the software. Second, the built system and its components are described along with the reasoning behind the design choices. Third, the verification of the system is described by creating a test plan to be used for confirming that the system performs as expected.

The testbed system architecture is a simple dynamometer EIL setup, which is similar to many other HIL environments presented in the literature, which were discussed in section 2. For better understanding of the designed system, a simple diagram of the system connections is shown in figure 15.

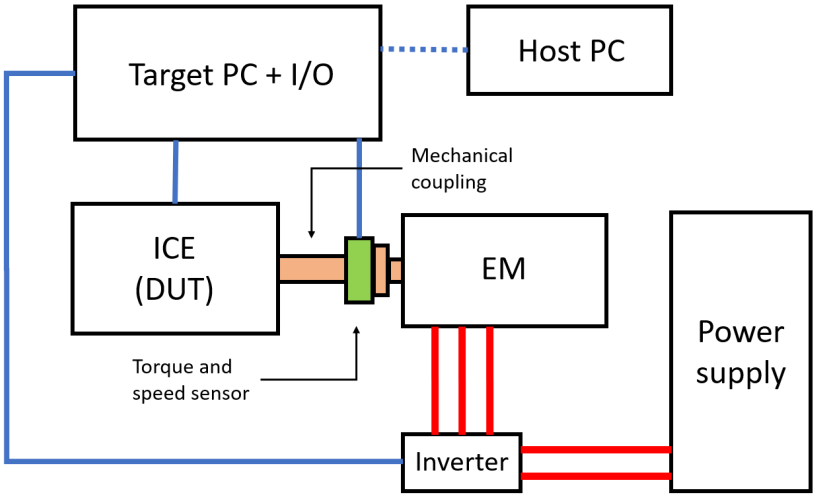

Figure 15. Simplified system layout of an engine dynamometer HIL testbed. Blue lines represent bidirectional data communication, dotted blue-line ethernet communication and red lines represent DC and AC electrical connections. The EM and the inverter together create the dynamometer system that emulates loads on the DUT.

3.1 Design requirements

The designed system will be used for applications such as engine emission testing, HIL-simulations and brake dust measurements. Generally, an engine dynamometer can be of many types, such as an eddy current based one, a hydraulic brake or a fan brake. However, brake dust measurement cannot be done with these kinds of dynamometers, which are solely based on power absorption. Rather, a reversed topology needs to be considered where a connecting shaft is rotated to emulate a vehicle's axle. All three applications can be achieved with an EM dynamometer. Therefore, the starting point for the system design and requirements is to build such a system.

One of the main requirements for the system is *for it to be easily transportable as one unit including all the main components*: a frame, an inverter, a motor, instrumentation and connections for power and cooling. Therefore, the frame base should be dimensioned so

that a common pallet truck can be used to move the whole system. This also sets weight requirements on the whole assembly. In turn, the system weight and size limit the power of the EM, but generally the dynamometer should be sized to be used for testing of typical non-road four-cylinder diesel engines. The cooling should be implemented with liquid cooling connections. Extra space and connections should be left available for future expansion of the system.

Additional aim of the testbed is to have a relatively low power consumption, although this will not be quantified or verified in this work. In practice, this could be achieved by energy recovery. Since the EM in the dynamometer works most of the time as a generator, it produces power. In many cases, this power is dissipated by a brake resistor, but by selecting the right components, it is possible to route this energy back into the DC bus, thus saving energy. However, the DC bus capacity may end up being quite small, and thus the energy recovery capability might not be of a practical use.

The design process was iterative, and requirements were added as the design evolved. First, the motor was selected, which then created further requirements for the inverter and the testbed frame.

3.1.1 Hardware requirements

The following section presents the requirements for the testbed hardware components individually. Detailed hardware requirements are not assessed for this work, as the final objective is not considered to be dependant of every detail. General requirement guidelines are put for the sake of reasoning the component choices. Table 2 presents the quantified hardware requirements, while the following subsections also discuss additional component requirements.

Motor

There are two main factors when it comes to choosing a motor. First off, the motor needs to follow given speed and torque profiles with minimal error and delay. Otherwise, the measured results are not valid. Secondly, the motor shall produce high torques quickly and change quickly between motoring and generating modes. This is important when it comes to simulating test cycles that present, for example, combined uphill and downhill driving. In addition, the power and torque produced by the motor must be close to those of the biggest engine to be tested. It is worth mentioning that in the initially planned test scenarios the motor will only rotate in one direction either as a load torque emulator or to emulate wheel rotation.

Inverter

A suitable inverter must meet the power demand of the motor and have high enough nominal voltage and current. The inverter unit should also be compact and have ports for liquid cooling. The inverter should have built-in speed and torque control of an EM, which communicates via a CAN protocol. Also, conversion from the motor/generator AC to common bus DC should be available to reduce overall power consumption of the testbed and to allow test measurements regarding energy recovery.

Table 2. Quantified hardware requirements for the eDyno testbed

Requirement	Subject	Variable	Value
Fits into predesignated test space	Testbed	H x (W) x D	< 2 000 x (1 500) x 1 000 mm
Can be moved with a pallet truck	Frame	Base slots	> 170 x 90 mm
	Testbed	Total mass	< 1 000 kg
		Width	< 1 000 mm
Meets the power demand of the typical applications	Motor	Power	> 150 kW
	Inverter		
Liquid cooling	Motor	Flow rate	20 l/min
	Inverter		10 l/min
Precise torque measurement for full torque range.	Torque sensor	Maximum torque	> 1 480 Nm
		Maximum speed	5 000 rpm
Real-time simulation and control	Analog high-speed input	Input voltage	0-10 V
		Input current	0/4-20 mA
		Number of channels	> 6 ch
		Sample rate	> 1 kHz
	Digital I/O	Number of channels	> 6 ch
		Sample rate	> 1 kHz
Normal analog I/O	Analog input	Voltage	0-10 V
		Current	0/4-20 mA
		Number of channels	16 ch
	Analog output	Voltage	0-10 V
		Number of channels	4 ch
Operation shutdown at safety threshold	On/Off relays	Number of channels	8 ch
Temperature measurement	Thermocouple	Thermocouple type	K
		Number of channels	16 ch
CAN bus protocol support	CAN	Protocol	SAE J-1939 or CANOpen
		Number of buses	2

Driveline

Test accuracy is somewhat dependent on the driveline design of the dynamometer. After a certain critical speed, the shaft will become unstable, resulting in torsional vibration, which makes the measurements inaccurate. Critical speed is dependent on shaft length, stiffness, weight and rotational speed. Therefore, the shaft should be kept as short, stiff and light as possible. [6]

Torque and rotational speed measurements should be taken directly from the shaft. Therefore, a recommended setup is to use a torque transducer directly mounted to the shaft. A transducer converts physical properties into physical signals. The transducer has to have a correct torque measurement range and compact size.

Design recommendations for torque sensor mounting and calibration are discussed in [53]. The paper also gives guidelines for shaft design to avoid measurement uncertainties. Such uncertainties may result, for example, from parasitic loads, i.e. off-axis loads. Regarding hardness and material decision, it is recommended to match the hardness's of the different driveline components as closely as possible. If an adapter piece is needed between the transducer and the shaft, some design principles should be followed: the material should be chosen so that the material strength of more than 900 N/mm^2 is achieved. The adapter should be dimensioned so that the flange thickness B is about twice the flange bolt diameter and the hub-to-flange diameter ratio should be $D_i/D_a < 0.6$, with the overall adapter length L of more than half of the flange diameter D_i. Figure 16 shows the general dimensioning of an adapter.

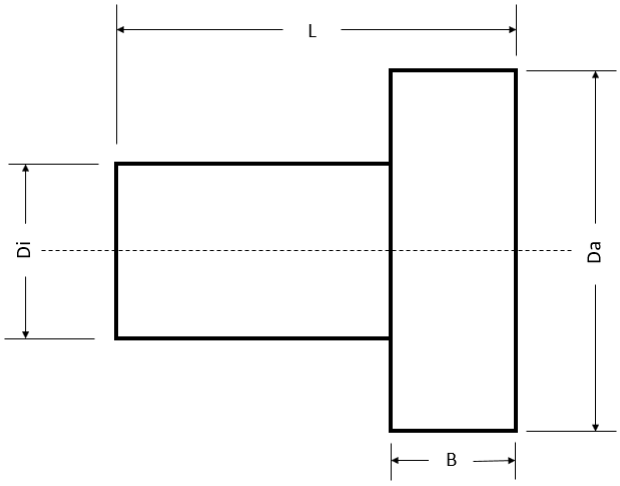

Figure 16. Flange adapter dimensions

Ideally, the torque sensor should be placed as close as possible to the dynamometer bearing so that it is holding most of the sensor weight, thus moving the critical speed further from the operating range. Parasitic extraneous loads need to be kept at minimum to prevent failures and measurement inaccuracies. [54]

The engine and the motor add vibrations on the connecting shaft when under load. In normal operation conditions, these should not have any noticeable impact on the measurements. However, if the vibration frequency gets close to the natural frequency of the system, the vibration is amplified. Figure 17 shows the effect of natural and operation frequency ratio on the displacement transmissibility. When the frequencies are equal, i.e. the ratio is one, the system is in resonance and has a high risk of a mechanical failure.

For the above reason, the stiffness and damping characteristics for the dynamometer shaft should be chosen so that the first resonant frequency is outside of the typical operating range of the engine [6, 57]. In some steady-state tests, it would be acceptable to have a low natural frequency below the operation points and transition quickly through the resonance point in the motor ramp-up phase. However, since the designed test system is required for transient engine testing, the driveline natural frequency should be above the maximum operational speed of the system. Damping of the driveline would reduce vibration excitation, but would compromise accurate torque transmissibility, which is often crucial for HIL.

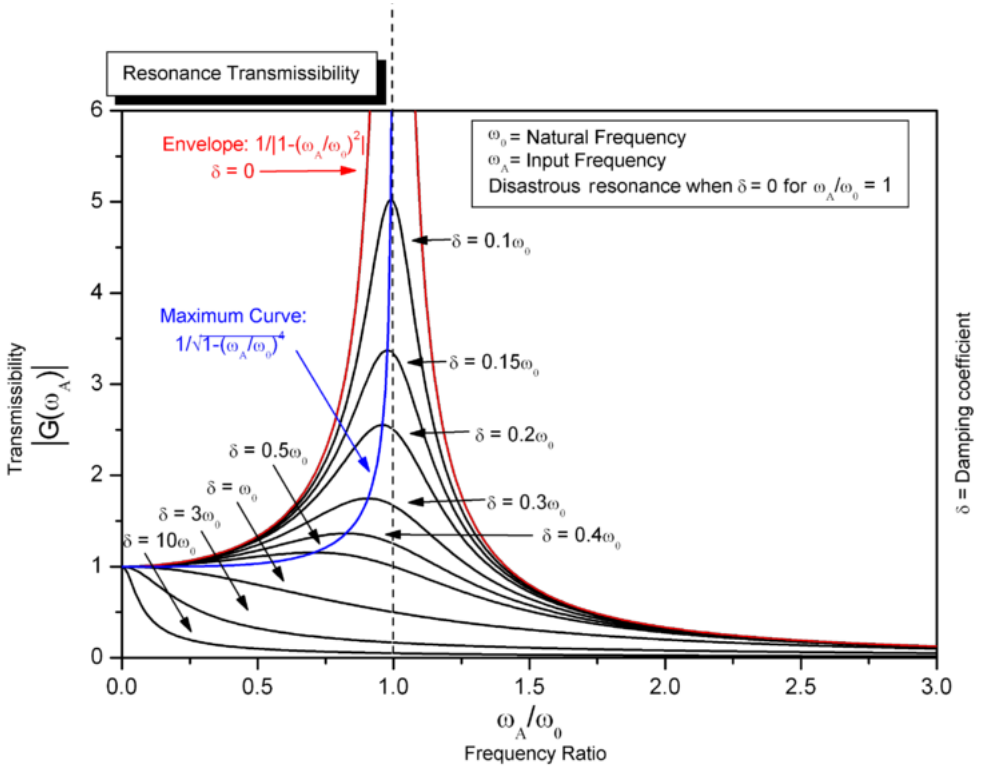

Figure 17. Effect of frequency ratio and dampening on transmissibility [55, 56]

Input/Output

Data collection and processing hardware have a few key requirements, which have to be met. First, the system has to be able to function in real-time. Therefore, high-speed I/O is required for some connections. Second, SAE J1939 standard [58] CAN buses are required for inverter control, and third, automatic safety switches are needed for safe operation, for example, in the case that torque or temperature limits are exceeded. The temperature should be measured with K-type thermocouples.

3.1.2 Software requirements

For engine applications, the system has to be controllable by uploading cycles of speed, torque and throttle profiles or a combination of those. In the simplest way, this could be done with an csv-file. The software must allow for different driving modes for the system. Both the engine and the dynamometer must be controllable using either a speed or a torque reference. A throttle position reference should also be used for the engine control. Dynamometer communication should be done by giving a CAN signal to the inverter. A 0-5 V analog signal would representing the throttle pedal position. Torque and speed measurements of the physical system should be measured for feedback control.

For HIL applications, a support for Simulink models has to be implemented so that the simulation is run in real-time with the physical system. The dynamometer and the engine should get their control inputs dynamically one time-step at a time from the simulation model rather than from premade profiles.

For the brake disk application, the dynamometer torque is predefined. Brake disc rotation

speed is also predefined so that during acceleration it is controlled by the inverter and during deceleration by the brake pedal position. Figure 18 shows the general idea between the connections for both engine (includes HIL) and brake dust applications.

In addition, there are few additional requirements set for the software. The software needs a possibility for setting safety thresholds to trigger relays to prevent unsafe system operation. Measurement related metadata should be automatically added to the results when data recording is enabled. The data should be exportable in excel compatible format. CAN bus configuration tool is also needed.

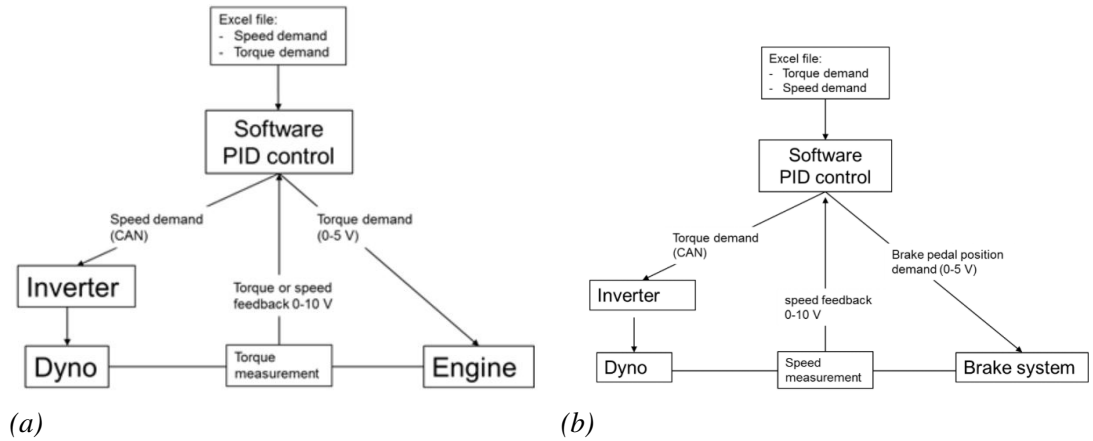

Figure 18. Dynamometer control schematics for engine (a) and for brake dust measurement applications (b)

3.1.3 Safety requirements

The safety requirements are selected according to national requirements, and to ensure a fail-safe real-time operation as defined in section 2.1.1. Fail-operational measures are not considered necessary, because an incorrect operation itself should not pose a significant risk.

In Finland, electrical equipment must fulfill safety requirements set in SFS 6000 standard series and machine safety standards SFS-EN-ISO 13849-1 and SFS-EN 60204-1:2006. The testbed will be designed and build to comply with the Finnish government decree 1434/2016: regulation of electrical installations. The regulation lists the essential safety requirements for electrical equipment. Below, a free translation and synopsis is presented of these requirements:

- Humans and pets must be protected from the dangers of touching or getting too close to live components. Protection must be achieved by preventing current flow through human or pet, or by reducing it to a harmless level. Usually this is achieved with touch prevention enclosure. If this is not feasible, the equipment must be positioned outside of reach. In research applications, other means are acceptable as long as outsiders are kept from accessing the equipment.
- Humans and pets must be protected from the dangers rising from equipment malfunction.

- The equipment structure must be so that there is no risk of ignition of flammable material due to high temperatures or electrical arc.
- The equipment must not cause danger of burns to humans or pets.
- Live wires with overcurrents must not cause such temperatures or faults that may cause dangers to humans or pets.
- Otherwise non-live conductors must not reach too high temperatures or cause mechanical danger in case of equipment malfunction.
- Safety equipment must work fast enough with such voltages and currents, which assure reasonable safety.
- Electrical safety system must be maintained operational and trustworthy throughout the lifetime of the equipment.
- Malfunction due to overvoltage must not cause danger to humans, pets or property.
- Voltage endurance and insulation of the equipment must meet the voltages present in the operational domain.
- The equipment must resist mechanical and environmental strains.
- The equipment must be assembled using component suitable for the intended use, and which fulfill the requirements set for them. The components must be installed using the manufacturer instructions.
- Personnel without proper electrical training must be able to operate the equipment as instructed without danger of touching live components.
- The equipment must be designed and positioned so that people unknown to its dangers are not able to touch live components.
- Possible exceptional dangers from connections to other special electrical equipment must be taken into account in design and safety.
- Equipment with exceptional dangers must be positioned in a space where the safety of such dangers has been taken into account.
- Electrical components must be compatible.
- The equipment must be such that the electrical and non-electrical components do not interact in a harmful way.
- The equipment structure must be so distinctive that no dangers arise from misunderstanding in operation or maintenance.
- The equipment must be equipped with safety markings and instructions, which clearly indicate its operation and maintenance. Safety equipment and conductors must be properly grouped and if necessary, labeled. Instruction regarding the assembly, operation and maintenance must be specified.

- The equipment structure must be such that all planned maintenance procedures can be done in a safe manner.
- The equipment must have enough breakers that separate components can be disconnected from the grid for maintenance or troubleshooting.
- Emergency electrical breaker must be installed so that it is easily and effectively accessible and usable.

Performance Level (PL) safety rating was derived according to safety standard SFS-EN-ISO 13849-1. PL is a simple way of assessing the risk of hazard of a machine by making assessment of the severity of resulting injury, frequency of exposure to a hazard and possibility of injury prevention. There are five possible results from *a* to *e*. In PL *a*, system control has a low impact on risk prevention and in PL *e* risk prevention is highly dependent on the system control. The assessment process is done by following a decision tree shown in figure 19.

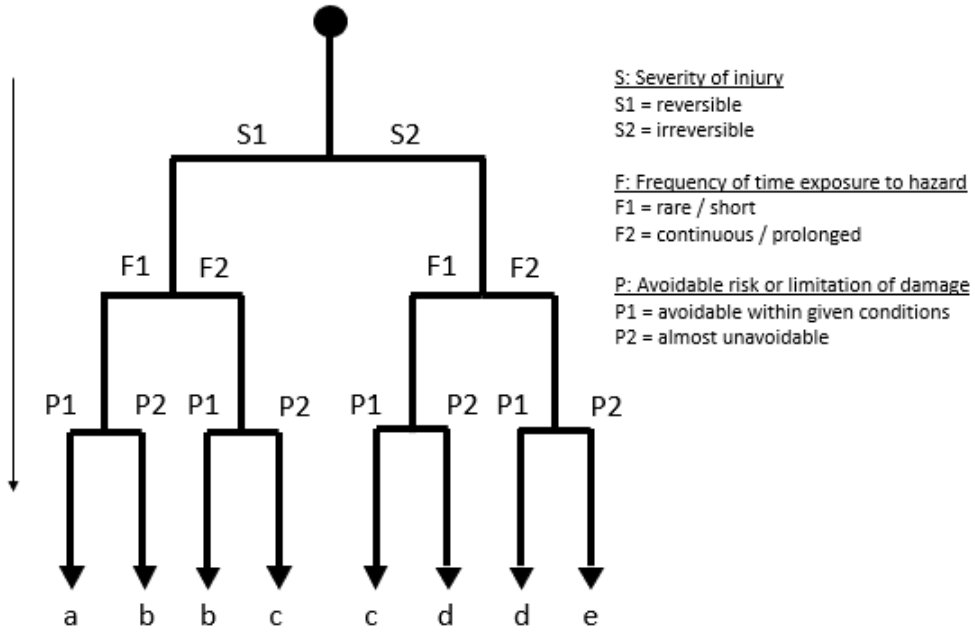

Figure 19. Performance level safety assessment rating

For the eDyno system, it was assessed that because of the high voltages and large rotating mass, the severity of injury may cause irreversible injury or even death, thus giving an S2 rating. At the time of writing, it is hard to estimate the frequency of testbed usage, but to be on the safe side, it is assumed that it will eventually be in nearly daily use, thus giving it an F2 rating. The system itself is quite simple and the electric and mechanical hazards are distinguishable, thus giving it a P1 rating. Following the tree, the resulting final safety assessment rating is PL *d*, meaning that proper measures have to be taken in ensuring safe operation.

3.2 Implementation

Given the requirements and the preselected components, the implementation was started with the design of the testbed frame. Concurrently, instrumentation hardware was selected, and the task for software development could be delegated to a third-party organization.

The design was carried out using Creo Parametric 3.0 computer-aided design software. 3D-models of all the manufacturable components were designed, and then 2D-drawings were made of those and sent to the manufacturers. The assembly and installation of the system was done inside VTT's own facilities. Also, the instrumentation wiring, power and cooling connections, and every other part of the physical implementation was carried out by respective professionals.

The system was installed inside a rather small laboratory room inside VTT's facilities. The room had two steel beam rails running across the floor, which were initially supposed to be removed. However, the removal of the rails was not considered necessary, and the system was installed on top of those, unlike the initial design suggested. Another large change to the overall test setup from the design requirements was the decision to leave the instrumentation cabinet separate from the testbed frame. The reason behind this decision is in ensuring a better resistance to electromagnetic interference coming from the high-voltage and high-current power lines running to the EM. Thus, the system is not transportable as one unit, as was initially required. Figures 20 and 21 show a Creo software rendering of the final eDyno design and the implementation at the facilities.

The rest of this section discusses and explains the design choices behind the main components of the testbed. Only the important dimensions and performance values are given as to generalize the system in this work. Appendix A presents a more thorough list of the used components. This section is divided to following subsections: frame, electric motor, inverter, coupling, cooling, power supply, safety measures, input/output connections and testbed operation.

Figure 20. Software rendering of the frame assembly

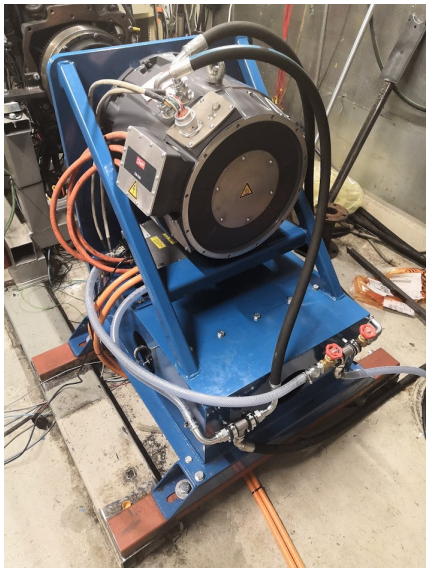

Figure 21. The eDyno testbed as it was at the end of this work

3.2.1 Frame

The frame was designed so that it can be constructed with easily available materials and tools. The design takes advantage of standard steel beam profiles and steel plates, which are water cut into their shapes. The frame is welded together with the exception of the bolted connections between the base plate and base beams. The motor, the inverter and the torque transducer are mounted with bolts for easy maintenance and assembly. Figure 22 shows the main assembly of the designed frame. The main body of the frame lies on a steel plate, which has bolted connections to the 100x100x10 mm thick base beams to provide additional possibilities for the testbed installation in different environments. By default, the base beams have large bolts, which are the primary installation connection to the laboratory floor. Bolted connections with oval-shaped bores are also used for the torque sensor mounting to allow accurate centering of the sensor, because fixed welding was considered to be too risky considering the small alignment tolerances for the torque and speed sensors.

Multiple iterations of the frame design were considered, but eventually it was decided that 6 mm steel plates would provide the best combination of light weight, structural stiffness and ease of manufacturing and assembly. The front plate was the only exception with a thickness of 20 mm. A thicker plate was needed to meet the requirement for the motor bolted connection penetration depth. A box-like structure with holesadded to the side plates was designed for the frame to allow routing of any wiring or piping, and to provide extra room for any future component extensions. Also, the frame length has some additional space for the same reason. The box structure also enables the inverter installation close to the motor so that the phase-cables can be as short as possible.

Even though the manufacturer specified motor mounting requirements were met using only the flange mounting connection, additional support was added to the back of the motor by welding a U-profile beam to the frame. This way the motor weight is supported more equally. After the final design was implemented, the testbed was further improved by bolting rib-like beams inside the box for increased torsional stiffness.

3.2.2 Electric Motor

The motor chosen for the eDyno application is a synchronous reluctance assisted permanent magnet motor by Danfoss, which essentially is a permanent magnet assisted synchronous reluctance motor. In both cases, reluctance torque and permanent magnet torque both significantly contribute to the total motor torque [59]. The motor model is EM-PMI375-T800-1900, and it has a high peak maximum torque of 1 480 Nm and a continuous torque and power of 933 Nm and 186 kW, respectively (at +40° C coolant temperature). For its advantages, the selected motor is said to have a compact and robust structure, which is able to produce high starting torques. The motor has high efficiency of 96% throughout its operation range. The maximum rotational speed of the motor is rather limited at 3 800 rpm but will be enough for most of the tested engines. For example, the validation tests will be done using an engine with a maximum speed of 2 250 rpm. The motor has relatively high moment of inertia at 0.63 kgm^2, which should be taken into account in dynamic HIL simulations for optimal results.

The motor is liquid cooled, which works well in the testing environment, where the inverter and the diesel engine are liquid cooled as well. The motor is of type IM 3001, which is classified in standard IEC 60034-7 [60] as a flange-mounted motor, with a large flange with

ITEM NO	PART NUMBER	QTY
30	ISO4032-M8-6	6
29	ISO4032-M20-6	4
28	ISO4032-M12-6	5
27	ISO4032-M10-10	12
26	ISO4032-M10-6	3
25	ISO4017-M8X25-8_8	6
24	ISO4017-M20X80-8_8	4
23	ISO4017-M12X30-8_8	5
22	EDYNO_TORQUE_SENSOR_SUPPORT	1
21	EDYNO_MOTOR_BACK_SUPPORT	1
20	EDYNO_INVERTER_SUPPORT_PLATE	1
19	EDYNO_FRONT_PLATE_SUPPORT_BEAM	2
18	EDYNO_FRONT_PLATE	1
17	EDYNO_FRAME_BOTTOM_RIGHT_SIDE	1
16	EDYNO_FRAME_BOTTOM_LEFT_SIDE	1
15	EDYNO_FRAME_BOTTOM	1
14	EDYNO_FRAME_BACK_PLATE	1
13	EDYNO_FLANGE_ADAPTER_ASSY	1
12	EDYNO_COUPLING_COVER	1
11	EDYNO_BASE_PLATE	1
10	EDYNO_BASE_BEAM	2
9	DINENISO7091-20	8
8	DINENISO7091-12	10
7	DINENISO7091-10	30
6	DINENISO7091-8	25
5	DIN912-M8X25-8_8	11
4	DIN912-M8X20-8_8	2
3	DIN912-M16X50-8_8	1
2	DIN912-M10X60-12_9	12
1	DIN912-M10X45-8_8	3

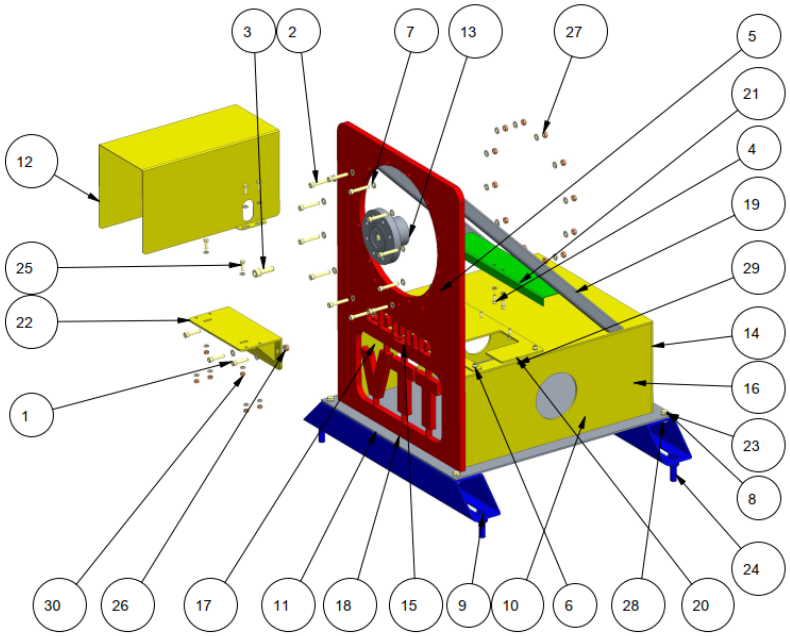

Figure 22. Main assembly of the testbed without the motor or the inverter

clearance fixing holes. In the same standard, motor D- and N-end are defined as (normally) the drive end and non-drive end of the motor, respectively. In our selected motor, the mounting flange is in the D-end of the motor and is of type SAE 3 according to standard SAE J617 [61]. For the testbed frame, a mounting flange was designed to meet the specified dimensions mentioned in this standard. Twelve DIN 912 M10 bolts were used for flange mounting.

3.2.3 Inverter

The selected inverter is also from Danfoss: EC-C1200-450, which is able to supply the motor with up to 300 kW of power at 500 VAC. The current is limited to 350 A. The inverter enclosure is compact and low weight and has good protection against electromagnetic interference.

The motor is supplied with a three-phase 500 V line-to-line voltage through the inverter. The electric power comes from 750 VDC power supply. For these power connections, cables were selected using table 3 from the standard IEC 60364-5-52 [62]. Manufacturer specified nominal current is 247 A, which translates to the selection of screened 70 mm^2 cables. This is also in line with the manufacturer recommendation.

Communication between the software and the inverter is by CANopen CAN-bus protocol. The inverter supports torque reference and speed reference motor control methods, which is important for the test applications. Speed control is capable of handling sample speeds of up to 1 000 Hz, which is more than enough for the intended purpose.

3.2.4 Coupling

For measurement of torque and angular velocity, a torque sensor is installed as part of the testbed. HBM T40B torque sensor was selected for its ease of installation and compact size. It is specifically designed for testbed purposes for measurements of static and dynamic torques

Table 3. Cross sectional area of current carrying conductors [62]

PVC insulation/Copper conductors
Conductor temperature: 70 °C/Reference ambient temperature: 30 °C

Nominal cross-sectional area of conductor mm²	Installation methods of table A.52-1						
	Multi-core cables		Single-core cables				
	Two loaded conductors	Three loaded conductors	Two loaded conductors touching	Three loaded conductors trefoil	Three loaded conductors, flat		
					Touching	Spaced	
						Horizontal	Vertical
							
	Method E	Method E	Method F	Method F	Method F	Method G	Method G
1	2	3	4	5	6	7	8
1,5	22	18,5	–	–	–	–	–
2,5	30	25	–	–	–	–	–
4	40	34	–	–	–	–	–
6	51	43	–	–	–	–	–
10	70	60	–	–	–	–	–
16	94	80	–	–	–	–	–
25	119	101	131	110	114	146	130
35	148	126	162	137	143	181	162
50	180	153	196	167	174	219	197
70	232	196	251	216	225	281	254
95	282	238	304	264	275	341	311
120	328	276	352	308	321	396	362
150	379	319	406	356	372	456	419
185	434	364	463	409	427	521	480
240	514	430	546	485	507	615	569
300	593	497	629	561	587	709	659
400	–	–	754	656	689	852	795
500	–	–	868	749	789	982	920
630	–	–	1 005	855	905	1 138	1 070

NOTE Circular conductors are assumed for sizes up to and including 16 mm². Values for larger sizes relate to shaped conductors and may safely be applied to circular conductors.

directly on stationary or rotating shafts. The selected model supports torque measurements up to 3 kNm, which is enough since the specified peak torque of the motor is only 1 480 Nm. In terms of linearity including hysteresis, the transducer has high accuracy of < 0.03 %. The torque sensor also has an added functionality of rotational speed measuring using a magnetic ring with a reference signal for absolute rotor position.

The torque sensor rotor and the motor shaft are incompatible as is. Therefore, a coupling between the motor shaft and the torque flange was designed according to dimensions and specifications presented in the user manuals of the components. The motor has a DIN 5480 type spline shaft with dimensions of W50x2x24x8f, where W50 stands for external spline with reference diameter of 50 mm (reference diameter is not minimum or maximum diameter in DIN 5480), 2 is the size of the tooth, 24 is the number of teeth and 8f is the tolerance class.

There are many types of installation methods for a shaft positioned torque sensor, but since the selected sensor is of a floating type, a placement shown in figure 23 is used, as recommended in [53, 54]. Similar to the picture, the eDyno sits two centimeters lower than the engine under test, a characteristic often used with flexible shaft connections.

The eDyno side connection is rigid. Suitable off-the-shelf adapters between torque sensor and the motor were not found, so one had to be designed and manufactured. Figure 24 shows

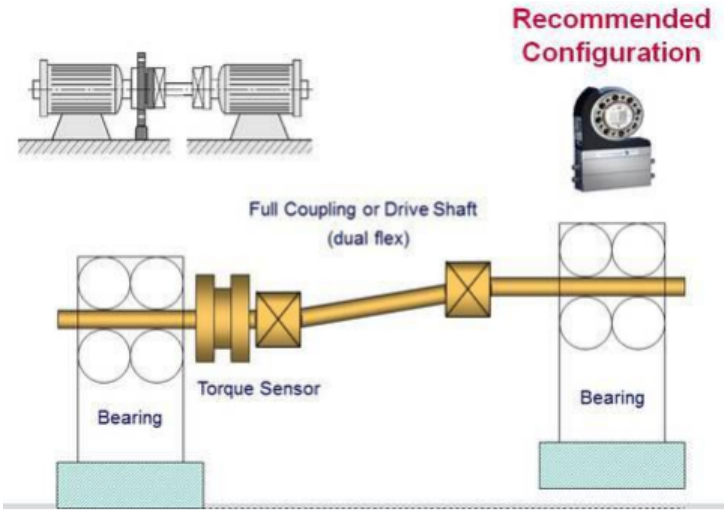

Figure 23. Torque sensor placement in the test setup [54]

the designed flange adapter assembly. To keep the motor-side connection rigid, the adapter flange was designed with a centering collar on the connecting surface, and an additional piece was welded to the flange to secure the assembly longitudinally to the motor shaft. The reason behind welding the two separate parts, rather than making one piece with the same features, was to reduce manufacturing cost. The motor shaft has DIN 332 compliant bore, which is used to screw the piece in place. An M16 screw was used and tightened to 300 Nm. The flange adapter hub has internal spline at the size of N50x2x24x9H, as was suggested by the motor manufacturer. The dimensioning of the adapter was done according to the literature guidelines, and the material was chosen to meet the strength requirements. The flange adapter is made out of 42CrMo4 (typical tensile strength of 900-1 200 N/mm^2) with the hub teeth induction hardened to 50-55 HRC. The hardness is a bit higher than recommended, as the torque sensor rotor hardness is around 46 HRC and the motor shaft hardness is 40-42 HRC. Eventually, this could cause grinding of the motor shaft teeth, but the effect was considered to be minimal as long as the shaft alignment is good.

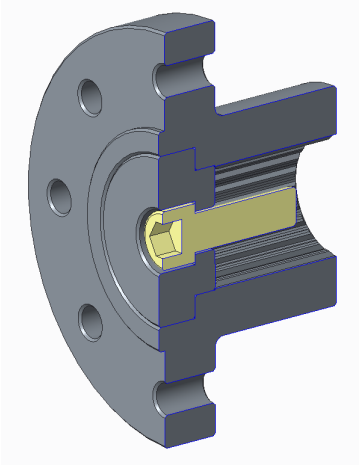

Figure 24. Initial design of the flange adapter between the motor shaft and the torque flange

During initial runs with only the motor running under no-load conditions, slight vibrations were detected with the adapter flange. It was determined that the motor manufacturer specified

fit between the shaft and the hub was too large for the application. To fix the issue, a sleeve was machined and fitted between the flange adapter and the motor shaft. The hole in the adapter piece also needed to be enlarged a little to make space for the sleeve.

The machining tolerances were carefully selected so that an interference fit would be achieved between the sleeve outer side and the adapter hole. For the 55 mm nominal diameter of the enlarged adapter hole, the fit was dimensioned as s6H7. The sleeve was first installed into the adapter assembly by thermal expansion/contraction, after which the sleeve's inner side could be machined to achieve a transition fit between the sleeve and the motor shaft so that the assembly can be removed if necessary without breaking. For the 45 mm nominal diameter of the motor shaft, the fit was dimensioned as g6M7

Machining the shaft-side of the sleeve while having it already assembled to the adapter ensured accurate centering of the entire flange adapter assembly and the motor shaft. Figure 25 shows the final components of the adapter assembly.

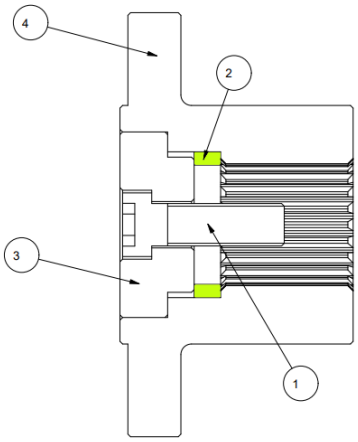

ITEM NO	PART NUMBER	QTY
4	FLANGE ADAPTER	1
3	LONGITUDINAL SECUREMENT PIECE	1
2	SLEEVE	1
1	DIN912 M16 BOLT	1

Figure 25. Updated design of the flange adapter between motor shaft and the torque flange with the sleeve highlighted

The natural frequency f_0 of the designed driveline could be calculated using equation 1. However, most of the inertias in the system are not known, and their measurement was not considered practical at this state of the project. With rough estimates, the resonance frequency should be high above the operational bandwidth. The actual vibration dynamics of the system are probably considerably lower, due to the use of a rubber clutch on the engine side. This dampening effect may result in the resonance getting inside the operation bandwidth, but due to the clutch's high damping, any vibrations should be smoothed out. However, the use of a rubber clutch is not optimal in terms of torque transmissibility, and it remains to be seen if the coupling assembly has to be changed for any tests with faster dynamic transitions.

The possible problems stated earlier in section 3.1.1 are noted, which is why the engine is connected to the torque sensor via a cardan shaft, which absorbs the extraneous loads resulting from any misalignment. The shaft is kept as short as possible to mitigate the complications from resonance vibrations and to increase torque transmissibility. The main reason for using a cardan shaft over a jaw-type flexible link shaft, is the ease of installation, because the tested engines might need to be swapped regularly. With cardan shafts, true axial alignment is not

required, and only parallel alignment is required. While jaw-type couplings offer protection from hardware failures in case of overtorque, cardan shafts have proved to be reliable for VTT. Just in case, the maximum torque rating of the cardan shaft is doubled to the maximum torque of the eDyno.

$$f_0 = \frac{1}{2\pi} \cdot \sqrt{C_\mathrm{T} \cdot (\frac{1}{J_1} + \frac{1}{J_2})} \tag{1}$$

where f_0 is the driveline natural frequency [Hz]
C_T is the torsional stiffness of the torque transducer [Nm/rad]
J_1 is the inertia of the left side connected to the transducer [kgm^2]
J_2 is the inertia of the right side connected to the transducer [kgm^2]

3.2.5 Cooling

Closed-circuit cooling infrastructure was already existing in the laboratory, including piping, reservoirs, heat exchangers and pumps. However, the capacity of the closed-circuit might have not been enough for the engine and the eDyno, which lead to the decision of taking cooling from the open-circuit water grid. This is not optimal and will be a temporary solution until the closed-circuit can be properly configured. The closed-circuit cooling would require more time for setup, as flows and temperatures would need proper monitoring. Ethylene glycol is recommended as cooling liquid but plain water is also viable.

In the open-circuit solution, the cooling input is split at the back of the frame into two separate loops for the motor and the inverter, respectively. The outflows meet again into a single line, which is directed straight into the laboratory drainage. Manual valves are used as placeholders to control the flow to meet the component specific cooling requirements. The valves are placed after the outports.

3.2.6 Power supply

The eDyno is powered by AVL BTS-BT-BS/320 combined battery tester and simulator. It is designed to be used especially in laboratories to supply DC voltage to electrical components such as EM/inverter systems. The benefits of using the battery simulator over a typical DC power supply is its programmability to emulate a vehicle battery system. This means that rather than supplying a constant DC voltage, the battery simulator can be made to behave like a real battery pack, i.e. voltage drop during a load step. This is good for future HEV powertrain HIL simulations where the physical part is extended to include an inverter or other electrical devices directly attached to the vehicle's battery pack. The system use as a tester is able to monitor energy storage systems connected in HIL. It also allows for BMS control strategy development. The AVL system supports direct integration of Simulink battery models without further hardware introduction. The BTS-BT-BS/320 is able to supply nominal voltage of up to 800 VDC, nominal current up to +/-600 A with nominal output power of 320 kW. This is well enough for the eDyno testbed.

3.2.7 Safety measures

At the time of finishing this thesis, the full safety measures are not yet realized, as the core operational performance was considered the main goal due to time constraints. However, only the personnel aware of the status of the testbed are allowed to work with it during this implementation period to enforce a safe operation of the unfinished system. Currently, there are shutdown switches on the test engine and on the instrumentation cabinet. If the instrumentation switch is turned off, the inverter will stop working as well. The ECU used for the test engine also has a stop button, which shuts the engine off.

Shutdown of the test system is implemented software-wise by allowing the user to set soft and hard limits for the system speed, torque, temperatures and pressures. If these thresholds are exceeded, the user interface will show an error and the system is automatically run into a safe operating state. The motor and the inverter on the eDyno already have manufacturer specified safety measures for temperature, short circuit, high-voltage interlock, overcurrent and overvoltage. Overcurrent and overvoltage are both implemented as hardware trips as well as programmable software trips. Also, the connection between the host and the target PC is automatically monitored continuously. If the connection is lost, the system is run down to a safe state.

Installation of a manual emergency shutdown switch/button is currently unfinished, but eventually one will be added next to the testbed and one in the control room, as was listed in the safety requirements. Also, after successful deployment of the system, either a full enclosure or shutdown door-switches will be installed to prevent anyone from getting close to the system as it is running and can be dangerous. The room, in which the system will first be installed, has two doors, which could both be triggered for emergency shutdown if the room is accessed when a test is running. Also, a traffic light system is recommended to be installed outside the room to let people know whether the room is safe to enter. However, these are likely to be installed only after the test system is validated.

The coupling between the eDyno and the engine is considered as the most mechanically dangerous component in the test system due to its high speed and high torque. The coupling is covered with 2 mm sheet metal cover from the sides and above to prevent unintentional contact to the shaft or from flying projectiles from a mechanical failure.

3.2.8 Input/Output connections

National Instruments hardware was selected for data connections. In the heart of the testbed system is a CompactRIO real-time processor, which is designed for distributed measurements, deterministic control and reliable monitoring. It runs a Linux-based operating system that allows real-time processing and user-accessible FPGA. The system specifications are presented in table 4. CompactRIO can be easily expanded with any combination of supported I/O-modules and can be extended with additional module boards using ethernet connection. The system is connected to the end-user's host computer via ethernet. A simplified schematic of the instrumentation is shown in appendix B. It is representative of the state of the initial tests, and thus some of the data signals to the I/O-modules are not drawn.

Table 4. Target machine specifications used in the eDyno

cRIO-9045	
System type	NI Linux Real-Time (64-bit)
Processor	Intel Atom E3930
CPU clock-rate (GHz)	1.3-1.8
Physical memory (Gb)	2

For low-speed analog input signals a module was chosen, which has eight input channels for both voltage and current measurement. For high-speed requirements, 100 kS/s/ch analog voltage input and output modules and a 100 ns bidirectional digital I/O-module were selected. A flexible data-rate, high-speed 1 Mb/s CAN bus module is used to send commands to the inverter. The hardware also involves two 16-channel thermocouple modules for temperature measurements and a solid-state field-effect transistor relay module for triggering the safety features. The high-speed modules are placed in the CompactRIO platform and the less critical low-speed modules are placed in the expansion platform.

The analog signals are conditioned using galvanic isolators. They are used to protect the signals from harmful effects, such as ground loop or motor noise. Galvanic isolation electrically and physically separates the input and output circuits. Rather, the information is passed through, for example, optically or via induction, as would be the case with common transformers. The isolators used in the testbed instrumentation use optical elements to transmit signals.

The velocity sensor uses a rotational encoder to create two differential frequency signals with a 90-degree phase difference. The order of the phases gives the direction of rotation, and the frequency gives the speed. This frequency signal is transmitted through a pulse signal converter into a voltage signal that can then be read at the target machine. For the torque measurement, a voltage between -10 V and +10 V linearly represents the torque. Zero torque is given as zero volts and positive rated torque as +10 V.

Only after the coupling between the motor and the torque sensor had been manufactured, was it noticed that the torque sensor would be installed "backwards" considering that the rotational sensor had a marked positive direction of rotation. Even though the coupling flange adapter could have easily been modified at this stage, it was easier to take the rotation direction into account inside the software by just taking the opposite of the measurement.

3.2.9 Testbed operation

A software was developed by a third-party company, which provides an intuitive user interface for the testbed operation. From the interface the operator can select recipes, i.e. test profiles, from premade test files or by loading a HIL simulation. The interface has tunable controllers, which are used for non-HIL testing, so that the engine and the eDyno follow the reference profiles. Soft and hard operation limits can be configured using a separate text file, which the software then reads. Multiple channels and digital displays can be monitored simultaneously, and the measured data can be stored in a database. The software is built upon NI LabVIEW. Additionally, the AVL battery simulator has its own software, which needs to be used to power up the electrical systems.

For HIL simulation, the ICE in the simulation model will be replaced with inport and outport blocks, after which it will be compiled to a NI Linux Real-Time target compatible format. This needs to be done separately with a computer that has the required programs and drivers installed. A LabVIEW file then imports the model and initializes the simulation parameters. It is also important to synchronize the model and LabVIEW real-time clocks to prevent problems from uneven sampling. LabVIEW is then responsible for the bidirectional communication with the physical hardware and execution of the fixed time-step iteration of the virtual model. Signal probes inside the Simulink model are ported to LabVIEW where these signals can be stored to a file for later examination. Physical measurement signals are also saved.

During testing, the state of the eDyno and the engine being tested can be constantly monitored and recorded using the user interface. The engine also has its own ECU software, which can be used to monitor engine data, such as pressures and fuel-mix-ratios. Importantly, the ECU software can override the other software settings, for example, to shut down the engine, adding redundancy to the operational safety of the system.

3.3 Testbed verification

Before the testbed can be taken into daily use, it has to be verified to be working properly. At this point, the system is verified using the layout shown earlier in figure 15. The eDyno's HIL capability can only be verified once the main function of the testbed is assessed as an engine dynamometer. The DUT is a non-road four-cylinder diesel engine by AGCO. The engine has a maximum power of 94 kW, with a maximum torque and speed of 551 Nm and 2 250 rpm, respectively. The goal is to run the engine according to a defined speed-torque cycle. The eDyno adds a resistive load to the engine, emulating loads from real-world driving operation.

The setup is tested gradually, starting from ensuring that the fundamental connections are working. The connection verification starts by building a network connection from the host PC to the target machine via software. Then it is checked that the instrumentation hardware and the designed software show matching connection ports and that their signal types have been correctly configured. Step-by-step, new functionalities are brought into the mix. This ensures the safest implementation of the system.

During the implementation, there are two main focuses: validation of the operational correctness and validation of the safety systems. However, validation of the safety systems is left out in this work, because not all the relay connections were installed. During the implementation and operational verification tests, pre-existing safety measures on the motor and the inverter should be enough to ensure safety when combined with extra caution and knowledge of the operator. After operational performance has been verified, safety systems and functions should be tested to ensure fail-safe operation of the eDyno. A following plan is suggested for the finished testbed:

- Emergency shutdown: each manual and software emergency stop cuts all power to the system and stops the engine immediately
- High coolant temperature: warning message on the user interface. Safe shutdown of the motor and the inverter, and prevention of running a test when the alert is on.
- High engine temperature: warning message on the user interface. Safe shutdown of the

motor, the inverter and the engine. Prevention of running a test when the alert is on.

- High engine pressure: warning message on the user interface. Safe shutdown of the motor, the inverter and the engine. Prevention of running a test when the alert is on.
- Overvoltage: warning message on the user interface. Safe shutdown of the motor and the inverter
- Overcurrent: Safe shutdown of the motor and the inverter
- Overtorque: Safe shutdown of the motor and the inverter
- Overspeed: Safe shutdown of the motor and the inverter

The verification of the operational correctness is a multi-stage process, which involves measurements of simple steady-state points, and finally transient operation in large range is tested. The correctness is verified by comparing test input signals to measurement values from the torque-speed sensor. One test cycle is run for steady-state operation, and its correctness is verified by cross-referencing the measurements to previously completed measurements of the same engine run under a different, verified, engine dynamometer. The standard transient test uses validation tools to define whether the test was successful. If both the steady-state and the transient tests can be considered successful, the eDyno's operational correctness is considered valid. The list below explains the different stages of the different test scenarios in the verification process:

- eDyno open-loop speed command, engine not connected
- Engine control test, eDyno not connected: The engine should have a working ECU, which is used to test the correct engine behavior
- Engine open-loop speed command, no added load
- Engine open-loop speed command, under load
- eDyno open-loop speed command, engine open-loop torque command, varying test points
- eDyno open-loop torque command, engine open-loop speed command, varying test points
- Engine closed-loop speed command, eDyno connected, no added load
- Engine closed-loop speed command, under load
- eDyno closed-loop speed command, engine closed-loop torque command, varying test points
- eDyno closed-loop torque command, engine closed-loop speed command, varying test points

- ISO 8178 C1, closed-loop eDyno speed command and engine torque command, no emission measurements: The ISO 8178 is an international standard for measuring non-road engine exhaust emissions. The collection includes several steady-state engine dynamometer test cycles, from which C1 cycle is used. The cycle goes through several steady-state setpoints with different weighing factors. Table 5 shows the setpoints for the 8-mode C1 test. In the table, engine torque is expressed as a percentage of the maximum available torque for the respective engine speed. Rated speed is the manufacturer specified speed, at which the rated engine power is specified. Intermediate speed is the speed, at which the engine's maximum torque is available. The interest in this test is only on the eDyno's ability to track the transient reference profiles, and thus the standard is only followed where appropriate.
- *Non-road Transient Cycle* (NRTC), closed-loop eDyno speed command and engine torque command, no emission measurements: The test cycle is developed for non-road diesel engine emission type-approval. It is used internationally and is part of multiple standards for non-road engines. Figures 26 and 27 show the normalized speed and torque profiles of the test cycle. The actual reference values are determined according to the equations and conditions presented in the regulation (EU) 2016/1628 annex VI [63]. However, the interest in this test is only on the eDyno's ability to track transient reference profiles, and thus the regulation is only followed where appropriate.

Table 5. Weighing factors to determine the setpoints for ISO 8178 C1 8-mode steady-state test cycle.

Mode number	1	2	3	4	5	6	7	8
Torque, %	100	75	50	10	100	75	50	0
Speed	Rated speed				Intermediate speed			Idle
Weighing factors	0.15	0.15	0.15	0.10	0.10	0.10	0.10	0.15

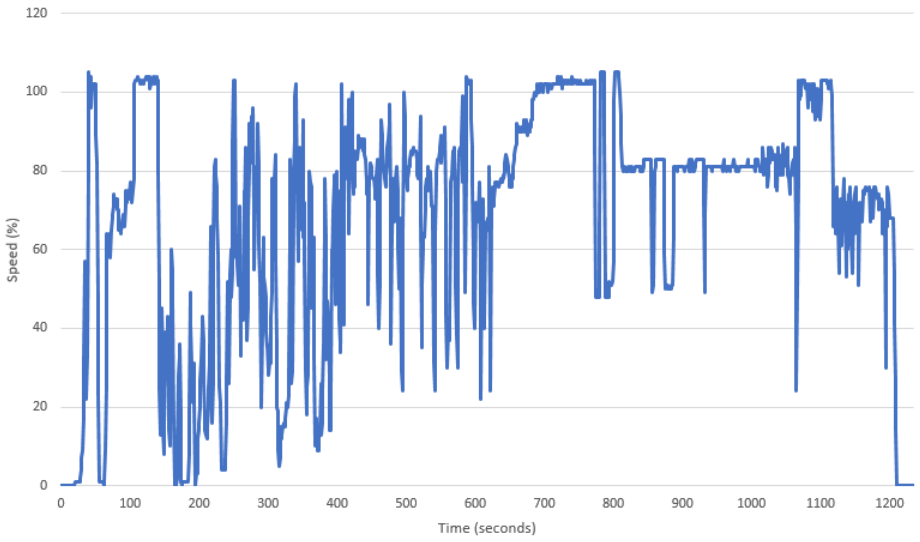

Figure 26. Normalized speed profile of the NRTC test cycle

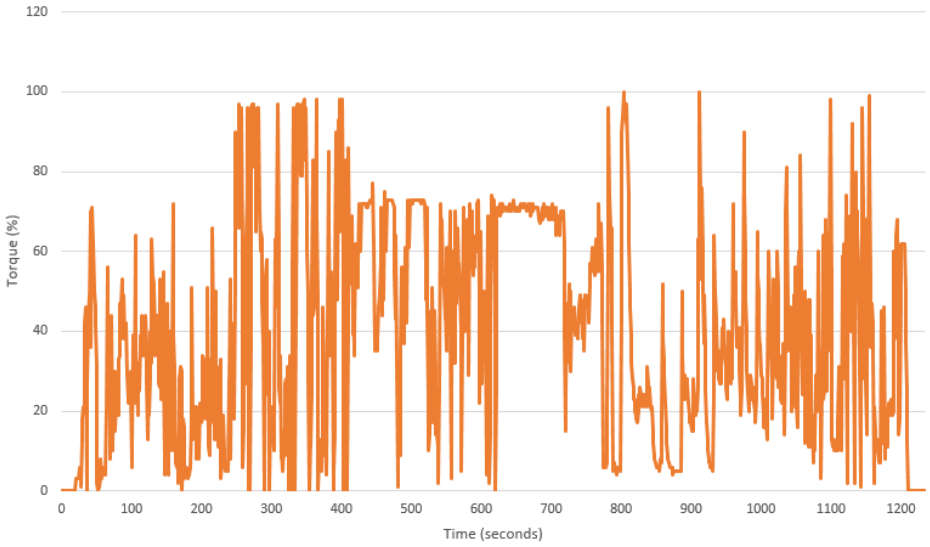

Figure 27. Normalized torque profile of the NRTC test cycle

4 Preparation for the HIL simulation

Part of the verification process of the designed testbed is to carry out a HIL simulation. For this reason, a simulation model is prepared. In addition, the model is validated to compile to a proper format for HIL simulation.

In the verification HIL simulation, only a diesel engine is used as the physical DUT, and thus the test setup could be verified with a simple model e.g. a conventional vehicle with simplified dynamics. However, since HEV applications are of a high interest for the testbed use, a series-parallel HEV model is built. The model is going to be a proof-of-concept, and thus many assumptions and generalizations are made during the modeling process. Still, the simulation model is going to require much more processing power than a simplified conventional vehicle model because of the added electrical components and the use of multiple controllers. The benefit of using an intensive model is to verify the calculation and tracking capabilities of the eDyno system for its intended purposes.

First, the modeling process of the vehicle is presented. Second, the test cycle is defined. Third, the simulation implementation to the eDyno platform is described.

4.1 Vehicle model

In his thesis, Echter [64] extensively studies the hydraulic work circuits of RCVs. According to the thesis, RCVs are currently undergoing a change towards greener operation, where powertrain hybridization is a key enabler. Reference vehicles in [65] only have conventional diesel engines, but as [65] and [66] show, the average power during operation is low at around 20 percent of the maximum engine power available. Thus, the ICE is not running in its efficient region. Therefore, powertrain hybridization is well suited for RCVs. VTT also has interest in the research of hybrid RCVs, which is why one is modeled for the purpose of this work.

This section describes the HIL simulation model by explaining the design choices, parameters and Simulink implementation for the overall vehicle model, engine model, traction motor model, power split device model, generator model, hydraulic circuit model and for the other supplementary model components.

4.1.1 Overall model architecture

The hybridized simulation model has a downsized ICE in combination with an EM. Literature [35, 66] typically suggests series hybrid or hydraulic hybrid powertrain topologies, but it was decided that a series-parallel topology would be used for this HIL simulation, since it results in more varying operating points for the ICE, better showing the capabilities of the designed testbed. The suggested powertrain topology is presented in figure 28.

The model is of a series-parallel hybrid RCV, with both ICE and EM providing traction. The traction motor is powered by a battery, which is charged by a generator or by motor regenerative braking. The generator is run by the ICE. A speed coupling in the form of a planetary gear is used to enable battery charging independent of the vehicle speed. An RCV also needs a method for waste collection and compression. For this, a hydraulic work circuit

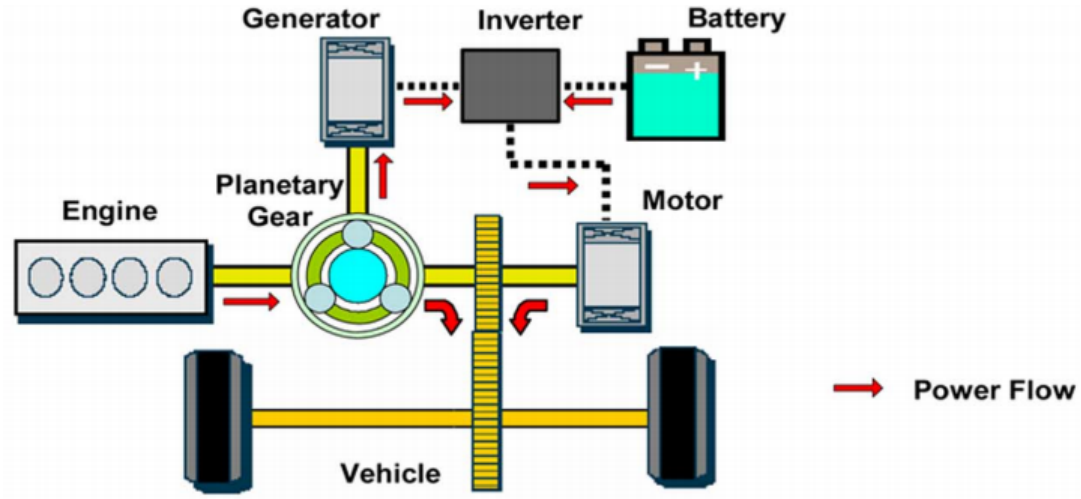

Figure 28. Typical series-parallel (power-split) HEV configuration [67]

is modeled. The pressure for the hydraulics is provided by another electric motor running a fixed displacement pump.

The modeling software used is Simulink. The model is constructed based on a ready-available series-parallel HEV model by Mathworks [68]. The model is further modified to suit the purpose of the simulation. The biggest modifications were done by adding a hydraulic work circuit to the template model. Additionally, the simulation control logic had to be updated, continuous blocks and subgroups were configured to support purely discrete simulation, the model parameters were almost completely re-done and the controller values were tuned. The causalities in the model caused many problems in controller tuning. For example, tuning of the traction motor controller would easily cause the DC bus voltage to oscillate in a way that would stop the simulation.

The overall simulation model architecture is shown in figure 29. The left-hand side of the model contains all of the control logic, which are described in section 4.1.2. The top side of the model has the hydraulic body ancillaries and the pump motor, which is connected to the DC bus. Rest of the model is arranged to match the positioning in figure 28. The Internal Combustion Engine block either has the virtually modeled engine or the inports and outports for the physical testbed integration.

The model is built as a forward-facing model following the reasoning in section 2.1.5. The forward-facing model also better tests the computation capabilities of the test setup than a backward-facing model, since it typically uses much more complex models, such as dynamical equations rather than lookup tables or state-space representations. Figure 30 shows the simplified longitudinal dynamics of a vehicle. Based on the forces acting on the vehicle, equations 2-4 derive the total power of the vehicle.

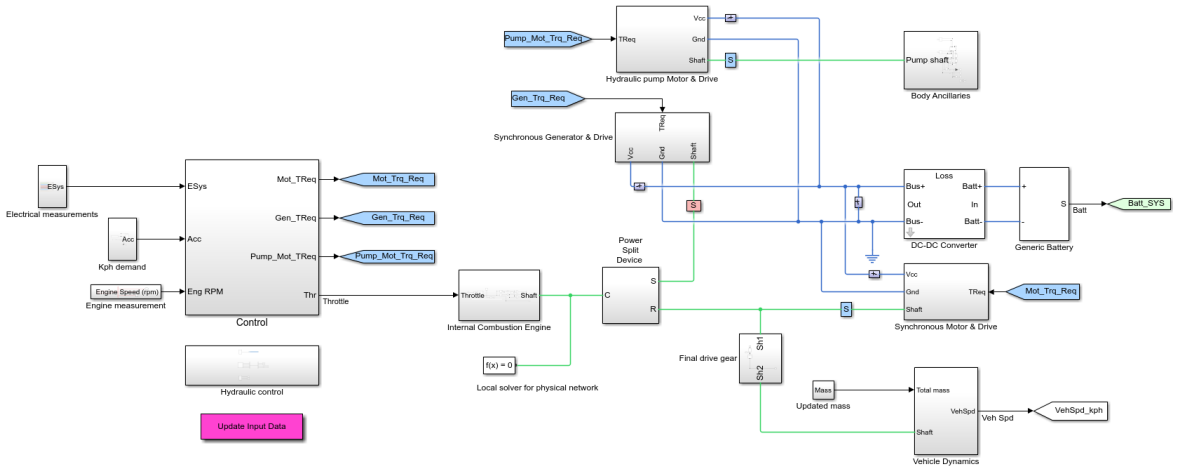

Figure 29. Overview of the designed hybrid RCV Simulink model. Blue lines create the electrical network, and green signals the physical network.

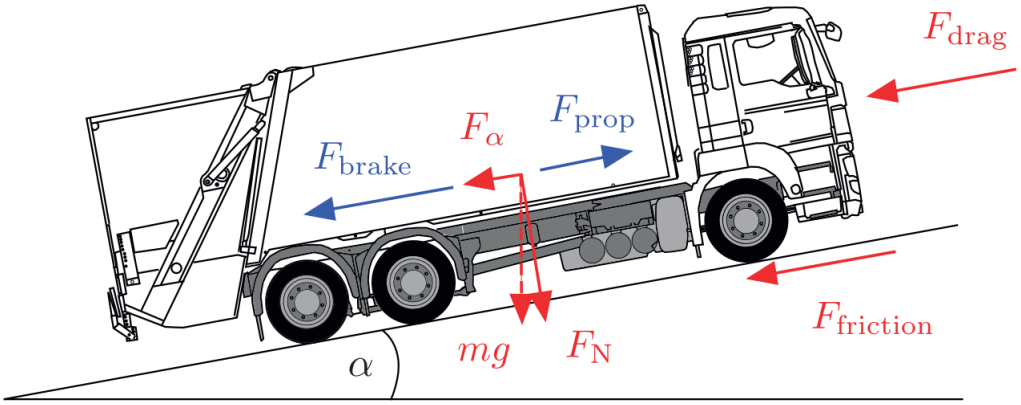

Figure 30. The vehicle longitudinal dynamics are a result of the acting forces on the RCV. Aerodynamic drag, (uphill) road grading and rolling resistance are considered as the only resisting environmental forces. Traction and braking forces are based on drivers initiative. Note that F_{N} is not part of longitudinal dynamics. [35]

$$F_{\text{total}} = F_{\text{prop}} + F_{\text{brake}} + F_{\text{N}} + F_{\text{drag}} + F_{\text{friction}} + F_{\alpha} \tag{2}$$

$$P_{\text{dyn}} = F_{\text{total}} v \tag{3}$$

$$P_{\text{total}} = \frac{1}{\eta_{\text{t}}}(ma + \tfrac{1}{2} C_d \rho A_{\text{f}} v^2 + mg f_{\text{r}} \cos(\alpha) + mg \sin(\alpha)) v + P_{\text{aux}} \tag{4}$$

where	F_{total}	is the total force acting on the vehicle [N]
	F_{prop}	is the accelerating (propelling) force at the tire-road contact [N]
	F_{brake}	is the braking force at the tire-road contact [N]
	F_{drag}	is the resisting aerodynamic force [N]
	$F_{friction}$	is the resisting frictional force [N]
	F_{α}	is the gravitational force resulting from the road grade [N]
	P_{dyn}	is the vehicle power need from the dynamic elements [W]
	P_{total}	is the total vehicle power need [W]
	P_{aux}	is the auxiliary power consumption [W]
	v	is the longitudinal velocity [m/s]
	η_t	is the transmission efficiency [-]
	m	is the vehicle mass [kg]
	a	is the acceleration [m/s^2]
	C_d	is the aerodynamic drag coefficient [-]
	ρ	is the air density [kg/m^3]
	A_f	is the vehicle frontal area [m^2]
	g	is the gravitational constant [m/s^2]
	f_r	is the rolling resistance coefficient [-]
	α	is the road inclination [%]

The vehicle model template had the dynamics implemented based on the above longitudinal dynamics. The model was further extended by factoring braking and vehicle mass increase during waste collection. Also, rolling resistance was not in the model template, so it was added. The vehicle dynamics model is shown in figure 31.

The model takes a different approach compared to the equations when considering the vehicle inertia. Rather than arbitrarily implementing vehicle dynamics to the whole vehicle as in the above equations, the acting forces are directly targeted to the drive shaft. And because the vehicle is mostly modeled using Simscape physical network signals, it is a more realistic approach to take the vehicle weight into consideration as an added inertia component in the shaft. Thus, the entirety of the longitudinal inertia of the vehicle is reduced to the drive shaft as shown in equation 5.

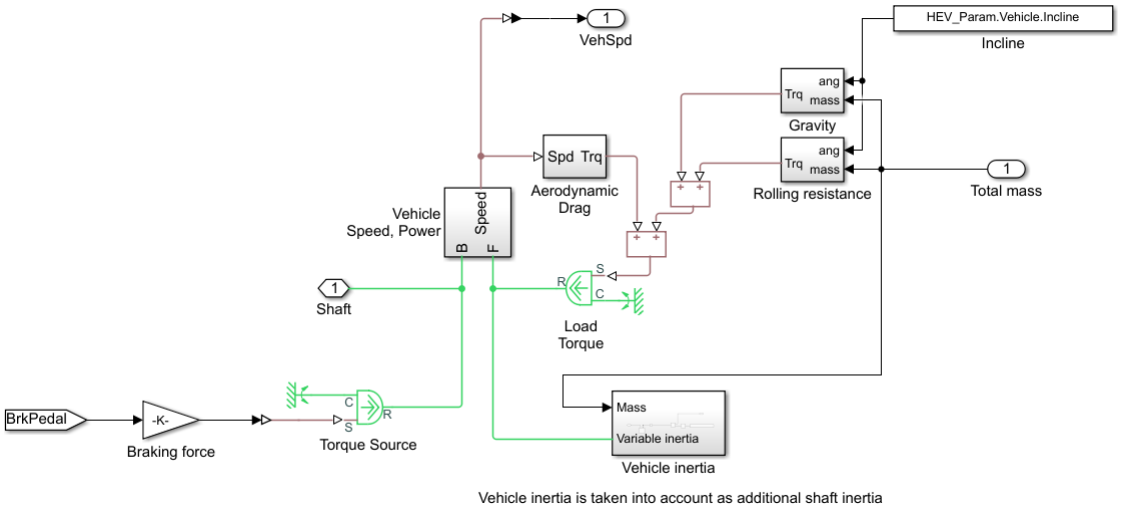

Figure 31. Vehicle longitudinal dynamics model

$$J_{\text{total}} = mr_{\text{e}}^2 + J_{\text{driveshaft}} + J_{\text{trans}} \tag{5}$$

where J_{total} is the total vehicle inertia [kgm^2]
$J_{\text{driveshaft}}$ is the driveshaft inertia [kgm^2]
J_{trans} is the rest of the inertias combined (gearbox, motor, etc.) [kgm^2]
r_{e} is the tire radius [m]

The parameters of a real RCV are not readily available. Therefore, for the verification simulation, the model is based on average weights, engine powers and drive cycles of EURO VI emissions rating RCVs, which were empirically tested for tail-pipe NO_x emissions in the Netherlands. EURO VI is the most common emission class for vehicles with GVW of over 3.5 tonnes in the Netherlands in 2018. [65]

The initial weight for the simulation model vehicle is derived by averaging actual RCV weight values presented in [65]. The model RCV receives an empty weight of 14 601 kg and a GVW of 26 778 kg. We assume that the vehicle is at the end of its duty cycle at the beginning of the simulation. Logged data from real-world operation in [66] shows that the total number of collected bins is typically between 144 and 194[1]. From fourteen logged routes the average total bin count was 167 bins. An assumption of 23 kg of waste per bin is made in [69]. However, in this simulation, the collected bins are made twice as heavy to better see any possible impact on vehicle performance from the waste collection. With these added masses, the overall RCV weight at the start of the simulation is 14 601 kg + (165 x 46 kg) = 22 191 kg. During the simulation, the weight increases with additional 2 x 46 kg.

The power requirements for the components is carried out to verify component selections. Component sizing optimization is not carried out in this work, since there is only one suitable diesel engine, which can be used as the DUT for the HIL simulation. The EM will therefore be used more for the vehicle traction, while the ICE is used more for battery charging.

Vehicle frontal area, tire radius, rolling resistance coefficient and aerodynamic drag coefficient are gathered from [70], which studied the optimal design of a series-parallel HEV powertrain for a heavy-duty truck. Tire radius is used to convert longitudinal velocities to rotational velocities according to equation 6 and is taken into account in vehicle inertia modeling.

$$v = \omega_{\text{w}} r_{\text{e}} \tag{6}$$

where ω_{w} is the wheel rotational velocity [rad/s]

Final drive gear ratio i_{g} is from [71], which proved to match well with the speed characteristics of the power sources. The planetary gear ratio k is later calculated in section 4.1.4 equation 16. The vehicle simulation parameters are presented in table 6.

[1] Route 15 omitted for its much higher bin count (266).

Table 6. Vehicle parameters used in the simulation model for a series-parallel hybrid RCV

Vehicle Parameters	
Initial mass, m (kg)	22 191
Tire radius, r_e (m)	0.5
Frontal area, A_f (m^2)	6.5
Aerodynamic drag, C_d	0.44
Rolling resistance, f_r	0.009
Planetary gear ratio, k	3.867
Final drive gear ratio, i_g	6.14
Air density, ρ (kg/m^3)	1.17
Gravity, g (m/s^2)	9.81
Road inclination, α (%)	0
Auxiliary power, P_{aux} (W)	1000

4.1.2 Control logic

The vehicle control can be considered as nested control loops, where the drive cycle speed tracking is the outermost and the slowest of the controls. The drive cycle tracking is implemented with a simple PI-controller, which represents the driver. The controller output is saturated between zero and one, both for acceleration and braking. The brake pedal signal is used in mode logic chart and in the vehicle model by implementing a constant brake pedal force gain to it. The acceleration signal is used to create the traction motor and the ICE speed controller speed demands.

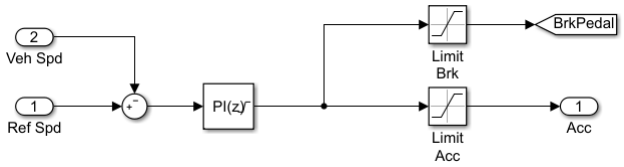

Figure 32. Vehicle speed controller Simulink scheme

Under the control subsystem, all of the three EMs have their own controllers, which are essentially PI-controllers. Their outputs are torque requirements, which are then routed to the component models. The models themselves are assumed to track the torque demands.

The traction motor and the ICE are controlled with the acceleration input, which is scaled so that the acceleration value of one represents the maximum speed demand. Zero value represents idle speed and zero speed for the ICE and the traction motor, respectively. The engine speed controller outputs a value between zero and one, which represents the throttle pedal position. The engine model then converts this throttle input into rotation and torque of the engine output shaft.

The pump motor reference speed is set to be constant. Practically the speed will vary during the hydraulic work cycle.

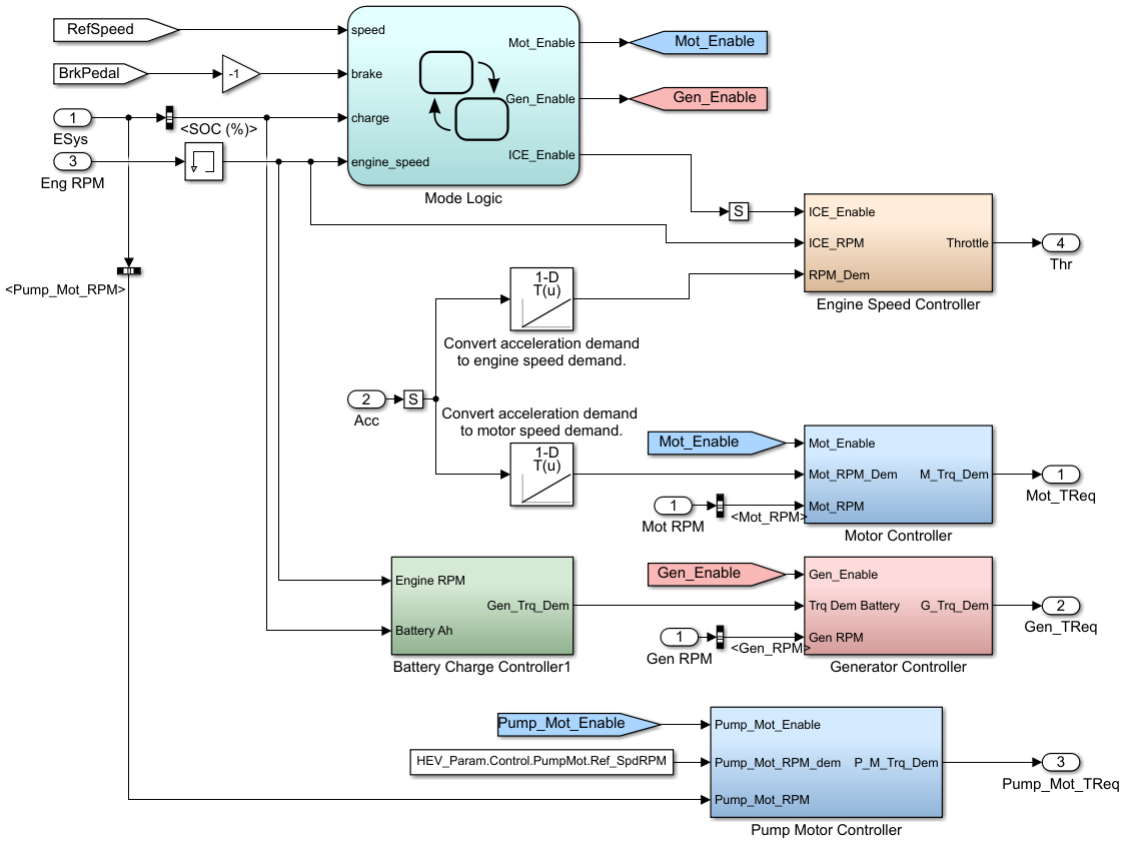

Figure 33. The Simulink model controller blocks and the flowchart-based logic block

Before the generator controller there is a battery charge controller. With the current mode logic, the generator controller works as a speed controller only at the beginning of the simulation, as it is used as a starter motor for the ICE. After the ICE reaches its idle speed, the battery charge controller's torque demand output is passed to the generator instead. Figure 34 shows the logic, which determines the torque demand for the generator when charging is enabled.

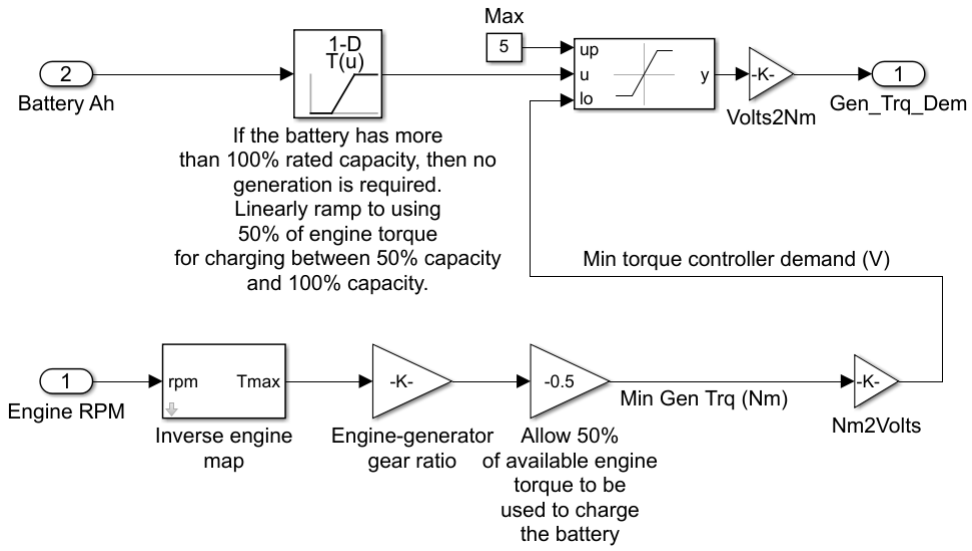

Figure 34. The battery charger controller logic in Simulink

The mode logic flowchart is presented in figure 35. The mode logic is modeled using Simulink Stateflow architecture. The mode logic chart block takes brake pedal position, battery SoC, vehicle speed and the engine speed as its inputs. Vehicle speed is not used in the current logic, but it is left available for further development of more sophisticated control logics. For example, the ICE could be activated only after a certain vehicle speed is reached.

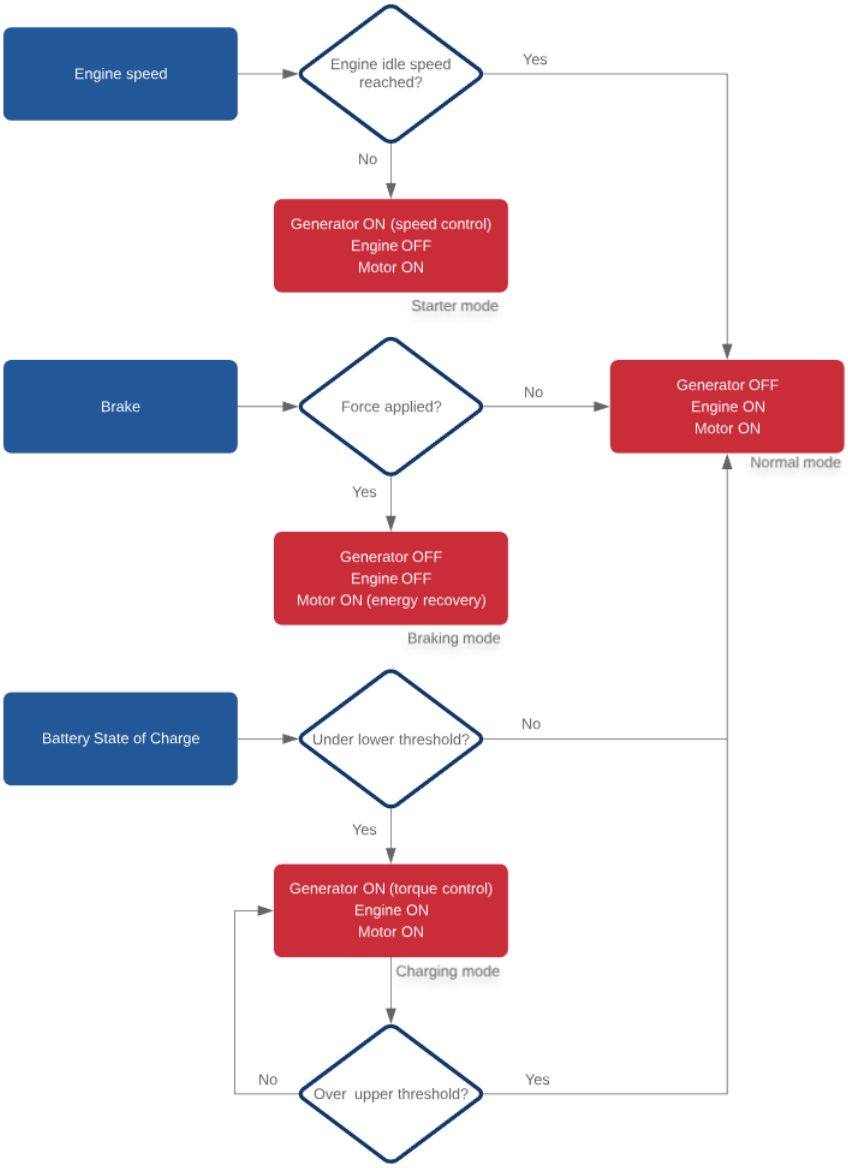

Figure 35. The traction motor, the generator and the ICE are activated according to the following mode logic

Under the hydraulic control subsystem, there are logics for hydraulic work cycle triggering as well as controlling of the hydraulic cylinders.

The actuation logic shown in figure 37 triggers the hydraulic work cycle on/off state. The user defines the actuation starting points and duration as parameters. The logic then switches the pump motor on for the duration of the work cycle with an additional five seconds to drive the valves back to their shut positions. Collection trigger signal is created and used to update the vehicle mass at the start of the work cycle.

Figure 36 presents the hydraulic cylinder controllers. PI-controllers are used to track the piston stroke length by actuating valve openings, which restrict fluid flow to the cylinders.

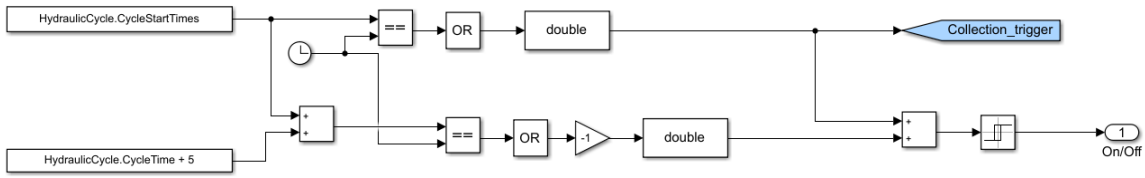

Figure 36. Simulink scheme of the hydraulic work cycle actuation logic

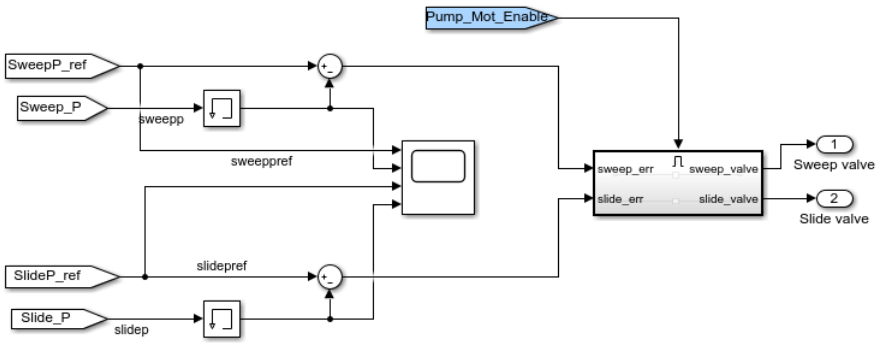

Figure 37. Hydraulic cylinder position controllers in Simulink. The enabled sybsystem contains PI-controllers for each cylinder.

4.1.3 Engine

The internal combustion engine in the simulation model is only to be used for pure simulations when designing the model. In a HIL test, the ICE model will be omitted and replaced with the physical engine. Because the ICE model parameters cannot be changed, it is used as a reference point when sizing the motor and the generator.

Since the engine model parameters are tied to the physical engine, it should be modeled as accurately as possible so that the HIL simulation would be comparable to the pure simulation runs. The ICE model used is a generic engine block from the Simscape Driveline library. The block is parametrized as normalized third-order polynomial matched to peak power. The engine model takes signal input between zero and one, which represents the gas pedal position. The engine model output is connected to a physical signal network representing the engine cardan shaft. Engine inertia is neglected for faster simulation and is compensated in the shaft inertia. Rotational velocity and torque measurements are taken from the shaft and are used for simulation control.

For the sake of guaranteeing a working simulation model, the sufficiency of the ICE power is verified analytically. The ICE should be able to provide enough power for cruising at 85 km/h even at full load i.e. GVW, since the typical speed limit for heavy road vehicles is limited to 80 km/h. In steady speed, the engine must provide power to overcome aerodynamic drag and rolling resistance. Using equation 4 derived from the longitudinal vehicle dynamics shown in figure 30, ICE power need is evaluated to be at least 87.5 kW. Auxiliary power need, such

as cabin air conditioning and low voltage electronics, were considered to be steady 1000 W. Also, a conservative transmission efficiency of 90 % is used to take into account frictional and inertia effort from the engine, transmission, driveline and wheels. Air density was considered to be 1.17 kg/m^3 and gravitational constant as 9.81 m/s^2. This calculation validates that the diesel engine available for the HIL simulation meets the requirement with its maximum power of 98 kW. The engine's main parameters are shown in table 7

Table 7. Engine parameters of the DUT also to be used in the simulation model of the hybrid RCV

Engine	
Maximum power (kW)	98
Maximum torque (Nm)	551
Maximum speed (rpm)	2250
Minimum speed (rpm)	825

4.1.4 Power split device

In series-parallel powertrain topologies the engine can both be used to provide traction to the wheels or to independently run, for example, to charge the battery via a generator. This speed coupling is most often done using a planetary gear unit, also known as a power split device [67, 70], shown in figure 38. The unit consists of a ring gear, a sun gear, a carrier and planet gears. The ring gear is connected to the main drive shaft that drives the wheels. The electric traction motor is also connected to the ring gear by having a connection to the drive shaft. This means that the traction motor shares the speed with the ring gear unless reduction gears are used in between. The generator, which is used to charge the batteries is directly connected to the sun gear. Planet gears are used to transmit the rotations between the planetary gear elements. The planet gears are connected to a planet carrier, which is coupled to the engine output shaft.

Planetary gear ratio k determines the relations between the drive shaft and the traction motor, the generator and the ICE. It is expressed as a ratio of teeth or radii of the ring gear to that of the sun gear. The ratio must be greater than one. This results in the sun gear having a proportionally greater rotational speed than the ring gear. The speed relations are expressed in equation 7:

$$\omega_{\mathrm{r}} = \frac{1+k}{k}\omega_{\mathrm{eng}} - \frac{\omega_{\mathrm{gen}}}{k} \tag{7}$$

where ω_{r} is the ring gear (motor) rotational velocity [rad/s]
ω_{eng} is the carrier gear (engine) rotational velocity [rad/s]
ω_{gen} is the sun gear (generator) rotational velocity [rad/s]

Any of the three main components can be locked in place, which inherently results in different operational behaviors, listed below. However, in typical power split operation all of the components are turning, as the ICE is charging the batteries, while the vehicle is moving.

1. When the sun gear is locked, the carrier (ICE) and the ring gear (traction motor) will turn in the same direction. The ICE will have a reduced speed compared to the traction motor. For example, with a planetary gear ratio of k=4, engine speed of 2 000 rpm results in ring gear speed of 2 500 rpm.

$$\omega_{\mathrm{r}} = \frac{1+k}{k}\omega_{\mathrm{eng}} \tag{8}$$

2. When the ring gear is locked, the carrier and the sun gear turn in the same direction and all of the engine power is used to charge the battery via the generator and the vehicle is stationary. Again with ICE speed of 2 000 rpm and a gear ratio of k=4, the generator will turn at a rate of 10 000 rpm.

$$\omega_{\mathrm{gen}} = (1+k)\omega_{\mathrm{eng}} \tag{9}$$

3. When the carrier is locked, the engine is cut off and the sun and ring gear are turning in opposite directions. With a traction motor speed of 2 000 rpm the generator will turn at a speed of 8 000 rpm, with a gear ratio k=4.

$$\omega_{\mathrm{gen}} = -k\omega_{\mathrm{r}} \tag{10}$$

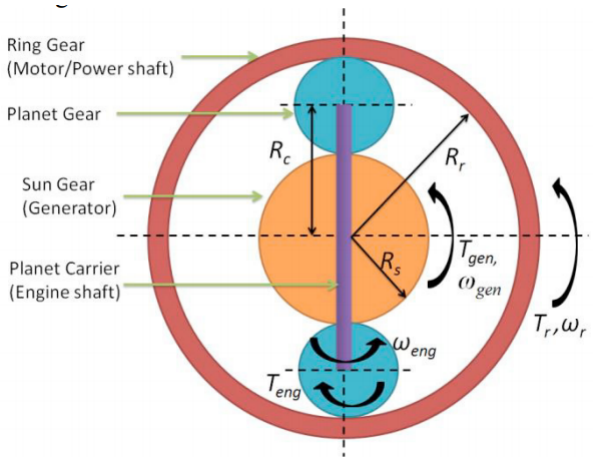

Figure 38. Torque and speed relations in a planetary gear unit [70]

The torque coupling of the series-parallel powertrain usually is a result of the power split device and a fixed reduction gear that connects the ring gear and the traction motor to the wheel axle, as shown in figure 28. The ICE torque is split between ring gear (traction motor) the sun gear (generator) according to equations 11 and 12, and the final torque at the wheels is shown in 13.

$$T_{\mathrm{r}} = \frac{k}{k+1}T_{\mathrm{eng}} \tag{11}$$

$$T_{\mathrm{gen}} = \frac{1}{1+k}T_{\mathrm{eng}} \tag{12}$$

$$T_{\text{wheels}} = \frac{1}{i_{\text{g}}\eta_{\text{t}}}(T_{\text{m}} + T_{\text{r}}) = \frac{1}{i_{\text{g}}\eta_{\text{t}}}(T_{\text{m}} + \frac{k}{k+1}T_{\text{eng}}) \tag{13}$$

where T_{r} is the ring gear torque [Nm]
T_{eng} is the carrier gear torque [Nm]
T_{gen} is the sun gear torque [Nm]
T_{m} is the traction motor torque [Nm]
i_{g} is the final gear ratio [-]

The planetary gear is simply modeled by using a planetary gear block from the Simscape Driveline library. It connects the three physical shaft signals to the block, representing the connections from the ICE, the generator and the traction motor.

The planetary gear ratio is determined by matching the ICE maximum speed to the maximum longitudinal velocity of the vehicle. The longitudinal velocity is reduced to drive shaft rotational velocity according to equations 14 and 15. Longitudinal Wheel slip is neglected in this work. Using the previously determined maximum speed of 85 km/h, tire radius and final drive gear ratio, the planetary gear ratio is calculated to be 3.868 according to equation 16. To use integer values for gear teeth ratio, an example of 58/15 = 3.867 is selected as the planetary gear ratio. It is also close to the values found in the literature [70, 71].

$$\omega_w = v/r_e \tag{14}$$

$$\omega_r = i_g \cdot \omega_w \tag{15}$$

$$k = \frac{\omega_{eng} r_e}{i_g v - \omega_{eng} r_e} \tag{16}$$

4.1.5 Traction motor

In the model, there are three EMs: the traction motor, the generator and the pump motor. Their power is supplied by a battery pack, which is modeled around a Simscape generic battery model. The battery voltage is slightly boosted via a DC-DC boost converter. In reality this DC voltage would be converted to three-phase AC voltage by an inverter, but in this simulation model those are omitted because DC servomotors are used to emulate the three-phase machines. The motors use torque-speed lookup tables for their parameters. The electrical models mainly use Simscape Electrical blockset components.

Using equation 4, the power need to meet acceleration requirements is produced. The requirement is referenced from [70] and scaled to match the RCV weight. The RCV at its maximum weight should reach 50 km/h in 24 seconds. The total power need is calculated as 281.6 kW. This means that the traction motor has to provide at least 281.6 kW - 98 kW = 183.6 kW, because the two power sources can also work in parallel configuration. The EM used in the eDyno is able to provide maximum peak power of 250 kW, so we can use

its parameters in the simulation model without any scaling, as its characteristics are already available from the EM supplier.

Table 8. Parameters for the traction motor to be used in the simulation model for a series-parallel hybrid RCV

Traction motor	
Continuous power (kW)	186
Maximum power (kW)	250
Speed at maximum power (rpm)	2 700
Maximum speed (rpm)	3 500
Maximum torque (Ñm)	1 480
Efficiency (%)	96

4.1.6 Generator

The modeling of the generator follows that of the traction motor. The generator is sized by deriving equations 17 and 18 from earlier equations 9 and 12. The engine parameters were already known, and the planetary gear ratio was determined based on the vehicle and engine specifications.

Now, the inequality equation 17 gives us the torque rating for the generator. To take full potential of the engine's battery charging capabilities, the generator has to have a minimum torque rating of 113 Nm. Maximum rotational speed of the generator happens in a situation where the engine is at its maximum speed and the traction motor is at its maximum negative speed. However, practically there is no need to reverse the vehicle at high speeds, which is why the generator's maximum speed can solely be specified by the engine speed. Inequality equation 18 results in a minimum speed rating of 10 700 rpm for the generator. A 5 % margin is added to both torque and speed to meet the requirements. The torque-speed curve from the traction motor is scaled for the generator, since no real component parameters are available for a generator that is close to the analytic values. Generator efficiency is referenced from [70].

$$T_{\text{gen,max}} \geq \frac{1+k}{k} T_{\text{eng,max}} \tag{17}$$

$$\omega_{\text{gen,max}} \geq \frac{1}{1+k} \omega_{\text{eng,max}} \tag{18}$$

Table 9. Parameters for the generator to be used in the simulation model for a series-parallel hybrid RCV

Generator	
Maximum power (kW)	71
Maximum speed (rpm)	11235
Maximum torque (Ñm)	119
Efficiency (%)	90

4.1.7 Hydraulic compactor

Accurate modeling of the hydraulic loader and compressor system is difficult and examples are hard to find from literature. Easier and computationally more effective method would be to create a torque demand for the EM running the pump by using real-world measured pump displacement and pressure during the work cycle, as was done in [64]. Thus, the only addition for the series-parallel HEV model in terms of the hydraulic compactor would be to include an EM to the electric DC circuit and to provide a torque input generated as a product of pump displacement and pressure. For this work, such data was not available.

Because the component parameters are not known, and hydraulic cycle data is not accessible, a combinatorial approach is taken, where the hydraulic circuit components are modeled to a decent fidelity and the pump and cylinder parameters are tuned until the pump's power, pressure and displacement values match the general values from the literature sources. This method also allows for further development of an even more accurate model, which the raw data based approach does not.

The hydraulic work circuit is implemented to the DC circuit by connecting the pump motor to it. The actuation command for the hydraulics is generated by the modified control logic. The hydraulic model was also modified from a model provided by Mathworks [72]. The hydraulic circuit and its components use Simscape Fluids library components. The hydraulic circuit consists of a fixed-displacement hydraulic pump, two open center, 5-way, 3-position directional valves, piping, pressure relief valve and two hydraulic cylinder actuators, which represent the sweep cylinder and the slide/pack cylinder found in common rear-loading RCVs. Figure 39 shows the overview of the hydraulic model.

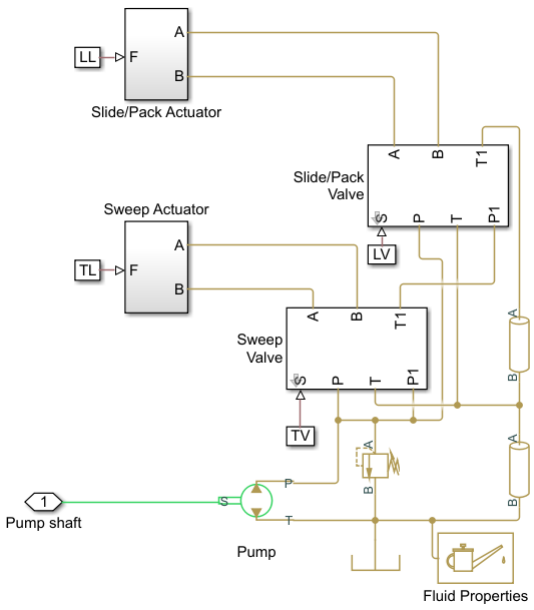

Figure 39. Overview of the hydraulic model in Simulink

The hydraulic pump's displacement and operating pressure are gathered from [64]. Table 10 from the paper presents values for refuse body values for rear, front and side loader vehicles. The average pump displacement value of 96 cc/rev is used in the simulation. The paper also

refers to a specific RCV: 2010 Mack TerraPro LEU613. Operation data of that specific RCV show that its pump is running between 800 and 2 000 rpm, with a pressure variation between 0 and 170 bar and a power from 0 to 42 kW during an operation cycle. The lower values are when the pump is idling, and under a work cycle the pump usually goes near its maximum values.

In the simulation model, the 2 000 rpm rotational speed will be used as the pump's nominal speed. Rather than idling the pump at 800 rpm, it will be run to zero speed. The reason behind 800 rpm idling speed in the reference pump is the fact that the hydraulic pump is fixed to the ICE running it. A pressure relief valve will be used to limit the system pressure to 170 bar.

Table 10. Refuse body values according to a manufacturer survey [64]

		Rear Loader	Front Loader	Side Loader
Hopper Size (m^3)	Min.	0.8	7.6	
	Max.	2.8	9.2	
	Ave.	2.2	8.4	1.1*
Body Size (m^3)	Min.	4.6	18	4.6
	Max.	25	34	37
	Ave.	15	28	23
Max Operating Pressure (bar)	Min.	124	155	124
	Max.	190	190	207
	Ave.	156	174	171
Pump Displacement (cc/rev)	Min.	56	133	54
	Max.	133	136	170
	Ave.	96	135	100*
Reservoir Volume (l)	Min.	83	178	91
	Max.	265	265	322
	Ave.	178	208	201

The cylinder piston and rod side areas are calculated to closely match the cylinder volumes presented in table 11 by using the piston stroke value from the template. The model consists of only slide/pack and sweep cylinders for the sake of simplicity. In reality, there are usually two cylinders per operation, but in the model there are only one of each. Thus, their volumes will be matched to the right-most column of table 11. Other parameters such as dead volumes, specific heat ratio and cylinder stiffness and damping remain the same as in the template. However, these values will be added to the parameter initiation file so that they can be easily modified later on. Table 12 shows the main parameters of the hydraulic model for the HIL testing.

Table 11. Values for average cylinder volumes according to a manufacturer survey [64]

Rear Loader	Piston Side	Rod Side	1 Cylinder	2 Cylinders
Slide/Pack Cylinder Volume (l)	9.8	4.3	14.1	28.2
Sweep Cylinder Volume (l)	5.5	2.4	7.9	15.8
Tailgate Cylinder Volume (l)	4.5	1.3	5.9	11.8
Ejector Cylinder Volume (l)	35.7**	9.3**	45.0**	N/A

The electric motor for running the hydraulic pump is sized using equation 19.

$$P_{\text{pumpmotor}} = \frac{Q \cdot \Delta p}{\eta_{\text{m}} \eta_{\text{V}}} \tag{19}$$

where $P_{\text{pumpmotor}}$ is the pump motor power [W]
Q is the hydraulic flow [m^3/s]
Δp is the pressure difference over the pump [Pa]
η_{m} is the mechanical efficiency [-]
η_{V} is the volumetric efficiency [-]

Table 12. Hydraulic circuit model parameters

Fixed Displacement Pump	
Displacement (cm^3/rev)	96
Volumetric Efficiency (%)	92
Total Efficiency (%)	85
Nominal Pressure (bar)	156
Maximum Pressure (bar)	170
Nominal Speed (rpm)	2000
Pump Motor	
Maximum power (kW)	56
Maximum speed (rpm)	3500
Maximum torque (Ñm)	300
Efficiency (%)	96

Slide/Pack Cylinder	
Volume (l)	28.23
Stroke (cm)	120
Piston side area (cm^2)	165
Rod side area (cm^2)	70
Sweep Cylinder	
Volume (l)	15.81
Stroke (cm)	43
Piston side area (cm^2)	263
Rod side area (cm^2)	113

4.1.8 Other modeling parameters

The utility electric components are not optimized, and their values are selected for this single simulation by iterating the simulation and coming up with values which provided a working model. The electric circuit is powered by a 250 kW battery pack with a capacity of 20.7 kWh. The capacity is rather small for the application, but was intentionally down-sized so that the battery energy generation could better be observed in the short simulation runs. The battery's nominal voltage is 690 V, which is slightly boosted by a DC-DC boost converter.

The DC-DC boost converter uses a PI-controller model to scale the Simscape electrical network signals from the battery into same format output according to a constant reference value of 750 VDC. The battery model uses components from the electrical blockset, and it uses general parametrization based on table values.

4.2 Test cycles

Best way to utilize the designed testbed for vehicle development is to emulate real-world conditions as closely as possible. For this reason, the test cycle should reflect real scenarios rather than take use of standardized drive cycles. For optimal solution, one should log driving data on-board from a vehicle in its characteristic operation. This collected data could then be used to create representative drive cycles to be used for testing. However, it may be hard and time consuming to evaluate the raw information, which adds benefit to using ready-made

drive cycles. There are tools available to automate the raw data processing such as DRIVE: Drive-Cycle Rapid Investigation, Visualization, and Evaluation Analysis Tool [73], which converts raw data into a drive cycle and evaluates its usefulness, for example, against any industry specific standard cycles.

In [65], drive cycle data from real-world RCV operation is presented. Actual averages cannot be drawn from that paper, because the full data is not available. Rather, some trends can be seen. The cycles often have a portion of high-speed driving, where the vehicle reaches a speed of around 80 km/h. This probably correlates to a section where the RCV drives on a highway to its designated suburban area where the actual operation begins. This section is unsurprisingly often at the beginning and at the end of the drive cycle. To keep our real-time HIL simulation relatively short, the high-speed section is placed at the end of the simulation and kept short. The other trend shown in the figure shows repetitive driving at low speeds with full stops. This correlates with the actual operation of emptying refuse bins and driving a short distance to the next stop. There is a lot of variation between the vehicle speeds in [65], but in many cases the peak speed in the suburban varies between 30 and 40 km/h. Thus, our simulation drive cycle consists of two sections where the vehicle reaches 30 and 40 km/h, respectively, with stops in between where the hydraulic compactor is actuated. Figure 40 shows the suggested drive cycle for the HIL simulation. The overall cycle time is kept relatively short, because the simulation is only meant as a proof-of-concept. The vehicle will idle for ten seconds after each stop, before the hydraulic collection cycle is initiated. The vehicle will start to accelerate while the hydraulic cycle is still ongoing. The hydraulic cycle lasts for 20 seconds and is done twice during the test cycle.

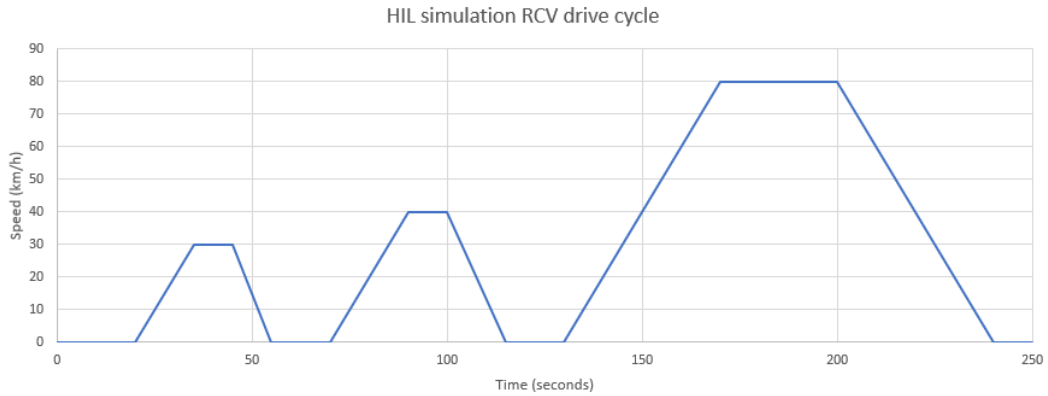

Figure 40. The simulation drive cycle starts by accelerating to 30 km/h, representing the transition from one bin to another. It then stops for 15 seconds to run the hydraulic mechanisms. This cycle is repeated with 40 km/h transition. Lastly, the vehicle accelerates to highway driving. The last deceleration is added to ensure safe operation point for the eDyno once the cycle stops. The overall cycle time is 250 seconds.

The hydraulic work cycle is the default one from the Mathworks hydraulic model template, as load forces are difficult to determine without actual measurements. The actuator default force loads are from 500 to 2 900 N and 1 000 to 24 000 N for the sweep and the slide actuator, respectively. The sweep actuator extends 0.4 m during the cycle, and the slide actuator extends 1.0 m. Figure 41 shows the hydraulic actuator cycle profiles once the cycle is triggered.

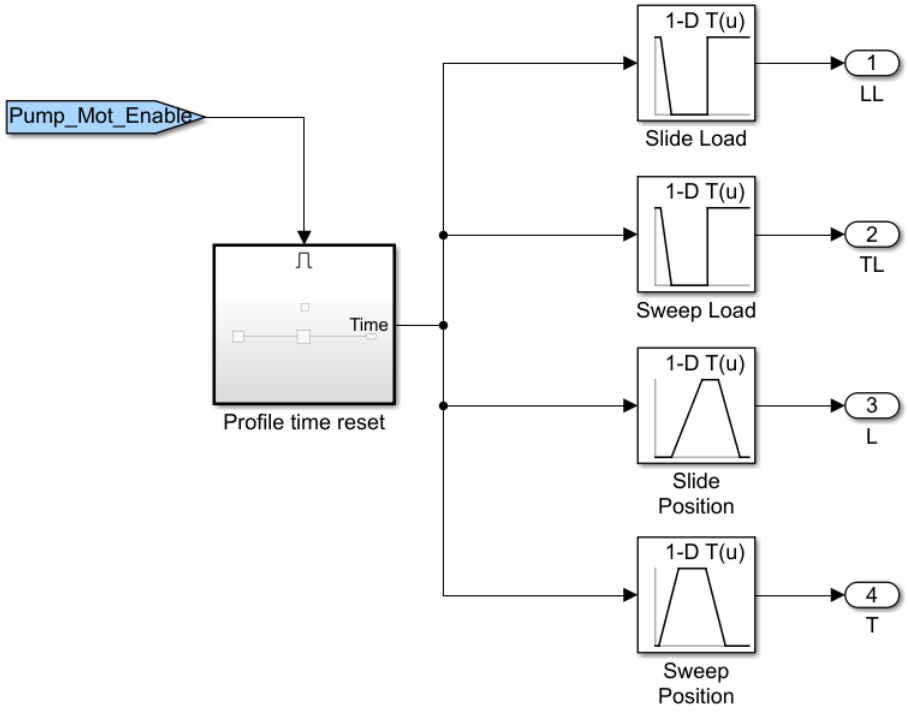

Figure 41. Cylinder force load and actuation position profiles in the Simulink model. An enabled subsystem is used to reset a simulation clock, which is used to read the lookup table values during the work cycle.

4.3 Physical/virtual interface configuration

The model and the simulation variables are parametrized to allow quick testing of different simulation profiles. Excel sheets were built to provide a template to input these variable values. Separate files were used to input lookup tables for the traction motor, generator, pump-motor and engine models. A script was written in Matlab as a startup for the simulation model. The script initiates the variables by reading the excel files.

The NI CompactRIO target machine requires a few extra steps for HIL implementation when compared to some other systems such as Speedgoat machines, which should have a more straightforward installation. First of all, a simulink model cannot be run directly on the target machine through the Simulink model interface. Where with some other platforms the model is first compiled to C-code by a generic real-time compiler, CompactRIO requires a separate compiler setup. The selected CompactRIO processor is Linux-based and thus, the model needs to be compiled to .so file type using NI VeriStand Model Framework and C/C++ Development Tools for NI Linux Real-Time, Eclipse Edition. Additionally the Simulink Coder Add-on is required for code generation.

After the necessary programs have been installed, the compiled model can be build inside Simulink. Before compiling, the model was cleared of errors using the Simulink upgrade and code generator advisor. The errors were mostly related to configuration settings, which were rather easily fixed. Code generation for NI Linux real-time system especially requires solver settings to be configured so that the simulation stop time is set to infinite and stepping is set to fixed-step. The solver is set to Fixed-step Discrete Solver for best compatibility and

computation speed. This also required that all continuous blocks needed to be replaced with discrete equivalents. For example, the model template had virtual sensor dynamic subsystems, which included continuous time integrators. For our purpose, virtual sensor dynamics do not need to be addressed, and rather a memory block was used in the feedback loops to delay the signal one simulation step to fix analytical loop errors. The Simscape physical network also required a local solver, which was needed to be set to be discrete.

Data logging is also disabled since it cannot be utilized once the model is implemented in the NI system. Rather, signals can be probed so that they are accessible in LabVIEW for signal monitoring. Also, inports and outports are placed to replace the diesel engine model, and LabVIEW recognizes these as model inputs and outputs, which are further communicated to the physical hardware. The correct compiler is set as NIVeriStand_Linux_64.tlc for Intel-based processors and the model can be built.

5 Results

The operational tests listed in section 3.3 were run with the eDyno. Data recording was not available for all of the first tests, but results are shown for manual closed-loop operation, two-setpoint steady-state tests, the steady-state C1 cycle and the NRTC. These test results are shown in this section. Actual physical HIL simulation tests could not be done due to the initial tests not giving satisfying results, and a properly functioning system is required for any HIL simulation. However, results from the pure simulation run are presented. These results are interesting when predicting how the model will run in physical HIL simulation.

5.1 Testbed validation results

The tests before the data-logged tests were considered more as checking for the proper connections and software functions than testing the performance of the system. However, it was noticed that the scaling from voltage to torque reference is incorrect, because there was a clear systematic offset between the input and the measured torque, when operating the engine in an open-loop. With the feedback controllers enabled, the system was able to track a steady-state reference in most cases, when running the engine in torque mode and the eDyno in speed mode.

A weird behavior was noticed when running the engine at 1 000 and 1 500 rpm, as the torque had a huge offset of even over 100 Nm in some cases. The torque would keep slowly creeping up, which can be seen in figure 42. This behavior was not noticed at any other speeds.

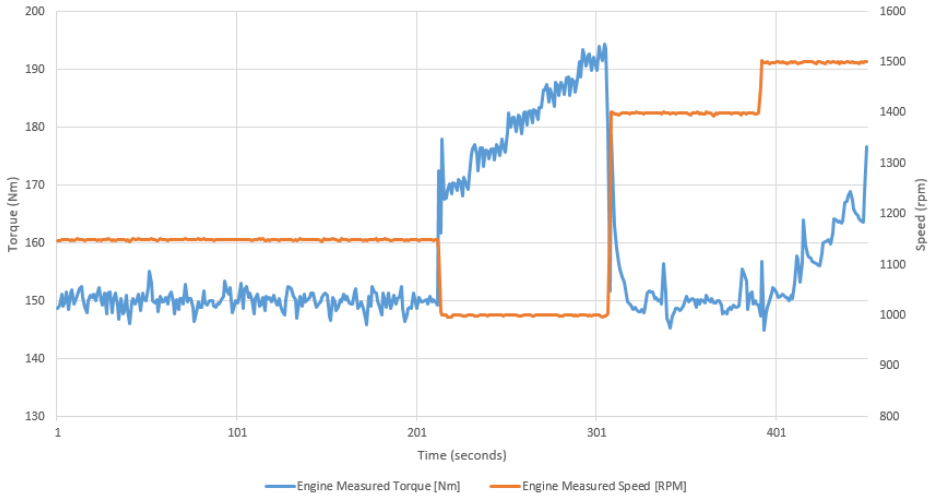

Figure 42. Part of an closed-loop test where speed and torque setpoints were varied. In the figure, the torque reference was constant at 150 Nm, but an offset and an increasing creep was noticed at 1 000 and 1 500 rpm. Also, the torque ripple was noticeable, but not alarming.

5.1.1 Two-setpoint test profile

The first tests had used manual inputs of the setpoints. Next, the software function of reading a .csv-file test profile was tested. The test consisted of two setpoints: 200 Nm at 1 400 rpm and 100 Nm at 1 800 rpm. The test was run at 1 Hz for both the reference and the measurement,

with torque demand for the eDyno and speed demand for the engine. At first, the engine stalled. The problem was troubleshooted to the input logic of the eDyno when running in a test profile mode. Because the eDyno is resisting the engine's rotation, a negative torque needs to be demanded from the eDyno. The manual open-loop controller already had the sign change implemented, but the recipe controller did not. After the simple fix, the recipe would run correctly. The tracking performance, however, was not yet very good. There was an offset between the input and the measured torque. The speed measurement would track the steady-state reference well, but the respond times were slow. When running the test in speed/torque mode for the eDyno and the engine, respectively, the controller would track the steady-state references well, but the torque transitions were unsatisfactory and the responses slow. Figures 43 and 44 show the test results for these tests.

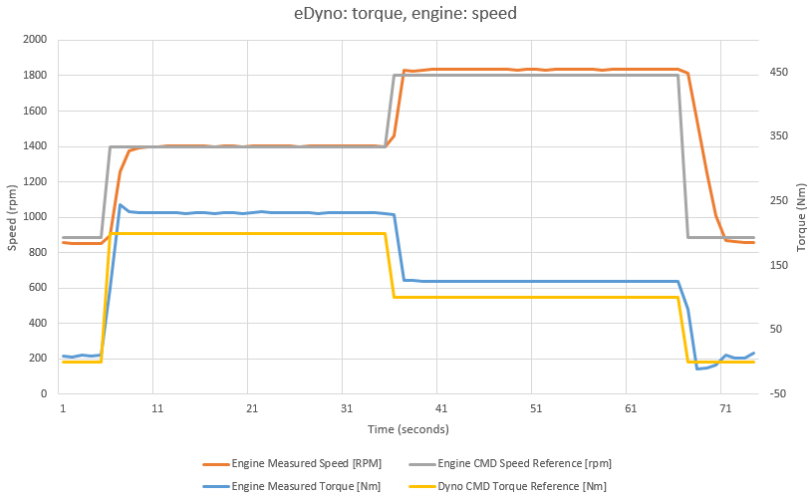

Figure 43. The two-setpoint test with the engine under speed control and the eDyno under torque control. The test cycle was run only once.

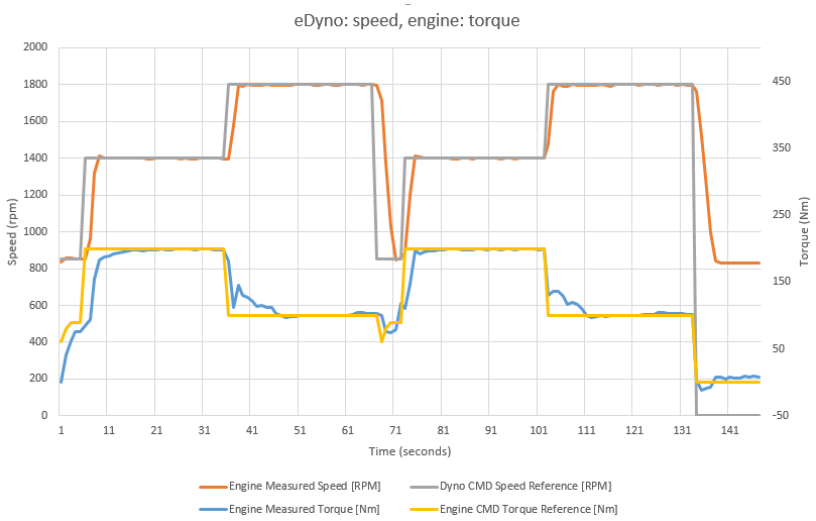

Figure 44. The two-setpoint test with the engine under torque control and the eDyno under speed control. The test cycle was run twice in a row. The beginning of each cycle had a torque ramp-up, which shows as a difference when compared to the previous test.

5.1.2 ISO 8178 C1 test profile

After the first tests, controller parameters were tuned for the next tests. The ISO 8178 C1 test was run in speed/torque mode for the eDyno and the engine, respectively. The cycle was drastically shortened from the standardized test, because the aim of this cycle was to only study the steady-state performance of the eDyno, similarly to the previous tests.

In the first run, shown in figure 45, a ramp-up was added at the start of the cycle, which should be neglected when comparing the test runs. The run showed the same behavior as the initial manual tests, where the torque control would not reach the reference and would start to creep up when demanding a speed of 1 500 rpm from the eDyno. At the end of the cycle the torque could not track the reference, because the engine idle speed had been set too low, meaning that the engine had to keep the torque high.

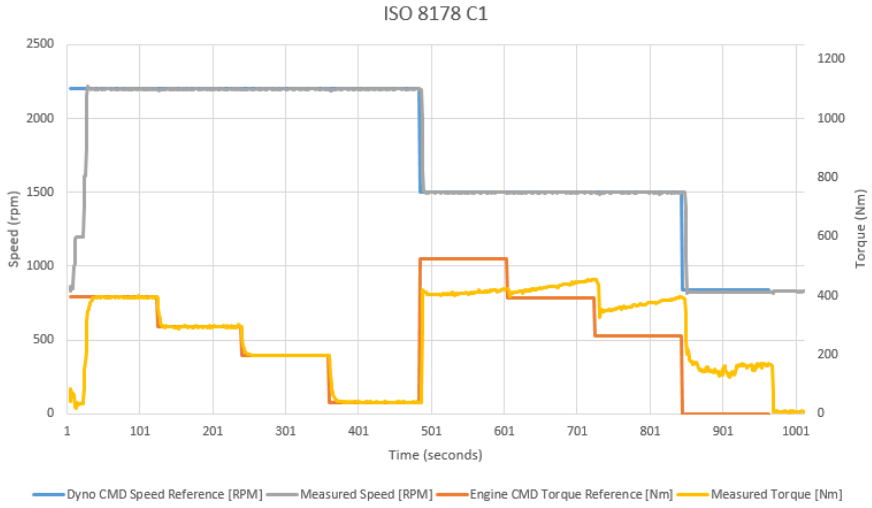

Figure 45. Torque and speed measurement of the eDyno under the ISO 8178 C1 steady-state test cycle

The C1 test profile was modified to see if the system would track the reference when the speed was changed from 1 500 rpm to 1 400 rpm. The idle speed was also raised from 825 rpm to 840 rpm. The results presented in figures 46 and 47 show that the previous behavior was not present and the system was tracking both references rather well. Speed tracking is much better than torque tracking, where the settling time is longer. The close-up shows that the tuning of the controller parameters made an improvement to the torque values when running in speed/torque mode. The response times are still quite long. Additionally, raising the idle speed reference point brought the torque slightly closer to its reference at the end of the cycle, but was not enough.

Figure 48 shows the full ISO 8178 C1 test cycle using another VTT's engine dynamometers. From the figure, torque and speed ripple is noticeable in the first ten minutes of the cycle. For comparative reasons, figure 49 shows only a small section of the transition from the third mode to the fourth, and is aligned with that of the the eDyno's cycle. It can be seen that the eDyno has slightly more ripple in its speed measurement, but not much. The roughly 10 rpm dip when the torque changes is more of a concern. However, the eDyno's torque measurement is better than that of the reference dynamometer.

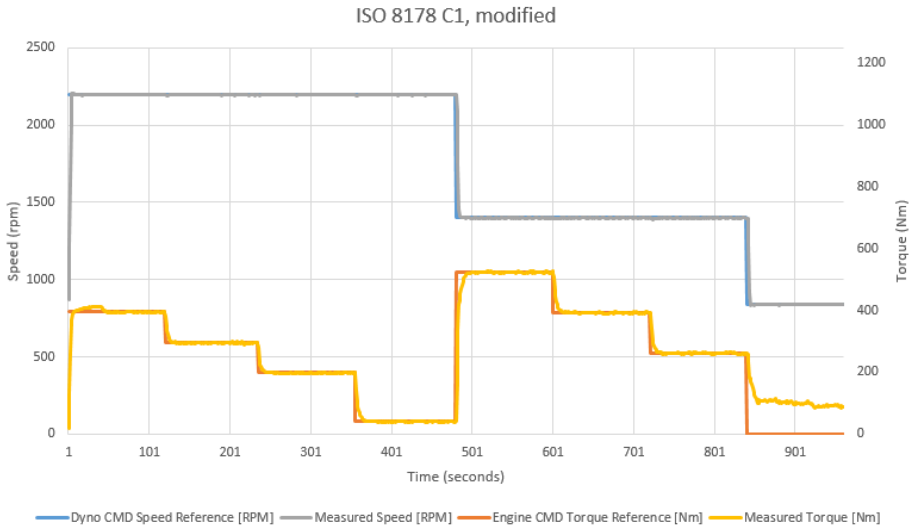

Figure 46. Torque and speed measurement of the eDyno under the modified ISO 8178 C1 steady-state test cycle. The problematic setpoint of 1 500 rpm was changed to 1 400 rpm.

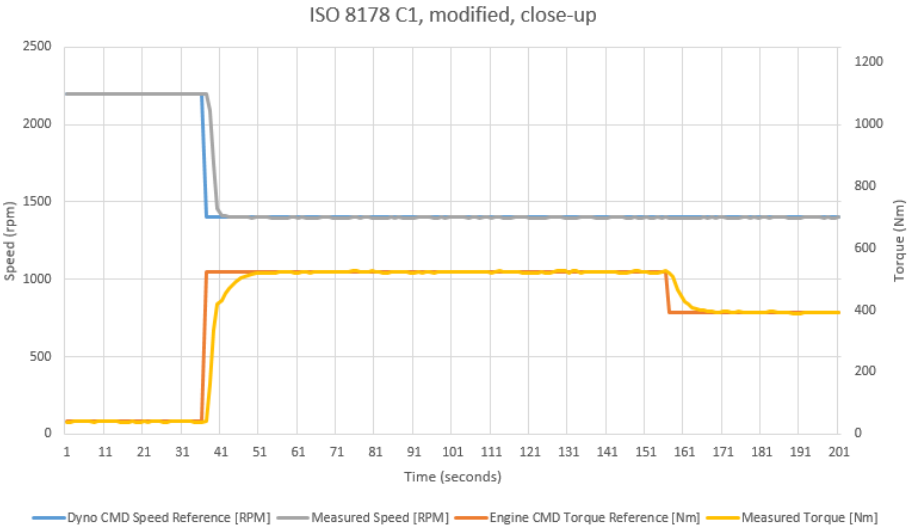

Figure 47. Close-up of the modified ISO 8178 C1 steady-state test cycle

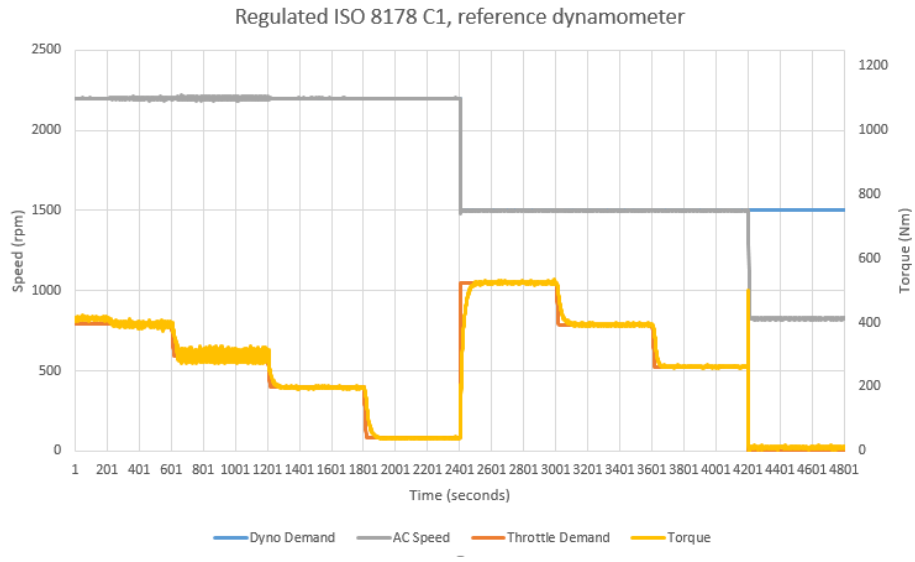

Figure 48. The ISO 8178 C1 previously run under regulated conditions for the same engine as in this work.

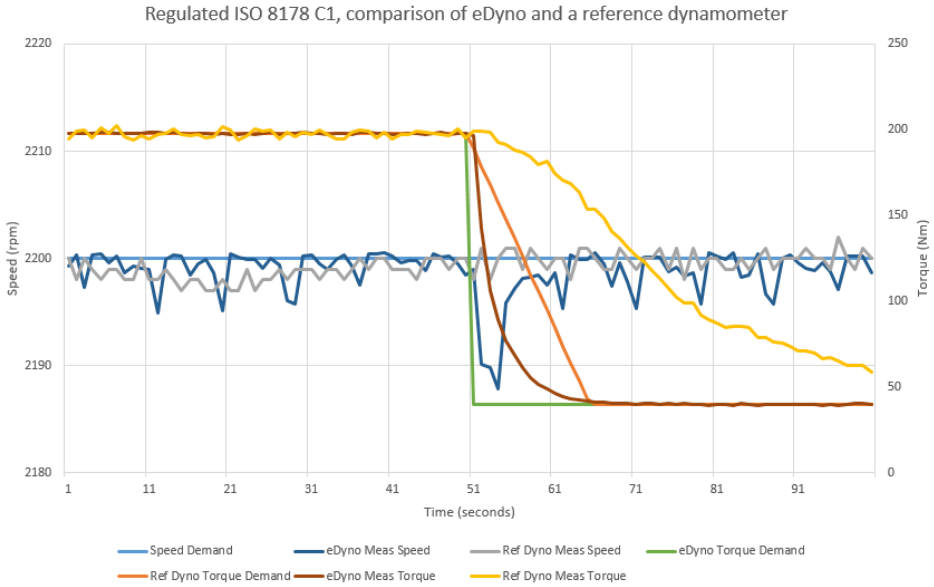

Figure 49. Close-up comparison of a small section of the ISO 8178 C1 cycle run with the eDyno and another dynamometer for the same engine

5.1.3 Non-road transient cycle

The NRTC was first run with the default values calculated using the testing regulation. However, because the eDyno does not work as intented when demanding engine idle, the speed reference values were limited to be above 850 rpm and the torque reference was limited to be above 20 Nm. Some additional tunings were also made, for example, the measurement sample rate was increased to 10 Hz. The test cycle was run in speed/torque mode. Figures 50, 51, 52 and 53 present the eDyno NRTC results. The results show that the speed tracking seems sufficient, while the torque tracking still needs adjustments. What concerns, is the approximately 1 second delay between the input and the response. If similar delay is present in HIL simulations, RT capabilities may not be met.

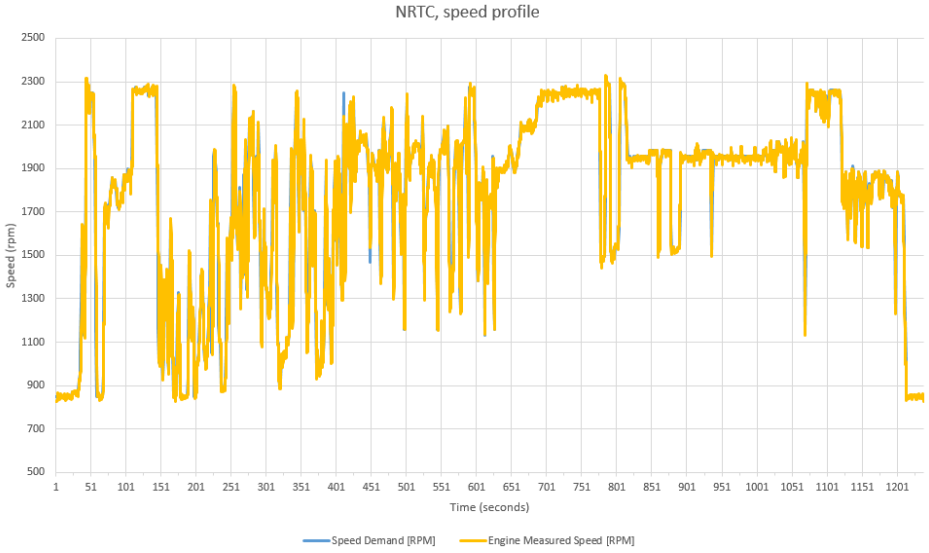

Figure 50. The NRTC results for speed tracking

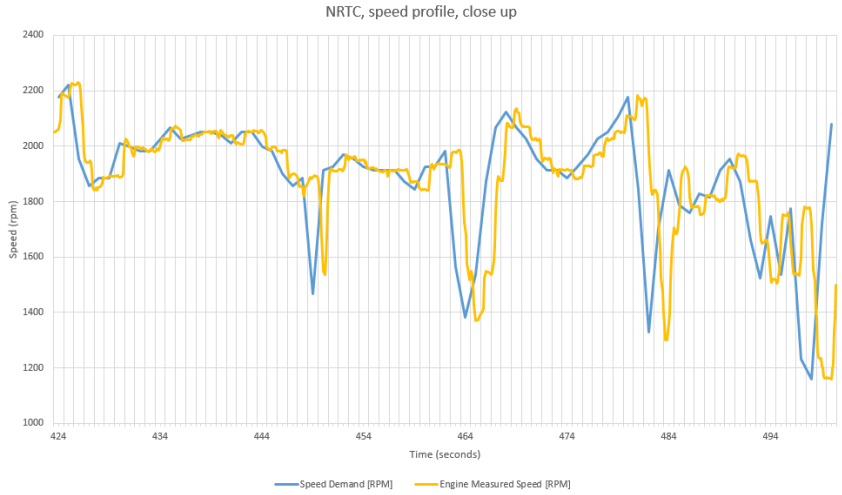

Figure 51. A close-up of the NRTC speed profile results. The tracking looks good if not for the delayed system response.

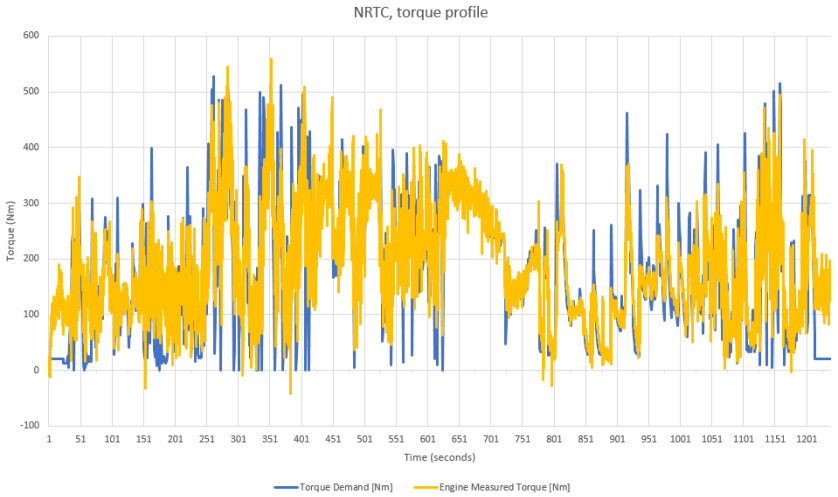

Figure 52. The NRTC results for torque tracking. It is clear that the system is not able to reach the profile peaks with the current controller parameters.

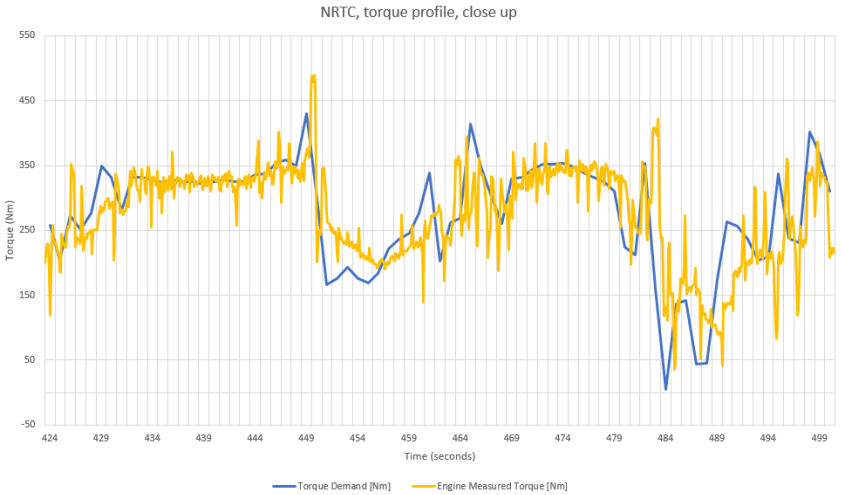

Figure 53. A close-up of the NRTC torque profile results. The tracking would look decent but the response is not good.

Figures 54 and 55 show the electrical measurements and powers during the NRTC, respectively. The figure timelines are cut after the first large power peak. The DC bus voltage remains constant at 750 V even during the power-intensive sections. With the tested engine, the currents stay well within the design limits, as the inverter and the cables are dimensioned for 350 A. The engine exceeds it's maximum specific power by almost 30 kW. However, this happens at short peaks, rather than at constant power, meaning that the dynamometer loads the engine throughout its operational range during the cycle, as it should. The motor power is taken from the CAN bus, and it is unclear what method is used, and if losses have been taken into account. Thus, the overall efficiency of the system cannot be derived without further knowledge or without a power meter.

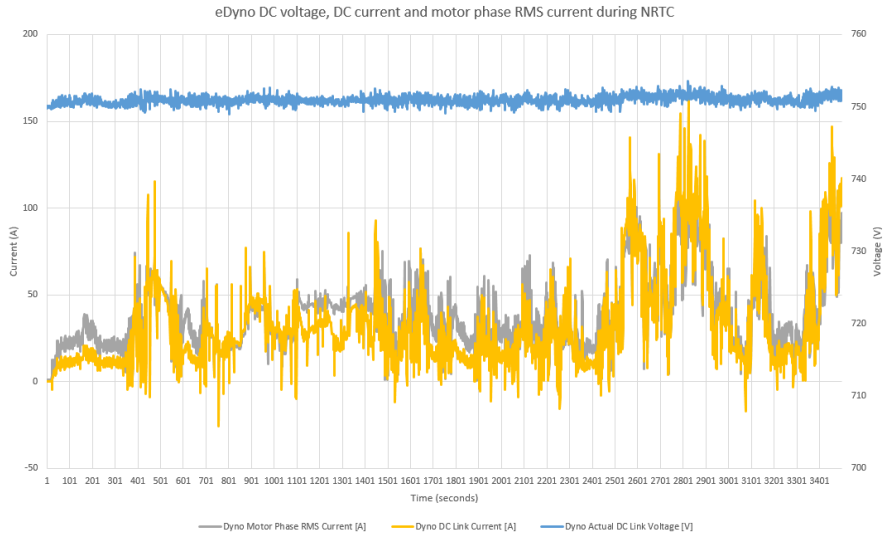

Figure 54. The NRTC results for eDyno voltage and currents. The electrical system seems to work fine under heavy testing.

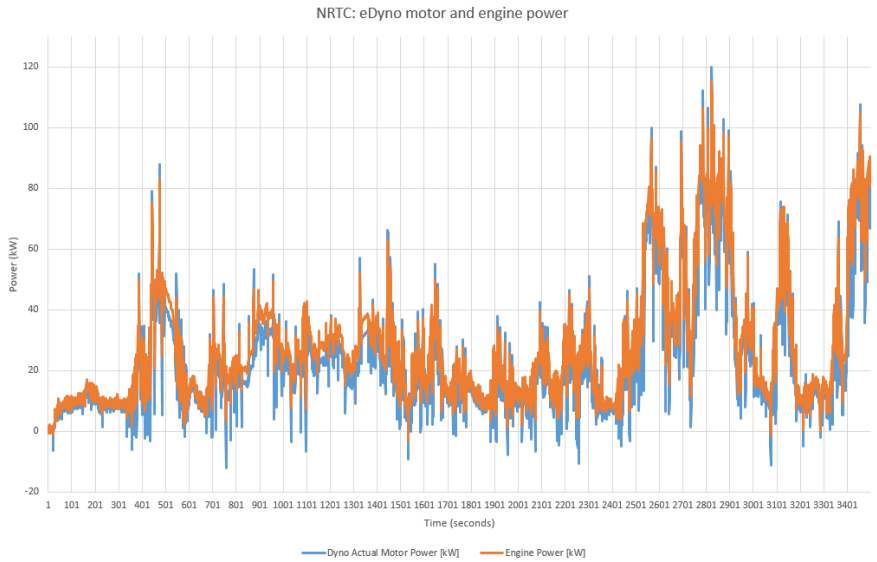

Figure 55. Motor and engine power needs during the NRTC. The engine power is analytical, while all required information is not available for the motor power, making the comparison not valid.

5.2 Reference simulation results

Initially, the goal was to have results from the pure simulation as a reference to compare the physical HIL simulation. However, the HIL tests could not be made. This section shows the reference simulation results to show that the model is working and ready to be implemented after the eDyno core functions are properly implemented and tuned.

The simulation model build in section 4 was run on a laptop, which specifications are shown in table 13. To give indication of the simulation performance on the HIL-platform, the same fixed step solver and settings were used as was when compiling the model to its proper file-format. Sample-rate of 1 kHz was used to test the limits of the simulation model. Faster sample-rates would not be possible to integrate for the eDyno due to hardware limitations. The simulation with a simulation time of 250 seconds took the laptop 54.6567 seconds to run. Interestingly, the simulation would not run completely when trying sample-rates of 10 Hz and 100 Hz, as the hydraulic system would lose pressure and start to cavitate. Additionally, this behavior happened in the parametrization process of the hydraulic circuit, meaning that the hydraulic system is currently only stable with the specified parameters.

Figure 56 shows the drive cycle tracking performance of the vehicle. Excellent tracking was achieved even with a simple PI-controller. However, the cycle itself is simple and more complex ones with faster transitions might require a more sophisticated predictive controller.

Table 13. Laptop configuration used to run the reference simulation

HP ZBook Studio G4	
System type	x64-based PC
Processor	i7-7700HQ
CPU clock-rate (GHz)	2.8
Physical memory (Gb)	8

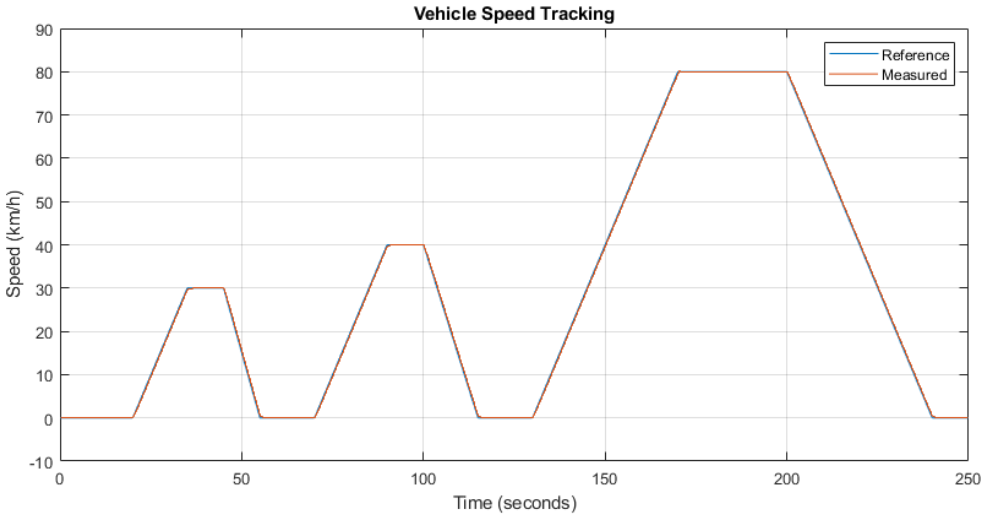

Figure 56. Drive cycle tracking of the hybrid RCV simulation

The component specific controllers performed well in the simulation as well. The drive cycle profile can be seen from all three components, which makes perfect sense, since they are connected to each other via the planetary gear at all times. The generator speed tracking does not match, since it is turned off after the engine has reached its reference. Thus, the speed controller will be entirely useless in the physical HIL simulation, because the engine will already be idling before the test cycle is initiated. The generator's torque tracking shows that at approximately 70 second mark, the battery charging is turned on.

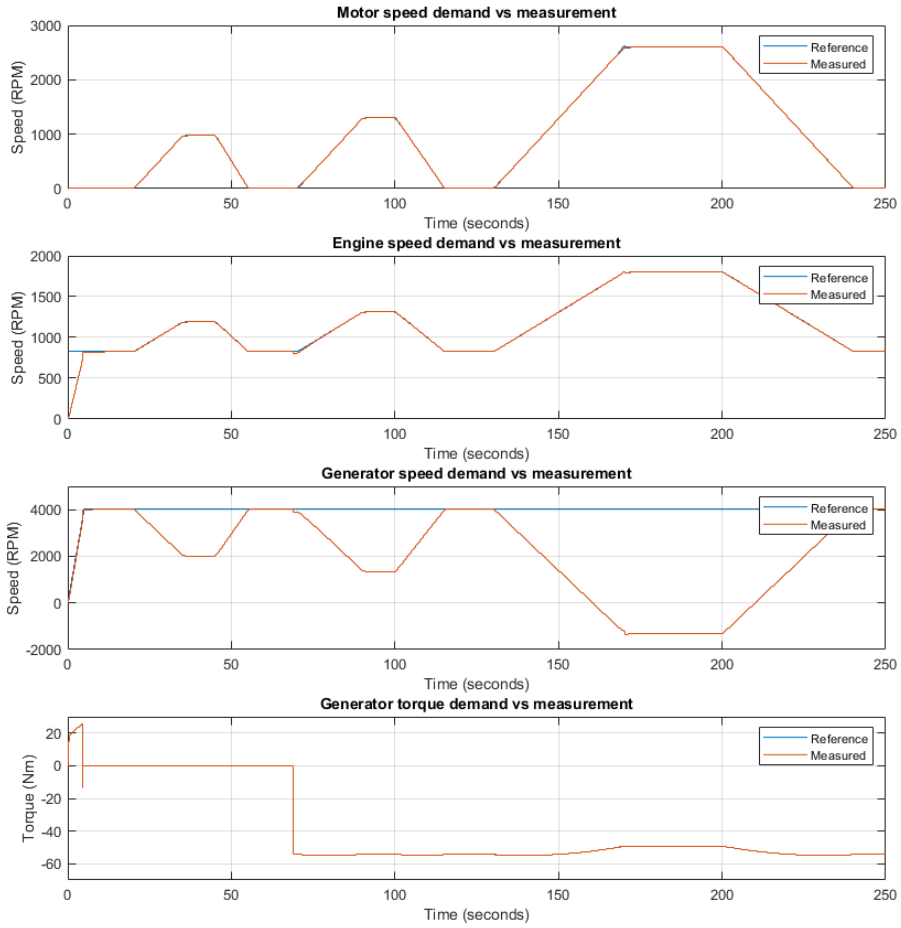

Figure 57. Controller results for the motor, the generator and the ICE of the hybrid RCV

The engine data in figure 58 shows some interesting transitions during the drive cycle. The traction motor has such a significant role in providing the vehicle traction that the engine is more or less useless. This should not be the case, and the drivetrain should be updated to include the ICE more in the total traction. Once the battery charging begins, larger torque and power are demanded from the engine. However, considering the testbed validation for HIL applications, the engine data provides very interesting profiles, where the physical engine will work in a large operational range with both fast and slow dynamics. As for the hydraulic circuit model, pump data from the entire drive cycle are presented in figure 59.

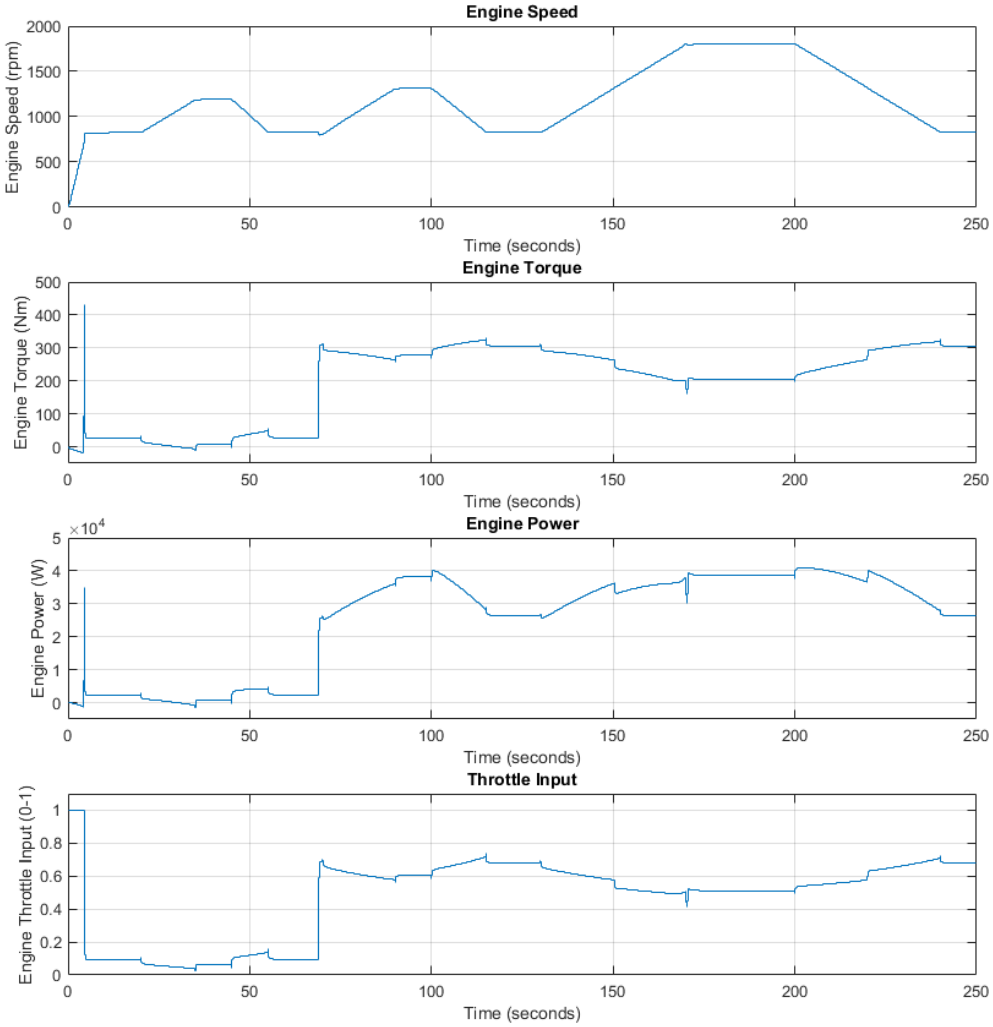

Figure 58. ICE performance during the hybrid RCV simulation

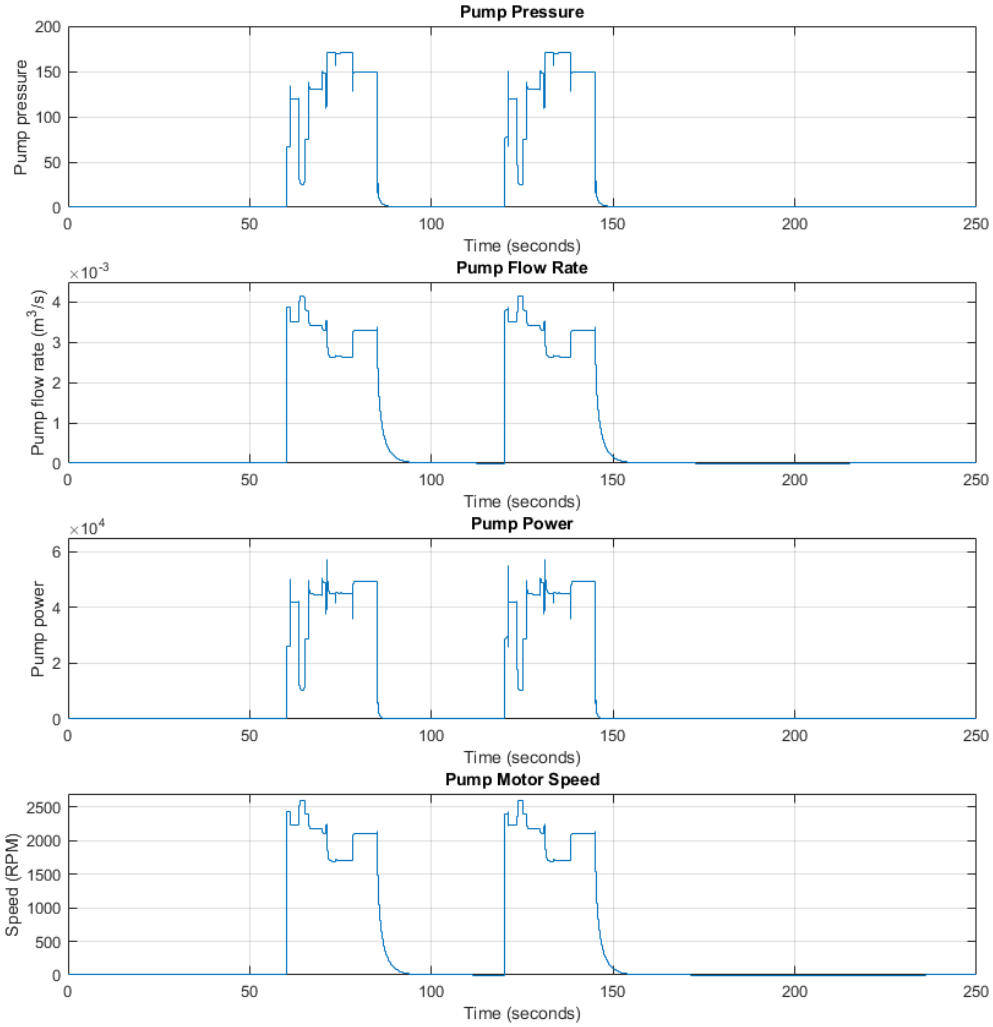

Figure 59. Hydraulic pump performance during the hybrid RCV simulation

6 Discussion and analysis

The testbed validation tests were performed to assess how well the system is able to track speed and torque references. In order for the system to be implemented for standardized testing protocols, it needs to have good tracking requirements. However, this work has only implemented one analytical assessment for determining when the desired performance has been reached. This is because the software and controller development is a rapidly iterating process, and from a design perspective it is faster to improve the system by stating the obvious problems and to look for a solution, rather than taking time to quantify the errors after each test.

The regulation for the NRTC sets requirements for the test procedure to ensure that the testbed does not affect the emission measurement results. Using a calculation template based on the regulation, the test was validated for the eDyno. The results are presented in table 14, which confirm that the eDyno could not be used for regulatory testing at its current state.

Table 14. NRTC tracking assessment for the eDyno testbed

	Correlation, r	r^2	min.	Pass/Fail
Torque	0.8922	0.796	0.88	Fail
Speed	0.9884	0.9770	0.97	Pass
Power	0.9095	0.827	0.91	Fail

The failed validation could be caused simply by the poor system response in the tests. The delay could be due to how the designed LabVIEW logic reads and writes the data from and to a spreadsheet file. According to the hardware specification, the system should be able to handle sample rates of up to 1 000 Hz, so most likely the problem lies in the data logging logic, rather than in the mechanical system performance.

As another tool for validation, the eDyno speed and torque tracking performance was visually compared to that of another dynamometer, which has been verified for standardized use, shown in figure 49. The same exact reference curve was not used for the eDyno test, because at the time of testing, it was not noticed that the reference dynamometer's torque reference had linear transitions from one point to another. Rather, eDyno test used a discrete transition step, making the results not directly comparable. In addition, it should be noted that the test comparison is not scientifically reliable, since the tests were run at completely different times on vastly different systems. For example, the comparison test is five times longer and may involve environmental differences, which could have affected the results. Also, the sensors and differences in data collection hardware could have drastic effect in the measurement accuracy. However, the torque tracking behavior can cautiously be considered better for the eDyno, while speed tracking is slightly worse. The cyclic behavior of the measured speed signal could indicate oscillation related to poor controller tuning, where a steady state is never really reached.

The torque ripple present in the measurements was noticeable, but in the end considered to be normal, because of the inherently uneven operation of an ICE. The ripple was more substantial when running the engine in torque control mode, as compared to the dynamometer's torque

control. This means that the larger torque ripple present in some of the tests were due to badly tuned engine torque controller rather than due to a mechanical vibration.

The behavior presented in figures 42 and 45 was unexpected. It is possible that at these discrete operation points, corresponding to 1 000 and 1 500 rpm, the system is in resonance. However, a resonance should only increase the torque ripple than create an offset and a creep. Based on this, the best guess is a logic fault in the torque controller.

For HIL verification, the prepared model gives good results for pure simulation when using the current parameters. The ICE speed and torque profiles do not seem too complex or fast, and the profiles excite the ICE in a wide operational range, even though the model behavior is not optimal from a vehicle control point of view. The purely virtual results are mostly in line with expectations and provide an acceptable starting point for future HIL model development. However, the model stability is questionable when changing parameters, and perhaps better modeling methods need to be considered, e.g. for the hydraulic work circuit.

Conclusions of the hydraulic circuit model's feasibility can also be made. The hydraulic energy during the refuse collection operation should be close to the values presented in the middle column of table 15. Integrating the flow rate and the power during the hydraulic cycle, a displaced volume and the needed energy are achieved. Analytical integration results in an energy need of 0.054 MJ, which is higher than the reference value. In addition, the displaced volume was 85.3 l, which is roughly doubled the reference.

Table 15. Flow and energy requirements for loading operation [64]

	Front Loader Lift Operation (Arm and Fork Cylinders)	**Rear Loader Pack and Sweep Operation**	**Rear Loader Sweep Operation**	**Side Loader Lift Operation (Grabber, Reach, Lift, Swing Cylinders)**
Displaced Volume (l)	50.3	43.9	15.9	9.8
Maximum Operating Pressure (bar)	190	190	190	207
Energy Needed (MJ)	0.990	0.832	0.301	0.187

The HIL performance of the system could not be assessed at this point, nor can clear conclusions be drawn from the pure simulation run on the laptop, because the system specifications of the laptop and the CompactRIO target machine are different. According to specifications, the laptop is more powerful, whereas the target machine is dedicated for real-time operation. For this reason, the computational performance of the two different systems could be similar. If that is the case, the laptop results indicate that the model should be computationally light enough for real-time simulation in the eDyno, since the simulation model was able to run at nearly five times the speed of real-time at 1 kHz sample rate.

7 Conclusions and recommendations

This section summarizes the thesis work by each subject and concludes whether the objectives were reached. Finally, recommendations are given as to how the work could be improved in the future.

7.1 Conclusions

The need for this work was explained by presenting background and current situation of the industry. Due to the need to develop economical and green vehicles, regulation changes in vehicle type-approval have been made in recent years. Eventually, the type-approval should match real-world driving conditions as closely as possible. HIL testing creates an attractive alternative between laboratory and real-world testing.

HIL testing combines a virtual model and a physical DUT, which enables taking actual measurements from the DUT with minimal physical requirements. The virtual and the physical components communicate bidirectionally with each other in real-time, creating a full representation of the system. Real-time systems have strict requirements regarding the execution time of each iteration step. HIL advantages include cost effectiveness, rapid prototyping, repeatability, non-destructiveness, condition emulation and safety. In turn, HIL requires, for example, hardware capable of handling real-time sampling, signal conditioning and proper modeling.

To prepare for the eventual testbed and simulation design, requirements and solutions for HIL testing were researched. In a simple configuration, HIL architecture consists of an operator interface (host PC), a target machine which has a real-time processor, I/Os and a DUT. Usually, the virtual environment and/or system properties are emulated to the DUT. For example, torque loads are emulated to a physical engine by using a dynamometer. The dynamometer receives the reference load from a virtual simulation model.

The virtual models in HIL have requirements for RT simulation. The simulation has to have fixed discrete time-steps. The model fidelity should not be too large or otherwise the target machine cannot compute the model within the given time-step. Fidelity can be reduced by using proper modeling algorithms, or by using low-fidelity modeling techniques, such as steady-state models or lookup tables. In HIL vehicle simulations, real-world causality forward-facing models should be used to achieve results comparable to real-world testing. However, computationally less expensive backward-facing modeling can be used in some cases, where absolute correctness is not of necessity.

Several HIL applications were presented from literature, describing projects where it was implemented for EV and HEV powertrain development, vehicle batteries, fuel cells, ultracapacitors and hydraulics.

Requirements for the testbed design were conducted with safety and high dynamical performance as key objectives. The testbed is essentially a highly responsive engine dynamometer. A safety level was set according to national regulations for electrical equipment. The testbed was assessed with a safety rating of PL *d*, meaning that system control plays a large role in risk prevention, and system failure could lead to serious injury or death, if not well prevented.

The testbed was designed according to the selected requirements and was built internally at VTT's facilities. Essentially, the system is built around Danfoss's electric motor and inverter, with instrumentation from National Instruments. Links to the component specifications are provided in appendix A.

The objective of this work was to *provide a functional setup, which can be applied for conventional engine dynamometer testing and the system is expected to be used for HEV HIL simulations, where a physical engine is used.* The function as an engine dynamometer was assessed by running steady-state and transient test cycles. After some initial tests, a steady-state C1 cycle and a transient NRTC were run on the system. The results were promising, but the system was still assessed to not be ready for operation. This also meant that the intented HIL simulation could not be run either. Thus, the main objectives were not reached in this work.

To prepare for the eventual HIL simulations, a model of a hybrid RCV was designed. The model topology and parameters were backed up according relevant literature, and the main dynamics of the system were described. Simulation methods were shown for the main components. The model was run as a pure simulation on a laptop to give an indication of how the simulation model would run in the designed system. The process behind simulation model integration to the control software was described but not implemented beyond compiling the model to a compatible format. The results from the pure simulation showed that the model should be able to run in a HIL simulation, thus the HIL capabilities were at least partially reviewed.

For the research problem of *whether a Hardware-in-the-Loop simulation for Hybrid Electric Vehicles is achieved with the designed engine dynamometer testbed*, currently, the answer is 'no'. However, there is confidence that following the recommendations given in the next section, the research problem can be answered positively. If the question was rephrased to *whether a Hardware-in-the-Loop simulation for Hybrid Electric Vehicles is achieved with AN engine dynamometer testbed*, the answer would undoubtedly be 'yes'. This is known based on the literature review done in this work. While this work could not reach its main objectives, the side objectives of *documenting the testbed design and implementation process* and *explaining the overall theory behind HIL simulations and providing reference for different HIL applications of HEVs* were reached.

7.2 Recommendations

As the very first step, it is recommended that the communication logic in the software is troubleshot for errors to see whether the delay in system response and the unexpected tracking behavior at the two discrete points could be caused by a programming error. If the system response cannot be otherwise improved, a possible solution would be to implement a predictive controller to the software. This way the system dynamics would be taken into account and the references should be tracked well. The use of lead-lag filtering for signal conditioning was mentioned in section 2.1.3, but was never fully realized.

If no errors are found for the tracking problem at the two discrete points from the software, possible mechanical resonance should be researched. The easiest way would be to change the flexible coupling into either a more damped or a more rigid one to shift the system's

natural frequency, and see if the problematic discrete points change. If that is the case, it is recommended to use as rigid driveline as possible to ensure optimal torque transmission for HIL applications, while having the resonance frequency above the operational range. However, this could cause a risk in mechanical reliability, as the parasitic extraneous loads are not dampened as well anymore.

Overall, the controllers need further parameter tuning. In addition, a logic should be added that when both the engine idle speed and zero torque is demanded, the system will actually be run idle without enforcing any speeds or torques, as was seen at the end of some of the tests.

Considering the HIL applications of the eDyno, the intention was to have a simulation model which could be used for rapid prototyping. This would require fast changes to the model parameters and even to the powertrain topology. For the simulation model, there is a great probability for it to not work when considerably changing the model parameters. Currently, the model updating process is not as effortless as was hoped, due to the requirement for accurate tuning of the controllers. The model could still be used for fine tuning after component specific parameters are set. For rapid prototyping, it is recommended that a backward-facing model would be built.

While it was not in the scope of this work to study the feasibility of the simulation model as an actual hybrid RCV, some recommendation can be given. When considering the power-split topology of the model vehicle, updates should be made. Currently, the ICE does not provide enough to the total traction force of the vehicle. The engine power only becomes significant when the battery is being charged. A clutch could be added to disengage the traction motor from the power-split device combined with a different control logic to achieve better traction and charging performance from the RCV. In addition, the hydraulic model parameters of the RCV should be updated if a more realistic representation is required. However, for a HIL simulation, this has little effect.

References

[1] Georgios Fontaras, Nikiforos-Georgios Zacharof, and Biagio Ciuffo. Fuel consumption and co2 emissions from passenger cars in europe – laboratory versus real-world emissions. *Progress in Energy and Combustion Science*, 60:97 – 131, 2017.

[2] Nils Hooftman, Maarten Messagie, Joeri Van Mierlo, and Thierry Coosemans. A review of the european passenger car regulations – real driving emissions vs local air quality. *Renewable and Sustainable Energy Reviews*, 86:1 – 21, 2018.

[3] Pierpaolo Cazzola, Marine Gorner, Renske Schuitmaker, Leonardo Paoli, Sacha Scheffer, Jacob Teter, Jacopo Tattini, Kate Palmer, and Till Bunsen. Global electric vehicles outlook - 2018. Technical report, International Energy Agency, 2018.

[4] Ari Hentunen, Panu Sainio, Jussi Suomela, Antti Leivo, and Matti Liukkonen. Hardware-in-the-loop verification environment for heavy-duty hybrid electric vehicles. In *IEEE Vehicle Power and Propulsion Conference (VPPC), Lille, France, 1-3.10.2010*, page 6, 2010.

[5] Andrew R Plummer. Model-in-the-loop testing. *Proceedings of the Institution of Mechanical Engineers, Part I: Journal of Systems and Control Engineering*, 220(3):183–199, 2006.

[6] G. R. Babbitt and J. J. Moskwa. Implementation details and test results for a transient engine dynamometer and hardware in the loop vehicle model. In *Proceedings of the 1999 IEEE International Symposium on Computer Aided Control System Design (Cat. No.99TH8404)*, pages 569–574, Aug 1999.

[7] Theodoros Grigoratos and Giorgio Martini. Brake wear particle emissions: a review. *Environmental science and pollution research international*, 22, 10 2014.

[8] Zoran Filipi, Jonathan Hagena, and Hosam Fathy. Investigating the impact of in-vehicle transients on diesel soot emissions. *Thermal Science - THERM SCI*, 12:53–72, 01 2008.

[9] Zoran Filipi, Hosam Fathy, Jonathan Hagena, Alexander Knafl, Rahul Ahlawat, Jinming Liu, Dohoy Jung, Dennis N. Assanis, Huei Peng, and Jeffrey Stein. Engine-in-the-loop testing for evaluating hybrid propulsion concepts and transient emissions - hmmwv case study. In *SAE Technical Paper*. SAE International, 04 2006.

[10] Jonathan Hagena Jeffrey L. Stein Hosam K. Fathy, Zoran S. Filipi. Review of hardware-in-the-loop simulation and its prospects in the automotive area. In *Proc. SPIE, Modeling and Simulation for Military Applications*, volume 6228, pages 6228 – 6228 – 20, 2006.

[11] H. Zhang, Y. Zhang, and C. Yin. Hardware-in-the-loop simulation of robust mode transition control for a series–parallel hybrid electric vehicle. *IEEE Transactions on Vehicular Technology*, 65(3):1059–1069, March 2016.

[12] Jane W. S. W. Liu. *Real-Time Systems*. Prentice Hall PTR, Upper Saddle River, NJ, USA, 1st edition, 2000.

[13] Phillip A. Laplante and Seppo J. Ovaska. *Fundamentals of Real-Time Systems*, chapter 1. IEEE, 2012.

[14] Loucas S. Louca and Umut Yilder. Modelling and reduction techniques for studies of integrated hybrid vehicle systems. *Mathematical & Computer Modelling of Dynamical Systems*, 12(2/3):203 – 218, 2006.

[15] National Instruments. Hardware-in-the-loop (hil) test system architectures. `http://www.ni.com/white-paper/10343/en/`. [Online; accessed 22-January-2019].

[16] Rui Xiong, Yanzhou Duan, Jiayi Cao, and Quanqing Yu. Battery and ultracapacitor in-the-loop approach to validate a real-time power management method for an all-climate electric vehicle. *Applied Energy*, 217:153 – 165, 2018.

[17] Y. Xiao-kun, H. Hong-wen, P. Lian-yun, and Z. Xiaolin. Hardware-in-the-loop simulation on a hybrid power system. In *2011 4th International Conference on Power Electronics Systems and Applications*, pages 1–5, June 2011.

[18] Loucas S Louca and Jeffrey L Stein. Energy-based model reduction of linear systems. In *Proc. of Int. Conf. on Bond Graph Modeling and Simulation*, 1999.

[19] F. Gao, B. Blunier, M. G. Simoes, and A. Miraoui. Pem fuel cell stack modeling for real-time emulation in hardware-in-the-loop applications. *IEEE Transactions on Energy Conversion*, 26(1):184–194, March 2011.

[20] Luis Herrera, Cong Li, Xiu Yao, and Jin Wang. Fpga-based detailed real-time simulation of power converters and electric machines for ev hil applications. *IEEE Transactions on Industry Applications*, 51(2):1702–1712, 2015.

[21] C. Dufour, T. Ishikawa, S. Abourida, and J. Belanger. Modern hardware-in-the-loop simulation technology for fuel cell hybrid electric vehicles. In *2007 IEEE Vehicle Power and Propulsion Conference*, pages 432–439, Sep. 2007.

[22] Vahid Jalili-Marandi, Zhiyin Zhou, and Venkata Dinavahi. Large-scale transient stability simulation of electrical power systems on parallel gpus. In *Power and Energy Society General Meeting, 2012 IEEE*, pages 1–11. IEEE, 2012.

[23] C. C. Chan, A. Bouscayrol, and K. Chen. Electric, hybrid, and fuel-cell vehicles: Architectures and modeling. *IEEE Transactions on Vehicular Technology*, 59(2):589–598, Feb 2010.

[24] Ganesh Mohan, Francis Assadian, and Stefano Longo. Comparative analysis of forward-facing models vs backward-facing models in powertrain component sizing. In *IET Hybrid and Electric Vehicles Conference 2013 (HEVC 2013)*, volume 2013, 01 2013.

[25] Sung Chul Oh. Evaluation of motor characteristics for hybrid electric vehicles using the hardware-in-the-loop concept. *IEEE Transactions on Vehicular Technology*, 54(3):817–824, May 2005.

[26] Matti Liukkonen. *Methodologies for development of series-hybrid powertrains to non-road mobile machineries*. G5 artikkeliväitöskirja, Aalto University; Aalto-yliopisto, 2013.

[27] Z Filipi and Y J. Kim. Hydraulic hybrid propulsion for heavy vehicles: Combining the simulation and engine-in-the-loop techniques to maximize the fuel economy and emission benefits. *http://dx.doi.org/10.2516/ogst/2009024*, 65, 09 2009.

[28] Mohd Azrin Mohd Zulkefli, Pratik Mukherjee, Zongxuan Sun, Jianfeng Zheng, Henry X. Liu, and Peter Huang. Hardware-in-the-loop testbed for evaluating connected vehicle applications. *Transportation Research Part C: Emerging Technologies*, 78:50 – 62, 2017.

[29] C Hardie, H Tait, S Craig, J G Chase, B W Smith, and G Harris. Automated tuning of an engine management unit for an automotive engine. *Proceedings of the Institution of Mechanical Engineers, Part D: Journal of Automobile Engineering*, 216(10):841–849, 2002.

[30] SAE J 1715. Hybrid Electric Vehicle (HEV) and Electric Vehicle (EV) Terminology. Standard, SAE International, October 2014.

[31] M. Ehsani, Y. Gao, and A. Emadi. *Modern Electric, Hybrid Electric, and Fuel Cell Vehicles: Fundamentals, Theory, and Design, Second Edition*. Power Electronics and Applications Series. CRC Press, 2009.

[32] Guang Wu, Xing Zhang, and Zuomin Dong. Powertrain architectures of electrified vehicles: Review, classification and comparison. *Journal of the Franklin Institute*, 352(2):425 – 448, 2015. Special Issue on Control and Estimation of Electrified vehicles.

[33] K. T. Chau and C. C. Chan. Emerging energy-efficient technologies for hybrid electric vehicles. *Proceedings of the IEEE*, 95(4):821–835, April 2007.

[34] Bin Wu, Chan-Chiao Lin, Zoran Filipi, Huei Peng, and Dennis Assanis. Optimal power management for a hydraulic hybrid delivery truck. *Vehicle System Dynamics*, 42:23–40, 12 2004.

[35] Frank A. Bender, Thomas Bosse, and Oliver Sawodny. An investigation on the fuel savings potential of hybrid hydraulic refuse collection vehicles. *Waste Management*, 34(9):1577 – 1583, 2014.

[36] Poria Fajri, Sangin Lee, Venkata Anand Kishore Prabhala, and Mehdi Ferdowsi. Modeling and integration of electric vehicle regenerative and friction braking for motor/dynamometer test bench emulation. *IEEE Transactions on Vehicular Technology*, 65(6):4264–4273, 2016.

[37] M.J. Marcel, T.A. Haskew, and K.A. Williams. Test facility for a hybrid fuel cell electric vehicle. In *Proceedings 2007 IEEE SoutheastCon*, pages 734 – 739, 04 2007.

[38] R. M. Schupbach and J. C. Balda. A versatile laboratory test bench for developing powertrains of electric vehicles. In *Proceedings IEEE 56th Vehicular Technology Conference*, volume 3, pages 1666–1670 vol.3, Sept 2002.

[39] A Castaings, Alain Bouscayrol, Walter Lhomme, and Rochdi Trigui. Power hardware-in-the-loop simulation for testing multi-source vehicles. *IFAC-PapersOnLine*, 50:10971–10976, 07 2017.

[40] Y. Zhang, R. Xiong, H. He, and W. Shen. Lithium-ion battery pack state of charge and state of energy estimation algorithms using a hardware-in-the-loop validation. *IEEE Transactions on Power Electronics*, 32(6):4421–4431, June 2017.

[41] J. V. Barreras, C. Fleischer, A. E. Christensen, M. Swierczynski, E. Schaltz, S. J. Andreasen, and D. U. Sauer. An advanced hil simulation battery model for battery management system testing. *IEEE Transactions on Industry Applications*, 52(6):5086–5099, Nov 2016.

[42] W. C. Lee and D. Drury. Development of a hardware-in-the-loop simulation system for testing cell balancing circuits. *IEEE Transactions on Power Electronics*, 28(12):5949–5959, Dec 2013.

[43] Yongjun Yuan, Xuezhe Wei, and Zechang Sun. Assessment of power consumption control strategy for battery management system using hardware-in-the-loop simulation. In *2008 IEEE Vehicle Power and Propulsion Conference*, pages 1–6, Sep. 2008.

[44] P. A. Lindahl, S. R. Shaw, and S. B. Leeb. Fuel cell stack emulation for cell and hardware-in-the-loop testing. *IEEE Transactions on Instrumentation and Measurement*, 67(9):2143–2152, Sep. 2018.

[45] D. Zhao, Y. Huangfu, M. Dou, and F. Gao. Hardware-in-the-loop validation of an air supply method for vehicular fuel cell applications. In *IECON 2014 - 40th Annual Conference of the IEEE Industrial Electronics Society*, pages 3968–3972, Oct 2014.

[46] W Backé. The present and future of fluid power. *Proceedings of the Institution of Mechanical Engineers, Part I: Journal of Systems and Control Engineering*, 207(4):193–212, 1993.

[47] Soroosh Mahmoodi, Hu Guoqing, and Mehrdad Khajavi. Investigation of control model in a new series hybrid hydraulic/electric system for heavy vehicles based on energy efficiency. *Chinese Journal of Engineering*, 2016:1–9, 03 2016.

[48] Markets Research and. Research and markets: Hardware in the loop market by vertical (automotive, aerospace, defense, power electronics, research & education & others) 2015 - global forecasts to 2020 for the $826 million industry. *Business Wire (English)*, 0012.

[49] W. Grega. Hardware-in-the-loop simulation and its application in control education. In *FIE'99 Frontiers in Education. 29th Annual Frontiers in Education Conference. Designing the Future of Science and Engineering Education. Conference Proceedings (IEEE Cat. No.99CH37011*, volume 2, pages 12B6/7–12B612 vol.2, Nov 1999.

[50] Flavio Padilha Queiroz, Francisco José Gomes, Luka Parma de Freitas, and Vinicius Athouguia Gama. Development of a foss-based hardware-in-the-loop platform for control engineering education. *Journal of Control, Automation and Electrical Systems*, 24(3):244–252, Jun 2013.

[51] H. Temeltas, M. Gokasan, S. Bogosyan, and A. Kilic. Hardware in the loop simulation of robot manipulators through internet in mechatronics education. In *IEEE 2002 28th Annual Conference of the Industrial Electronics Society. IECON 02*, volume 4, pages 2617–2622 vol.4, Nov 2002.

[52] T. Horiuchi, M. Inoue, T. Konno, and Y. Namita. Real-time hybrid experimental system with actuator delay compensation and its application to a piping system with energy absorber. *Earthquake Engineering & Structural Dynamics*, 28(10):1121–1141, 1999.

[53] J Andrae. Measurement and calibration using reference and transfer torque flanges. In *Proceedings of the 17th International Conference on Force, Mass, Torque and Pressure Measurements, IMEKO TC3*, pages 17–21, 2001.

[54] Mark Minda. 21 tips on how to install a torque sensor. `https://www.hbm.com/en/4432/21-tips-on-how-to-install-a-torque-sensor/`. [Online; accessed 18-December-2018].

[55] A. Ghatak. *Optics*, page 6.10. McGraw-Hill, 2005.

[56] K. Ogata. *System Dynamics*, page 617. Cram 101. Pearson/Prentice Hall, 2004.

[57] Markus Lutz. Design and construction of electric motor dynamometer and grid attached storage laboratory. Master's thesis, Colorado State University, Colorado State University. Libraries, 2011.

[58] SAE J1939. Serial Control and Communications Heavy Duty Vehicle Network. Standard, SAE International, August 2018.

[59] Jorma Haataja and Juha Pyrhönen. Permanent magnet assisted synchronous reluctance motor: an alternative motor in variable speed drives. In Francesco Parasiliti and Paolo Bertoldi, editors, *Energy Efficiency in Motor Driven Systems*, pages 101–110, Berlin, Heidelberg, 2003. Springer Berlin Heidelberg.

[60] IEC 60034-7. Rotating electrical machines - Part 7: Classification of types of construction, mounting arrangements and terminal box position (IM Code). Standard, International Electrotechnical Commission, February 2001.

[61] SAE J617. Engine Flywheel Housing and Mating Transmission Housing Flanges. Standard, SAE International, April 2014.

[62] IEC 60364-5-52. Low-voltage electrical installations - Part 5-52: Selection and erection of electrical equipment - Wiring systems. Standard, International Electrotechnical Commission, February 2011.

[63] Annex to the commission delegated regulation (eu) 2017/654 supplementing regulation (eu) 2016/1628 of the european parliament and of the council with regard to technical and general requirements relating to emission limits and type-approval for internal combustion engines for non-road mobile machinery. *OJ*, L 102:4–5, 2017-04-13.

[64] Nicholas Echter. Parallel hydraulic pressure assist/work circuit hybrids for automated side loader refuse vehicles. Master's thesis, Colorado State University, Colorado State University. Libraries, 2012.

[65] RJ Vermeulen, RN van Gijlswijk, D van Heesen, EG Buskermolen, RP Verbeek, and S van Goethem. Tail-pipe nox emissions of refuse collection vehicles with a euro vi engine in daily operation in the netherlands. Technical report, TNO, 2018.

[66] Francisco Soriano Alfonso. *A study of hybrid powertrains and predictive algorithms applied to energy management in refuse-collecting vehicles*. Doctoral thesis, Universitat Politècnica de Catalunya, 2015.

[67] J. Liu and H. Peng. Modeling and control of a power-split hybrid vehicle. *IEEE Transactions on Control Systems Technology*, 16(6):1242–1251, Nov 2008.

[68] Mathworks. Hybrid-electric vehicle model in simulink. `https://se.mathworks.com/matlabcentral/fileexchange/28441-hybrid-electric-vehicle-model-in-simulink`. [Online; accessed 1-March-2019].

[69] Thuy T.T. Nguyen and Bruce G. Wilson. Fuel consumption estimation for kerbside municipal solid waste (msw) collection activities. *Waste Management & Research*, 28(4):289–297, 2010. PMID: 19723822.

[70] Swagata Borthakur and Shankar C. Subramanian. Optimized design and analysis of a series-parallel hybrid electric vehicle powertrain for a heavy duty truck. *IFAC-PapersOnLine*, 51(1):184 – 189, 2018. 5th IFAC Conference on Advances in Control and Optimization of Dynamical Systems ACODS 2018.

[71] Rajit Johri, Simon Baseley, and Zoran Filipi. Simultaneous optimization of supervisory control and gear shift logic for a parallel hydraulic hybrid refuse truck using stochastic dynamic programming. In *ASME 2011 Dynamic Systems and Control Conference and Bath/ASME Symposium on Fluid Power and Motion Control*, pages 99–106. American Society of Mechanical Engineers, 2011.

[72] Mathworks. Front-loader actuation system. `https://se.mathworks.com/help/physmod/hydro/examples/front-loader-actuation-system.html`. [Online; accessed 1-March-2019].

[73] National Renewable Energy Laboratory. Drive: Drive-cycle rapid investigation, visualization, and evaluation analysis tool. `https://www.nrel.gov/transportation/drive.html`. [Online; accessed 1-April-2019].

Appendices

Appendix A. Table of the Main Hardware Components. 1 page.
Appendix B. Instrumentation Schematic. 1 page.

Appendix A. Table of the Main Hardware Components

Component	Qty	Name	General purpose	Link to the specification
Electric motor	1	Danfoss EM-PMI375-T800-1900	Creates high torque rotational movement	https://assets.danfoss.com/documents/DOC305757641928/DOC305757641928.pdf
Inverter	1	Danfoss EC-C1200-450+MC	Speed and torque control of the connected electric motor	https://assets.danfoss.com/documents/DOC302657040147/DOC302657040147.pdf
Torque flange	1	HBM K-T40B-003R-MF-S-M-DU2-2-U	Measurement of torque and rotational velocity	https://www.hbm.com/fileadmin/mediapool/hbmdoc/technical/B03406.pdf
Target machine	1	National Instruments cRIO-9045	On-board data processing. Ports for communication modules	http://www.ni.com/pdf/manuals/376783f_02.pdf
Extension module	1	National Instruments NI 9145	Provides extra ports for communication modules	http://www.ni.com/pdf/manuals/378015a_02.pdf
Analog input module	2	National Instruments NI 9207	8 channels of both voltage and current input	http://www.ni.com/pdf/manuals/375206b_02.pdf
Temperature module	2	National Instruments NI 9213	16 channels for K-type thermocouple inputs	http://www.ni.com/pdf/manuals/374916a_02.pdf
High-speed analog input module	2	National Instruments NI 9215	4 differential input channels for up to 100kS/s/ch	http://www.ni.com/pdf/manuals/373779a_02.pdf
High-speed analog output module	1	National Instruments NI 9263	4 differential output channels for up to 100kS/s/ch	http://www.ni.com/pdf/manuals/373781b_02.pdf
Bidirectional digital module	1	National Instruments NI 9401	8 high-speed digital input and output channels	http://www.ni.com/pdf/manuals/374068a_02.pdf
Relay module	1	National Instruments NI 9485	8 channels of Solid-State Relay (SSR) digital output	http://www.ni.com/pdf/manuals/374820a_02.pdf
High-speed CAN module	2	National Instruments NI 9862	CAN bus interface for the inverter	http://www.ni.com/pdf/manuals/373243e.pdf
Galvanic isolator	>16	Advantech ADAM-3014	Isolated DC input/output signal conditioning	http://www.lima.com.tr/Advantech%20eAutomation/Manuals/ADAM-3014%20Manual.PDF
Pulse converter	1	Nokeval 6420	Frequency conversion into analog voltage or current signal	https://nokeval.com/wp-content/uploads/2019/04/6420-datasheet-230902.pdf
Battery tester/simulator	1	AVL BTS-BT-BS/320	Used only as a power supply for the testbed	N/A

Appendix B. Instrumentation Schematic

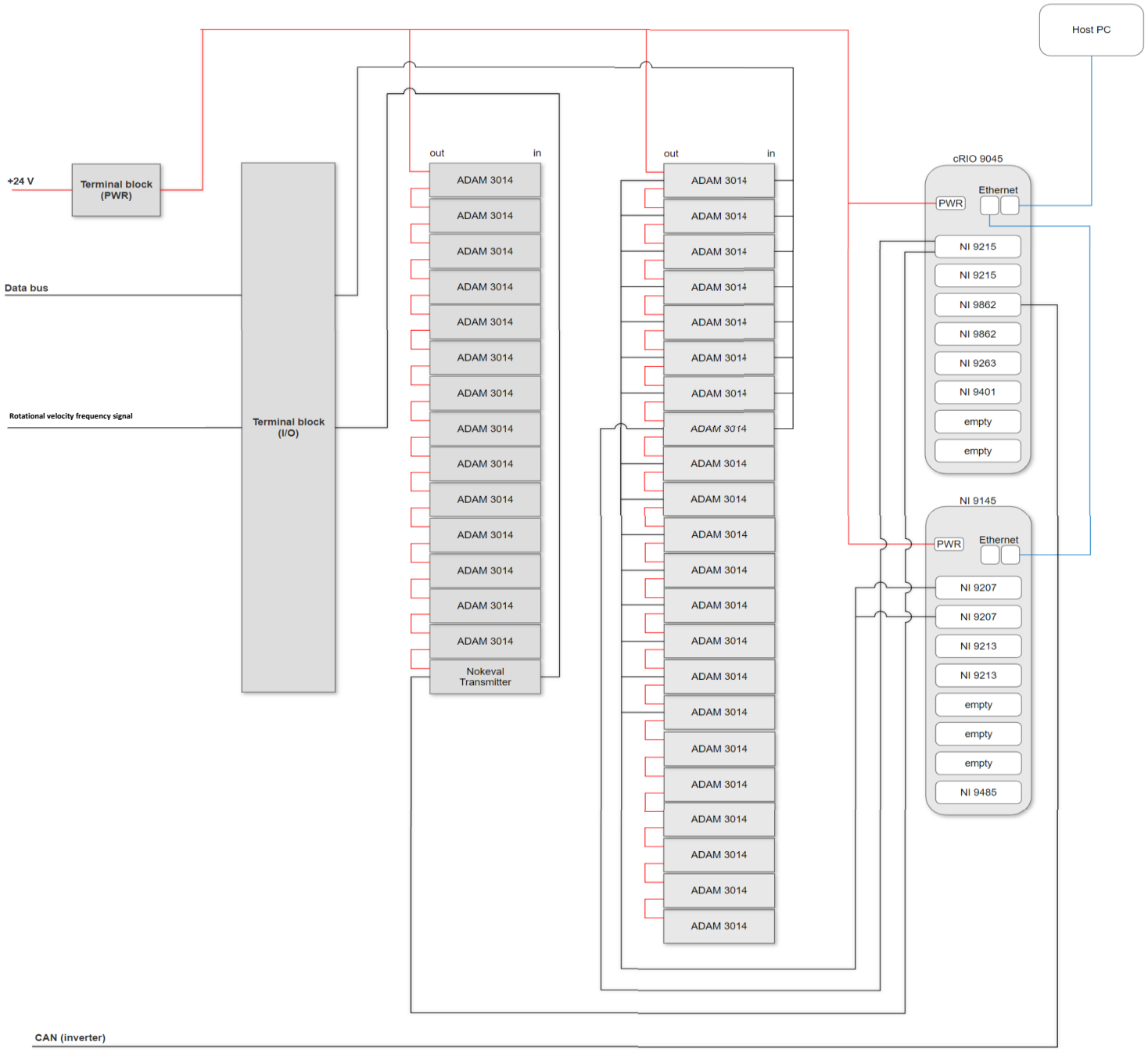

Blue lines represent ethernet connections, red lines power connections and black lines data connections. Grounding wires are excluded.